2012

Design and Analysis of Cloaked Fluorophores for Rapid Detection and Visualization of Cancer Cells Containing NAD(P)H:Quinone Oxidoreductase-1

William Silvers
Louisiana State University and Agricultural and Mechanical College, wsilve1@lsu.edu

DESIGN AND ANALYSIS OF CLOAKED FLUOROPHORES FOR RAPID DETECTION AND VISUALIZATION OF CANCER CELLS CONTAINING NAD(P)H:QUINONE OXIDOREDUCTASE-1

A Dissertation

Submitted to the Graduate Faculty of the
Louisiana State University and
Agricultural and Mechanical College
in partial fulfillment of the
Requirements for the degree of
Doctor of Philosophy

in

The Department of Chemistry

by
William Silvers
B.S., Texas State University, 2007
December 2012

This dissertation is dedicated to my family:

My dad, Charles W. Silvers

My mom, Charlotte A. Silvers

My brother, James V. Silvers

And to

My wife, Molly A. Silvers

ACKNOWLEDGMENTS

First and foremost I would like to express my deepest gratitude for my advisor, Dr. Robin L. McCarley, for his amazing guidance and support throughout the years while in his group. While sitting in his office for the first time to meet him I knew I wanted to join his group within the first ten minutes of talking to him. But little did I know what I was getting in to. I never imagined being able to work for someone so caring and compassionate, while pushing his students to be the best they could be and giving them the scientific freedom in the laboratory everyone yearns for. Because of him I have not only become a well-rounded scientist with a broad spectrum of skills, but a better person too. Not everything will work out as anticipated, but it will work out.

I would like to thank the McCarley research group for the scientific support, but mostly their friendships which will last a lifetime. It was a wide variety of backgrounds and cultures which made up this group and which made it very special. I especially would like to thank Dr. Sreelatha Balamurugan, Dr. Matt Brown, and Dr. David Burk for all of the help which they provided; my work would have never been as successful as it was if it wasn't for them.

I would also like to thank my committee members, Dr. Doug Gilman, Dr. Carol Taylor, and Dr. Kermit Murray. I couldn't have asked for a better collection of peers to be there and aid me when I needed it.

To my friends, I'm thankful every day that I've met you. Though we happened to meet through school, school is the last reason why we stuck together. Every one of you made graduate school a complete joy and made this process exponentially better than I ever anticipated.

To my family, without your love and support, none of this would have even come close to happening. You sacrificed more than I know to put me in the position where I am today, and you have no idea how grateful I am for it.

Lastly, I would like to thank my lovely wife, Molly. I absolutely have no idea how you have been able to put up with me these past five years. You have been there to comfort me and push me and I am so grateful to be married to you. I couldn't have asked for a better soulmate.

TABLE OF CONTENTS

LIST OF FIGURES

LIST OF SCHEMES

LIST OF ABBREVIATIONS AND SYMBOLS

AA	Ascorbic acid
AAP	Activatable aptamer probe
ACPP	Activatable cell penetrating peptide
AZQ	2,5-bis(carboethoxyamino)-3,6-diazirdinyl-1,4-benzoquinone
BSA	Bovine serum albumin
CCD	Charge-coupled device
CPP	Cell penetrating peptide
CT	Computerized tomography
CV	Cyclic voltammetry
Cy5.5	Cyanine 5
DCPIP	2,6-dichlorophenolindolphenol
DDS	Drug delivery system
DIC	Differential interference contrast
DNA	Deoxyribonucleic acid
DPNH	Diphosphopyridine nucleotide
DTT	Dithiothreitol
ECM	Extracellular matrix

EGFR	Epidermal growth factor receptor
EPR	Enhance permeability and retention
ER	Endoplasmic reticulum
FAD	Flavin adenine dinucleotide
$FADH_2$	Reduced flavin adenine dinucleotide
FAM	Fluorescein-5(6)-carbonyl
FBS	Fetal bovine serum
FE	Fluorescence enhancement
FLARE	Fluorescence-assisted resection and exploration
FOV	Field of view
FRET	Förster resonance energy transfer
GGT	γ-glutamyltranspeptidase
GSH	Glutathione
HD	Haloalkane dehalogenase
HER	Human epidermal growth factor
HIV-1	Human immunodeficiency virus type 1
HNSCC	Head and neck squamous cell carcinomas
ICG	Indocyanine green
ICT	Internal charge transfer
LED	Light emitting diode
MHz	Megahertz
MMC	Mitomycin C
MMP	Matrix metalloproteinase

MMP-2	Gelatinase A
MMP-9	Gelatinase B
MP	Multiphoton microscopy
MRI	Magnetic resonance imaging
NADH	Reduced nicotinamide adenine dinucleotide
NADPH	Reduced nicotinamide adenine dinucleotide phosphate
NIB	Narrow-band imaging
NIR	Near-infrared
NQO1	NAD(P)H:quinone oxidoreductase-1
NQO2	Mammal NAD(P)H:quinone oxidoreductase-2
NQO3	Bacteria NAD(P)H:quinone oxidoreductase-3
NQO4	Fungi NAD(P)H:quinone oxidoreductase-4
NQO5	Archaebacteria NAD(P)H:quinone oxidoreductase-5
hNQO1	human NAD(P)H: quinone oxidoreductase-1
mNQO1	mouse NAD(P)H:quinone oxidoreductase-1
rNQO1	rat NAD(P)H:quinone oxidoreductase-1
NSCLC	Non-small cell lung carcinoma
OeT	Oxidative electron transfer
PBS	Phosphate-buffered saline
PDE	Photodynamic Eye
PEG	Poly(ethylene glycol)
PeT	Photoinduced electron transfer
PET	Positron emission tomography

PGA	Penicillin G acylase
PMT	Photomultiplier tube
PSMA	Prostate-specific membrane antigen
PTK7	Protein kinase-7
PVP	Polyvinylpyrrolidone
Q_3	Trimethyl-lock
QD	Quantum dot
RAFT	Regioselectively addressable functionalized template
RES	Reticuloendothelial system
ReT	Reductive electron transfer
RFU	Relative fluorescence units
cRGD	Cyclic tripeptide arginine-glycine-aspartic acid
Rho-Morph	$Rhodamine_{110}$-morpholino urea
RNA	Ribonucleic acid
ROS	Reactive oxygen species
SBR	Signal-to-background ratio
SCLC	Small cell lung carcinoma
SHE	Standard hydrogen electrode
TPNH	Triphosphopyridine nucleotide
VEGF	Vascular endothelial growth factor
$Na_2S_2O_4$	Sodium dithionite
ε	Molar extinction coefficient
ΔG	Energy change

$E_{1/2}$	Half-wave potential
$E_{p,c}$	Cathodic reduction peak
λ_{ex}	Excitation wavelength
λ_{em}	Emission wavelength
k_{cat}	Catalytic constant
k_{cat}/K_m	Enzyme efficiency
K_m	Michaelis constant; substrate affinity
V_{max}	Maximum theoretical turnover rate

ABSTRACT

The development of fluorogenic substrates for real-time tumor cell detection has led to a vastly expanding field for personal oncology. Fluorophores have been studied as appendages to larger scaffolds leading to accumulation of these dyes in tumor cells or their surrounding environment, taking advantage of tumor anatomy. A new class of fluorophores has been developed in which the dye is an active participant in the mechanism of cancer cell detection. These dyes have been conjugated such that their fluorescence has been eliminated or altered and will undergo a change to reveal their fluorescent signal upon activation by a mechanism that is unique to tumor cells.

The research presented in this dissertation encompasses the design, synthesis, properties, and utilization of latent fluorophores that are specifically activated by an enzyme that is highly upregulated in tumor cells, NAD(P)H:quinone oxidoreductase-1 (NQO1). These dyes utilize the 2-electron reduction of quinones to hydroquinones, which NQO1 specifically catalyzes. A dye's fluorescence can be quenched by conjugating a quinone directly to the fluorophore, only to have its signal uncloaked after activation by NQO1. The objectives in this research will be achieved by: (1) the characterization of properties (stability in biological environments, quantum yields) of the quinone, dyes, and their conjugated counterparts; (2) determination of kinetic parameters (Michaelis constant (K_m), theoretical maximum velocity

(V_{max}), catalytic constant (k_{cat}), enzyme efficiency (k_{cat}/K_m) of the substrates towards NQO1 and the way solvent affects such parameters during assay conditions; and (3) utilization of a latent fluorophore for in vivo NQO1 analysis (widefield imaging, confocal single-/two-photon microscopy, flow cytometry) and determining the fate of the released fluorophore. Integration of these studies led to the development of two different latent fluorophores that are readily activated by NQO1. Of these two fluorogenic cancer sensors, one was found to possess a highly novel quenching mechanism between the quinone and the dye.

CHAPTER 1

INTRODUCTION

1.1 Research Goals and Aims

The goal of this research is the design and characterization of latent fluorophores used as sensors for the detection of NAD(P)H:quinone oxidoreductase-1 (NQO1) in tumor cells.[1-4] In particular, the design of the fluorogenic sensor is such that it will need to contain a cleavable substrate that is selectively activated by NQO1 and a fluorophore that will have its fluorescence quenched when conjugated with said substrate. Both the quenched dye and the free dye will be tested to ensure high stability while in a biological milieu. Both the capped dye and free dye had their optical properties examined to ensure a high probability of success in their application as an "off-on" type sensor. These fluorogenic sensors will be tested in vitro with cancer cell lines known to contain NQO1 and cells known to be devoid of the enzyme.

Sir George Gabriel Stokes first observed fluorescence in the early 19th century and coined the term "fluorescence" after noticing a blue light emitting from a solution of quinine sulfate. Since then, fluorescent dyes have made an immense impact in biological sciences, and more recently in the field of biomedical imaging.[5-6] Biomedical imaging has become a crux in the field of screening and disease treatment of cancer patients.[7] Statistics such as 1,638,910 new cancer cases and 577,190 deaths projected in the year 2012 provide motivation for the need of better detection and treatment of such a widespread disease.[8] Biomedical imaging has been at the heart of the cancer treatment by assisting with prediction, screening, biopsy guidance for detection, staging, prognosis, therapy planning, therapy guidance, therapy response, recurrence, and palliation.[9] Techniques involved in cancer detection and diagnosis are: magnetic resonance imaging (MRI), positron emission tomography (PET), X-ray, radiography, ultrasound, and nuclear medicine. But, these techniques lack specificity, sensitivity, and may yield radioactive

risks.[9] With a better understanding of the processes in the human body and the anatomy/biochemistry of tumors, better optical imaging agents and techniques have emerged. This type of imaging has been promising because it is non-invasive, potentially provides real-time information, and can provide high spatial resolution of cancerous tissues.[10]

Though the research into fluorophores relevant to cancer diagnosis/treatment has been expanding rapidly, there are currently only three clinically-approved exogenous fluorescent tracers.[11] Fluorescent sensors can be broken down into two categories: always on and off-on. These can be classified into two subcategories of organic and inorganic fluorophores.[10] Always-on fluorophores are typically conjugated to larger scaffolds such as macromolecules, peptide sequences, and antibodies, and they have been utilized for tumor imaging through a receptor-mediated process or accumulation from enhanced permeability and retention (EPR) within tumors.[12] The drawback to this process is long accumulation time within the body, leading to poor contrast when imaging.[13] Off-on type activatable sensors have been shown to be superior to always-on fluorophores due to the low background signal produced in the quenched state and the large fluorescence enhancement (FE) after activation and subsequent release of the fluorophore.[14] Even with the fact that NQO1 is a highly upregulated enzyme in cancer cells that selectively reduces quinoid compounds via a 2-electron reduction, no dyes have been reported for use in real-time in vitro sensors of this enzyme.[15]

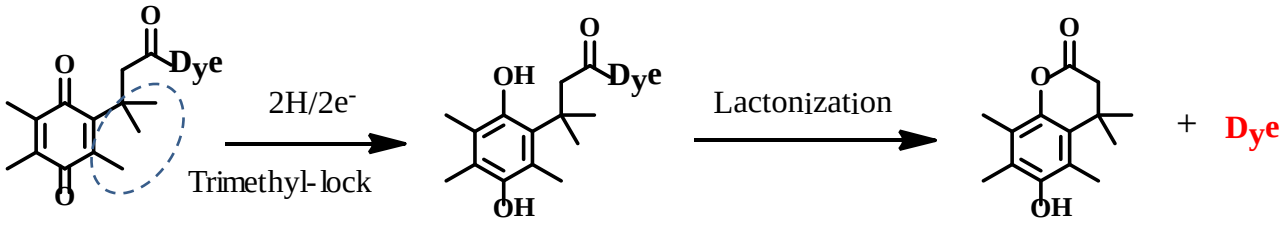

Scheme 1.1. Illustration of the NQO1-activatable substrate and dye release mechanism.

The first aim of this research is the development of two NQO1-activatable fluorescent sensors to be used as intracellular probes. The base of these dyes will be the activatable quinone substrate that is selectively activated by NQO1. The quinone unit will contain a trimethyl-lock (Q_3) motif, which has been shown to substantially increase the rate of cyclization and subsequently should lead to a rapid dye release.[16] The first fluorophore synthesized will contain a rhodamine-morpholino urea dye conjugated to Q_3. This rhodamine-based dye has been previously shown to have a high intensity in the mono-conjugated form and be nearly completely quenched when di-conjugated.[17-19] The second dye will pair a naphthalimide dye with the Q_3 moiety via a short spacer. This "fluorophore-spacer-receptor" dye has its fluorescence quenched as a result of a novel use of photoinduced electron transfer (PeT).[20] After each dye was synthesized, they were tested to ensure rapid release of the attached dye subsequent to quinone reduction. To this end, the quinone units were chemically reduced with a strong reducing agent (sodium dithionite, $Na_2S_2O_4$), and the fluorescence intensity was followed over time. To confirm the quinone activating group was highly stable and could withstand the known reducing intracellular environment, the Q_3 capped rhodamine dye was investigated while under physiological conditions in the presence of biological reductants. This fluorophore was incubated with NADH ($E_{1/2}$ = -0.31 V)[21], ascorbic acid ($E_{1/2}$ = 0.051 vs. SHE)[22], glutathione ($E_{1/2}$ = -0.22 V)[23], and dithiothreitol ($E_{1/2}$ = -0.33 V)[24], and the fluorescence signal was observed in order to determine if release was taking place. To confirm the capability of the Q_3-capped naphthalimide dye to be quenched via PeT, the reduction/oxidation potentials of the quinone unit and the naphthalimide dye were determined using cyclic voltammetry (CV), and they were used to calculate the energy change (ΔG)[25] from the Rehm-Weller equation.

The second aim of this work is characterization of the optical properties of the fluorophores and determination of the effectiveness at which NQO1 activated the sensors by performing enzyme kinetics. To determine the FE from pre- and post-activation of the dyes, a quantum yield for each dye was determined. To determine the quantum yield for the capped and free dyes, the fluorescence signal was compared to a compound with a well-known quantum yield; for the rhodamine-based dyes, fluorescein was used, while quinine sulfate was compared to the naphthalimide dyes.[17, 26] Enzyme assays and the kinetic parameters they yield provide information for how effective the sensors are as substrates for NQO1 and can be related to other published compounds. By assaying the capped sensors with human NQO1 (hNQO1), kinetic parameters of K_m (Michaelis constant, substrate affinity), V_{max} (maximum theoretical turnover rate), k_{cat} (catalytic constant), and k_{cat}/K_m (enzyme efficiency) were produced.

The final aim of this research is determination of the applicability of the fluorophores as in vivo sensors of hNQO1. To complete this objective, multiple cell lines of different origins that are known to contain or be devoid of hNQO1, were purchased and incubated with the dyes and subsequently analyzed using: fluorescence plate reader, flow cytometry, and fluorescence imaging using a widefield microscope and single-/two-photon microscope. From these analyses, it is possible to determine if each sensor was selectively activated in the cell lines known to contain hNQO1 or remain inactivate in the cell lines devoid of the enzyme. If the sensor was found to be activated, its fate was determined post-activation using colocalization experiments (confocal microscopy).

From the information presented in this work, I have demonstrated a novel use of NQO1 as a rapid in vivo sensor in tumor cells. The results presented in this work lay the groundwork for the next steps in NQO1 sensor utilization, possibly leading to ex vivo and in vivo analysis of

tumors. Illustrated is a first-generation sensor which has great potential to lead to further advancements in creating fluorophores for the detection of NQO1. Also, there is potential to create a better understanding of the role NQO1 plays in tumors and possibly in cancer analysis and treatment.

1.2 Biomedical Optical Imaging

Biomedical optical imaging has rapidly emerged as a field with the potential to impact all areas of cancer research and personal oncology, from the molecular level to a living system, and from the bench to the bedside. In the clinic, biomedical imaging plays a major role in all facets of cancer management by non-invasively detecting and visualizing biological processes within a living system.[27] These major involvements include: prediction,[28] screening,[29-30] biopsy guidance for detection,[31] staging,[32-34] prognosis,[35] therapy planning,[36-37] therapy guidance,[38] therapy response,[39-42] recurrence,[43] and palliation.[9] On the research (preclinical) side, imaging assists in the fundamental understanding of molecular pathways involved in carcinogenesis, aids in drug discovery, and provides a better understanding of the morphologic and biochemical processes within individual cells, tumors, and whole organs.[27] The instrumentation predominantly used in cancer management include: magnetic resonance imaging (MRI), positron emission tomography (PET), computerized tomography (CT), X-ray, radiography, and ultrasound. Though these methodologies are common place in the clinic, they lack specificity, sensitivity (Figure 1.1), and may yield radiation.[10] The only clinically used techniques with sufficient sensitivity for molecular imaging are nuclear imaging techniques. However, nuclear imaging techniques have severe drawbacks, such as: a cyclotron is used to develop radiotracers, radioactivity handling, lack of shelf life for the radiotracers, and the need to balance the half-life of the radiotracer with the pharmacokinetics of the targeting agent.[44] Also, the majority of the biomedical imaging

techniques are impractical in the research lab due to cost and spatial resolution when compared to optical imaging techniques.[27]

Figure 1.1 Relative sensitivity of imaging technologies; from Fass (2008).

Optical imaging in both clinical and preclinical applications has been expanding due to the low cost, real-time analysis, non-invasiveness, ability to image at microscopic and macroscopic level (subcellular to whole animal body to human organ), specificity of probes, and sensitivity. Optical imaging in cancer diagnostics originally observed changes in the contrast of endogenous sources. Due to neoplastic tissues forming from cancer, biochemical and morphological alterations could be observed by changes in absorbance, light scattering, fluorescence, and polarization properties.[27] One such characteristic change is a decrease in the fluorescence in the green region from stromal collagen cross-links as they are broken down from carcinogenesis.[45] Similarly, an increase in fluorescence from nicotinamide adenine dinucleotide (NADH) and flavin adenine dinucleotide (FAD) have been attributed to an increase in metabolic activity.[46] One of the benefits of imaging endogenous sources is there is no need for administering exogenous agents that require approval for clinical use. However, these sources of

optical contrast are rarely limited to only carcinogenesis.[27] Currently, the most common approach to increasing contrast and sensitivity in optical imaging is the use of exogenously introduced fluorophores. These can be used as individual species or conjugated to larger scaffolds; examples are shown in Figure 1.2.

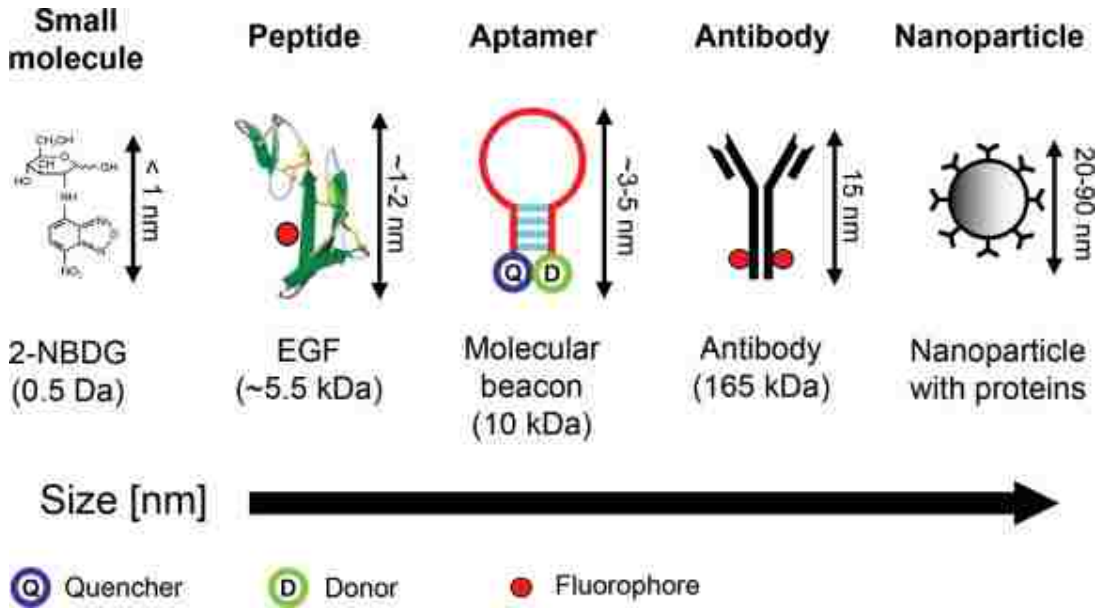

Figure 1.2. Five classes of molecularly-specific optical contrast agents. From left to right in order of increasing size: small molecules including glucose and peptides can be functionalized with fluorescent dyes. Aptamers can be designed to form activatable ‘‘smart probes,’’ with fluorescence quenched until target binding. Antibody probes are generally functionalized with fluorescent dyes in the Fc domain. Targeting molecules can be coupled to nanoparticle-based optical reporters, including gold nanoparticles and quantum dots; from Pierce et al. (2008).

Each of the fluorophore categories in Figure 1.2 can be utilized in a variety of techniques, from preferential accumulation in tumor sites[47-48] to specifically targeting of endogenous ligands[49]. Other such non-specific fluorophores have been used to increase contrast in optical imaging,[50-52] while new off-on sensors are being studied to switch from a nonfluorescent state to a fluorescent state in the presence of a specific biochemical event.[12] The existence of all imaging probes and fluorophore-scaffolds is to provide high sensitivity and specific interactions with the biological targets, though the path to that goal may vary. Optimal imaging fluorophores must

possess large Stokes shift for minimum interference between absorption and emission, high molar extinction coefficient, high quantum yield, photo-stability, biological stability, and water solubility with minimal aggregation.[10] Depending on the imaging application, specific wavelengths may prove to be more valuable to provide the essential signal-to-background ratio (SBR). With in vitro and ex vivo optical imaging, a wider spectrum of wavelengths may be used due to less endogenous interference. With in vivo and clinical applications, it is of great value to develop probes in the near-infrared (NIR) region (650 to 900 nm). This is due to the scattering and absorbance of light in tissue components, oxy-/deoxyhemoglobin, and water, Figure 1.3.[53]

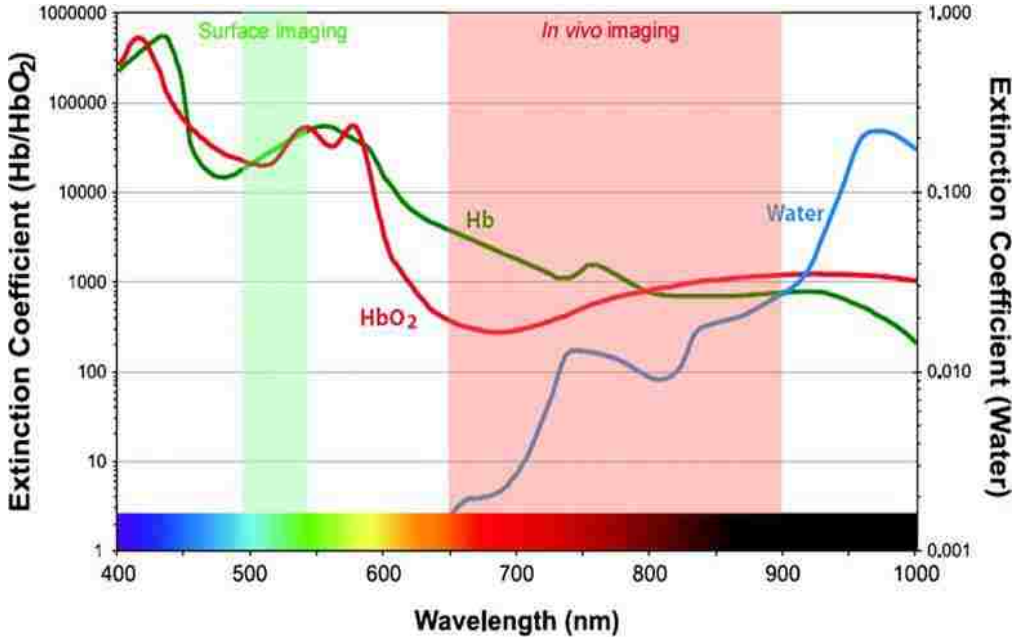

Figure 1.3. Extinction coefficient value of water, oxy- and deoxyhemoglobin are plotted ranging from visible to near-infrared wavelength; from Kobayashi et al. (2010).[53]

1.2.1 Instrumentation

The instrumentation used for optical imaging can vary greatly, depending on the application and biochemical or physiological process being observed. Benchtop (research lab)-based imaging can require subcellular resolution to obtain information on intra-/extracellular biochemical and biophysical processes,[54] and up to macroscopic resolution to observe

physiological events in whole animals.[55] Optical imaging in the clinical aspect ranges from cellular resolution for surgical guidance in resecting tumors[56] to whole organ imaging for cancer diagnosis.[57-58] Outside of image-guided invasive biopsy, current biomedical imaging technologies are not performed at the same time as the treatment. The use of fluorescence-based optical modalities offers the opportunity for both real-time in situ diagnosis and treatment at the same time as surgical procedures.[44] Detailed below is a non-exhaustive list of common techniques, descriptions, and current work utilizing preclinical and clinical modalities for the optical imaging of exogenously introduced fluorophores.

Confocal microscopy has become a common imaging technology in the laboratory due to its high contrast and high resolution (between 0.21 to 0.58 μm spatially and 0.44 to 3.44 μm axially)[59] of thin samples, such as cells and tissue. The primary characteristic of the confocal microscope is the use of continuous wave lasers to excite samples and use a pinhole aperture to remove out-of-focus light from non-observed emitting samples. Images are built point-by-point as the imaging laser scans a sample, leading to the ability to produce high quality 2D and 3D images.[27] This type of imaging is ideal for preclinical in vitro analysis, because it is non-destructive and has the ability to image cellular samples in their physiological state. In vitro imaging is also a more controlled environment than in vivo analysis, providing a better determination of the future efficacy of the compound under study. With confocal microscopy, protein interaction can be observed[60] and the fate of exogenous agents can be determined after compartmentalization and intracellular trafficking by using multiple contrast agents in a single sample.[61] By obtaining a better understanding of the intra/extracellular biochemical components and processes of cancerous cells, it is possible to gain better insight into the processes of the formation of neoplastic tissue during carcinogenesis. The intracellular fate of drugs, drug

delivery systems, and imaging agents yields crucial information in providing insight into future efficacy, such as in vivo analysis, and aids in future development of new drugs and imaging systems. Confocal imaging is also a rapid analysis technique when evaluating active targeting fluorogenic probes against specific cellular epitopes.[62] With the constant miniaturization of imaging technology, new methodologies are being developed from older instrumentation. Work has been done to create a portable endoscopic confocal imaging device that utilizes multiple flexible/narrow-diameter fiber optic cables, miniature lenses, and compact scanning mechanisms, Figure 1.4.[63-64] This imaging platform has been able to achieve a lateral resolution of 2.0 μm and an axial resolution of 25 μm;[65] it has also been used in clinical studies to image the gastrointestinal tract,[64] colon,[66] and ovaries.[65]

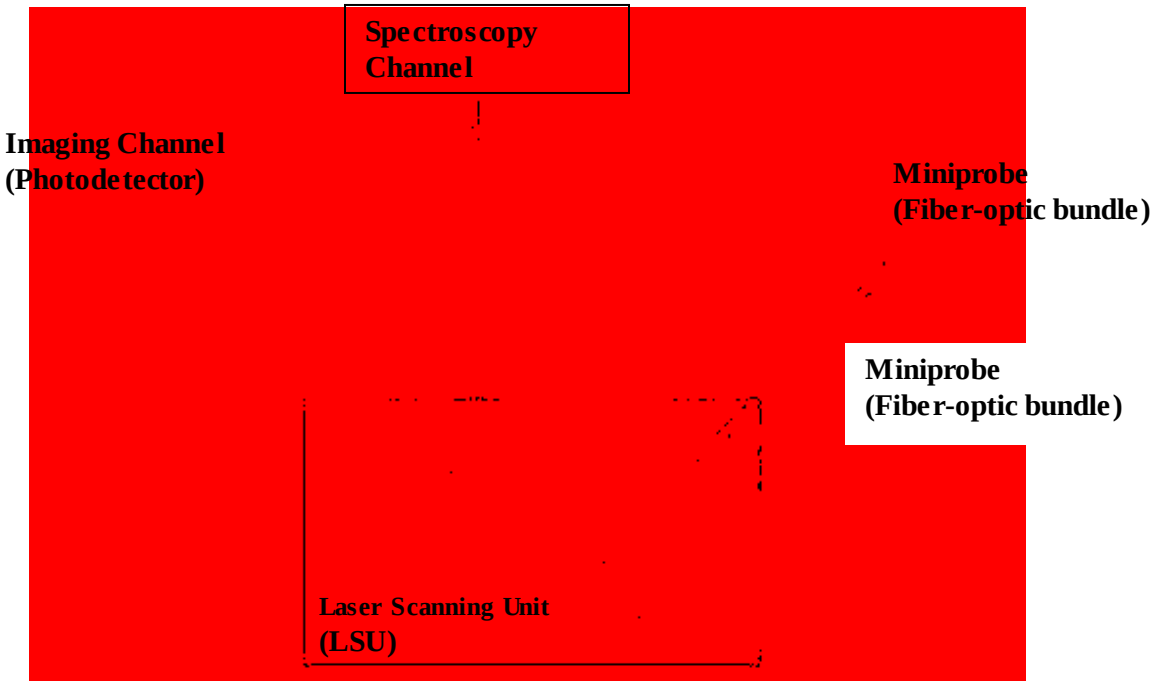

Figure 1.4. Schematic diagram of the prototype F400/S (Mauna Kea Technologies), a dual fibered confocal imaging and spectroscopic platform; from Thiberville (2007).[64]

As a result of the need for deeper tissue penetration and the existence of the highly successful confocal microscope, multiphoton microscopy was developed. This technique

exploits the high-resolution capabilities of the confocal microscope, but uses a pulsed laser with longer wavelength excitation. This longer wavelength generates less Rayleigh scattering and allows for deeper sample penetration for optical imaging. In this method, fluorophores are excited by near-simultaneous absorption of 2 (or more) photons at half the energy of the single-photon transition, Figure 1.5. This is possible by rapidly pulsing (~100 fs pulse width, 80 MHz pulse frequency) the sample with the laser beam.[27] Whereas continuous wave lasers in confocal microscopy excite all fluorophores in the path of the laser beam, pulsed lasers only generate sufficiently excited molecules (to generate fluorescence) at the focal point, Figure 1.5.[67] This modality has not only provided superb in vitro analysis of carcinogenesis.[27]

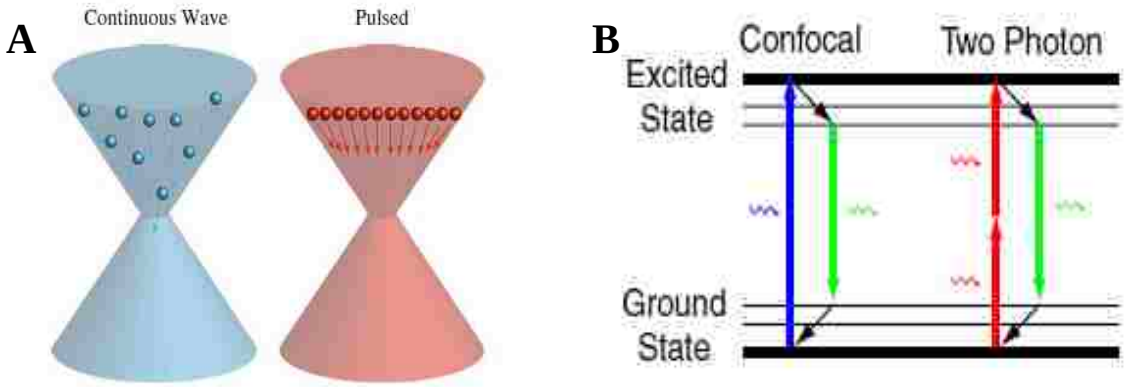

Figure 1.5. Continuous-wave vs. pulsed laser: a continuous-wave laser can be thought to consist of a steady stream of photons. A pulsed laser beam can be thought to be composed of a stream of evenly spaced, tightly grouped photon packets (**A**). Jablonski diagrams for confocal (one-photon) and two-photon fluorescence interactions (**B**); from Christensen and Nedergaard (2011).[67]

Brown et al. have shown that multiphoton microscopy used for in vivo imaging of tumor models in live mice can provide insight into tumor physiology by measuring gene expression, angiogenesis, blood-flow velocities, leukocyte/endothelial interactions, and permeability of tumors.[68] Runnels et al. were able to fluorescently label vascular endothelial cell adhesion molecules so as to obtain spatial and temporal relationships and build 3D images of the

vasculature, while also following specific populations of cells.[69] This use of live animals for multiphoton imaging leads to the possibility of studying inflammation, angiogenesis, and atherogenesis.[69] While multiphoton microscopy has become vital in the imaging of in vitro and in vivo settings and has provided unprecedented insights into the process of carcinogenesis, the ability to miniaturize the methodology has been hampered due to the translation of the pulse laser to utilize fiber-optic cables.[27] Though the miniaturization has been slower compared to confocal microscopy, there have been recent reports of imaging endoscope systems utilizing multiphoton microscopy.[70-72]

Though the goal for optical imaging modalities remains to be real-time analysis of the area under investigation, many real-time optical imaging instruments for clinical use have emerged since the first clinical applications of fluorescently guided surgery using indocyanine green (ICG) to aid in the resection of the sentinel lymph node.[56, 73-77] The basic setup for each imaging system includes light emitting diodes (LEDs) or lasers that emit a narrow bandwidth, band-pass filters to limit possible detection of the excitation source, and a charge-coupled device (CCD) camera for the collection of the emission signal.[11] One of the first clinically used fluorescence-guided optical imagers was the fluorescence-assisted resection and exploration (FLARE) system, which was designed and used by the Frangioni research group.[75] This widefield imaging device is capable of exciting fluorophores at 656 — 678 nm and 745 — 779 nm, and it contains a CCD camera with band-pass filters at 689 to 725 nm and 800 to 848 nm.[11] It possesses a field of view (FOV) between 3.7 to 195 cm^2, and uses more than one imaging camera to allow for image overlay between visual and fluorescence images. Since the inception of the FLARE imaging device, Frangioni has developed a second-generation machine called the mini-FLARE, Figure 1.6.[78] This imaging device contains the same imaging parameters as

FLARE, with updated technology and a shorter working distance: 45 cm for flare and 10 to 32 cm for mini-FLARE.[11]

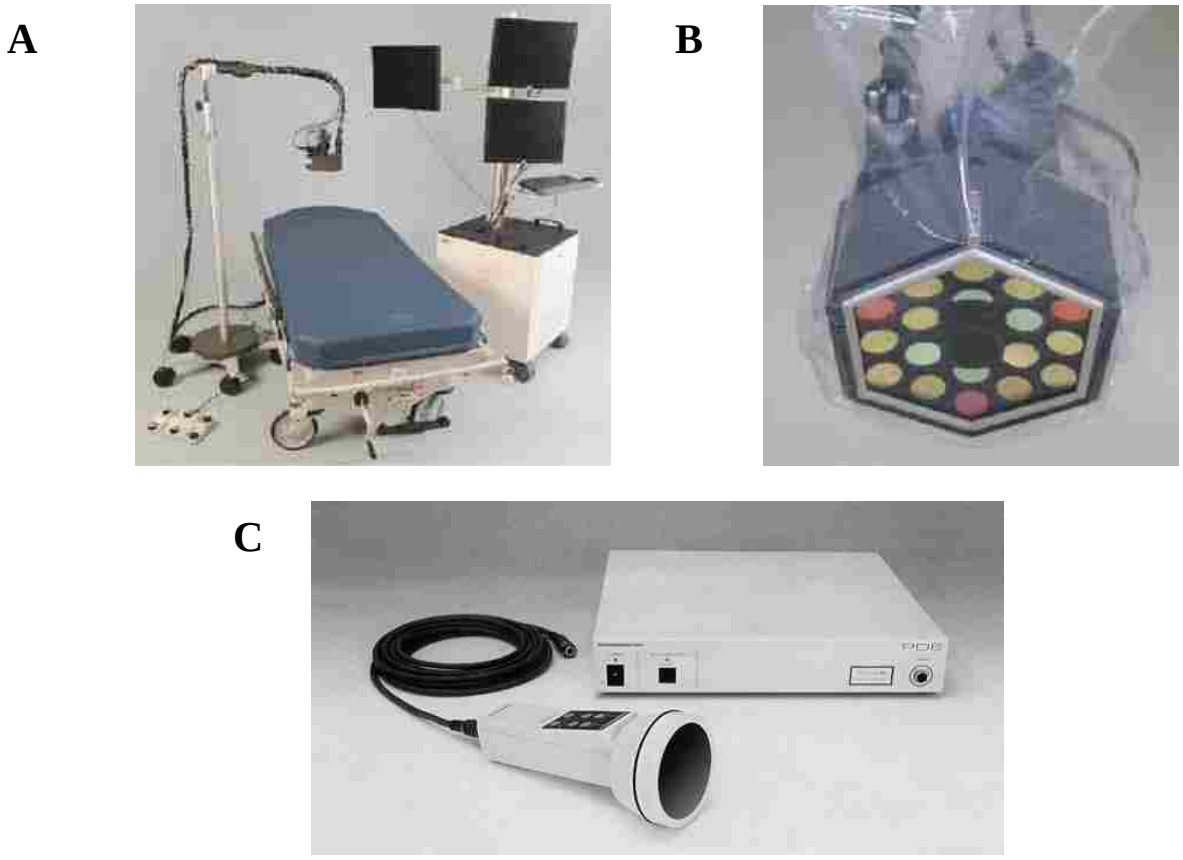

Figure 1.6. The Mini-FLARE portable near-infrared fluorescence imaging system, composed of electronics/monitor cart and counterweighted imaging system pole (**A**). Sterile drape/shield attached to the imaging head (**B**). The portable/hand-held Photodynamic Eye (**C**); from Mieog et al. (2011) and Tagaya et al. (2008).[74, 78]

As technology progresses, there is a desire to utilize the ever decreasing size of electronics and optics in newer imaging systems. The Photodynamic Eye (PDE, Photonics, Hamamatsu, Japan) is a commercially-available system that is a more portable optical imaging system compared to the (mini-)Flare system, Figure 1.6. With the reduction in size, it has fewer capabilities than other systems. The PDE only provides black and white images of the area of interest, and only excites at 760 nm with 36 LEDs.[79] Another advantage of this reduction in size

is the ability to produce laparoscopic imaging systems for minimally invasive surgery. To date, there are only four clinically-approved systems: the D-light[80] and D-light NIR[81] systems, Olympus narrow-band imaging (NIB),[82] and an integrated system[52] for the da Vinci Si Surgical robot.[11]

1.2.2 Nanomaterial-Based Sensors

Of all the in vivo imaging probe types, nanomaterials have certainly been one of the more intriguing. The most beneficial aspects of nanomaterial-based probes are their photostability, brightness, narrow excitation/emission bands, utilization of the EPR effect to allow for their passive accumulation in tumor sites, and ability to functionalize the exteriors as to allow for their association with different functionalities.[83] However, the major drawbacks in the use of these sensors in the clinic are concerns about their toxicity,[84-85] poor biodistribution due to uptake by the reticuloendothelial system (RES), only having a 2:1 to 4:1 signal-to-background ratio with passive uptake probes, and the inability to passively accumulate intracellularly (though this can be achieved through mediated endocytosis) due to the size of the particles. The two main types of nanoprobes are organic-based nanoparticles (polymer-core nanoparticle, polymer micelles, polymersomes, liposomes, lipid micelles, and lipid-core nanoparticles) and inorganic nanocrystals (semi-conducting quantum dots (QD) and silica nanoparticles), Figure 1.7.[83] Due to their intense fluorescent signal, ability to shift excitation/emission wavelengths by adjusting particle size, and photostability, QDs have emerged as useful tools in the optical imaging field and have led to a plethora of commercially-available dyes. The most common QDs are ZnS, CdSe, and CdTe, and typically have their surface coated with organic material (i.e. poly(ethylene glycol) (PEG)) to prolong blood lifetime between 48 and 72 hours and prevent protein adsorption.[83, 86] The size of the nanoparticles has been found to have a profound effect

on the ability to accumulate in tumor sites in in vivo experiments. Nanoparticles in the range of 111 to 141 nm were found to accumulate efficiently, while particles larger than 166 nm were rapidly removed by the RES.[87]

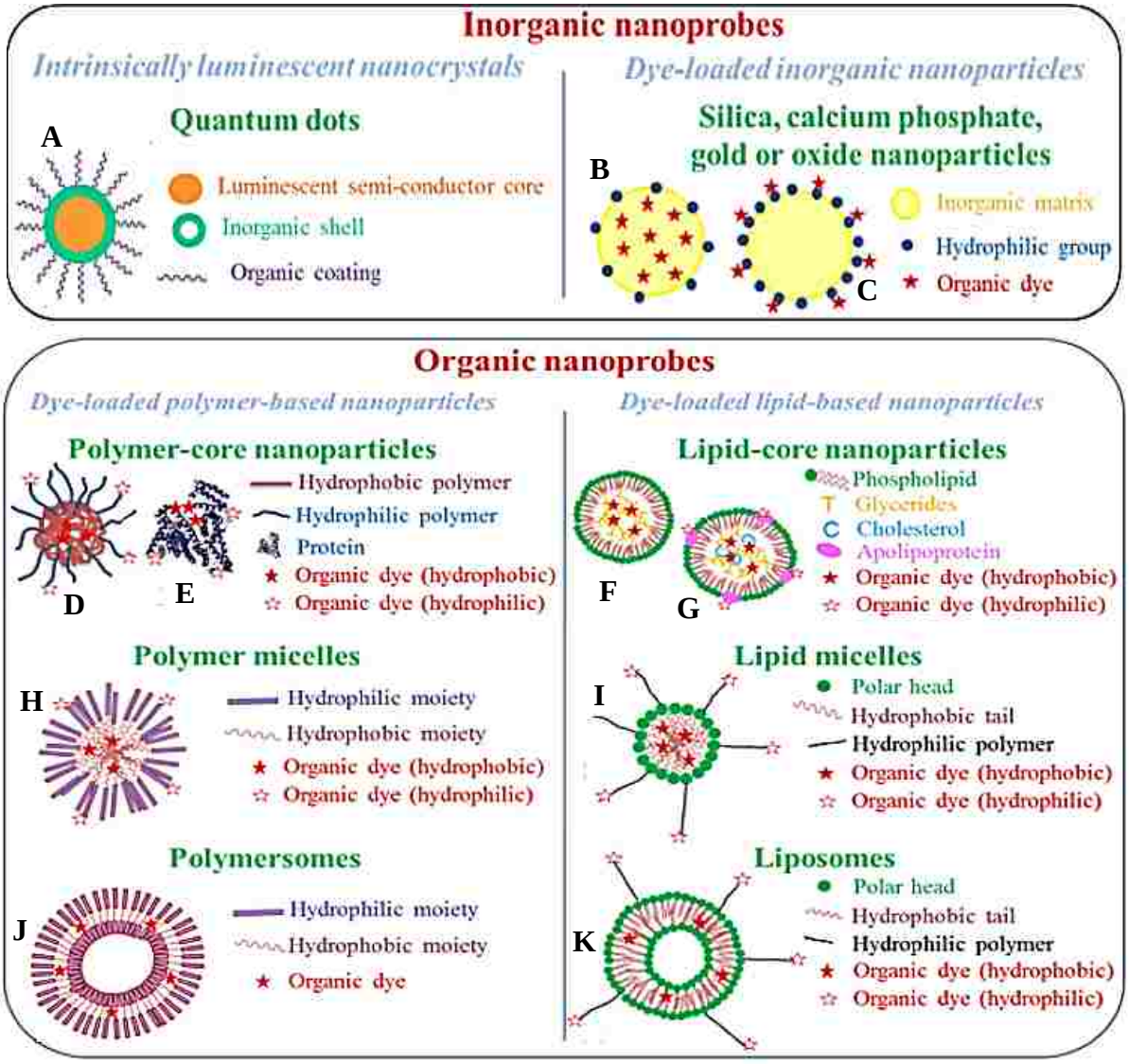

Figure 1.7. Inorganic nanoprobes are quantum dots (**A**) or dye-loaded silica, calcium phosphate, gold or oxide nanoparticles, for which the organic dye can be included in the inorganic matrix (**B**), or grafted on the nanoparticle surface (**C**). Organic nanoprobes can be divided in two main families: dye-loaded polymer-based and dye-loaded lipid-based nanoparticles. In each family, different architectures can be found: polymer- or lipid- core particles (polymer nanospheres (**D**), proteins (**E**), lipid nanoparticles (**F**), lipoproteins (**G**)), self-assembled constructions (polymer (**H**) or lipid (**I**) micelles), nanocapsules (polymersomes (**J**) or liposomes (**K**)). The fluorescent organic dye can be either included in the hydrophobic core or shell of the structure, or grafted on the nanoparticle surface (hydrophilic organic dye). From Merian et al (2012).[83]

One of the first in vivo imaging experiments was performed by Gao et al., where they successfully synthesized a tri-block polymer-coated CdSe QD with prostate-specific membrane antigens (PSMA) attached. This attachment of PSMA to the outer shell of the nanoparticle allowed the QDs to effectively adhere to prostate tumor cells in mice (from a xenograft), allowing for sensitive and specific in vivo imaging.[86] Cai et al. similarly produced a polymer-coated QD using arginine-glycine-aspartic acid as the targeting ligand, which binds to the $\alpha_v\beta_3$ integrin that is known to play a role in angiogenesis and metastasis.[88] This imaging probe produced maximum intensity after 6 hours post-injection, with good contrast in a mouse model.

Organic-based nanocarriers have been studied extensively over the last several decades as drug delivery systems, with several clinically-approved applications.[83, 89-90] Because of this, these nanocarrier systems have been studied extensively, and their in vivo fate and biodistribution have been determined. Similar to QDs, organic-based nanocarriers are typically conjugated to PEG to minimize removal by the RES and to extend blood circulation time. Tumor targeting ligands—such as antibodies, peptides, and saccharides—have also been attached so as to increase targeting efficacy.[83] The use of organic-based nanocarriers has only recently been studied as a vehicle for in vivo fluorescent probes. One of the main systems studied is the dye-loaded lipid based liposome, due to the vast amount of previous work using liposomes as drug delivery systems. Here, liposomes encapsulate fluorophores and will accumulate in tumor sites in vivo due to the EPR effect. Sandanaraj et al. demonstrated the use of an egg phosphaditylcholine, cholesterol, and 1,2-disteroyl-*sn*-glycero-3-phosphoethanolamine-*N*-methoxy-(poly(ethylene glycol)2000)-based liposome that contains cyanine 5.5 (Cy5.5) and indocyanine green (ICG) as an in vivo probe for tumors and arthritis disease models in mice.[91] This system was observed to be highly stable for up to 70 days, and it

was found to passively accumulate in tumor sites due to the EPR effect. Portnoy et al. synthesized liposomes from phospholipon 50 and noncovalently-attached ICG, and monoclonal antibodies for epidermal growth factor receptor (EGFR) to them.[92] EGFR is an extracellular ligand that has been found to be overexpressed in carcinomas. This dye system was optically imaged in vitro and was found to selectively bind to membrane bound receptors, which led to endocytosis.

1.2.3 Antibody-Based Sensors

Another option to increase contrast for intraoperative tumor analysis (in vivo and in vitro imaging) is the direct conjugation of always-on fluorophores to antibodies with known associations pertaining to specific cell types. This process is commonly used for immunohistochemical labeling of fixed cells and cell assays. Some of the drawbacks to this method are the possibility of loss of antibody recognition after dye conjugation, loss of fluorescence signal after conjugation, limited availability of antibodies, localization of epitopes, and the need to maintain proper controlled environmental conditions that prevent antibody degradation.[10, 27] As with always-on nanoprobes, antibody-based imaging constructs require sufficient clearance time in vivo to obtain an optimal SBR when imaging. Soukos et al. produced a monoclonal antibody against EGFR and subsequently conjugated it with the NIR Cy5.5 dye to test for immunophotodiagnostic properties for oral precancer and as a surrogate marker for disease progression.[93] For this work, they used this probe to image a hamster cheek pouch carcinogenic model in vivo. While they were successful in producing a probe that specifically labeled the tumor site and provided high contrast, the amount of time for the maximum contrast was rather high (between 4 to 8 days). Rosenthal et al. similarly used an EGFR-Cy5.5 probe to image in vivo head and neck squamous cell carcinomas (HNSCC) in

xenografts in mice.[94] They were also able to localize tumor sites using fluorescence imaging at 24, 48, and 72 hours after injection of the probe. Terwisscha et al. labeled antibodies for vascular endothelial growth factor (VEGF) and human epidermal growth factor (HER) 2 with the NIR dye IRDye 800CW for a proof of concept in intraoperative tumor detection in xenograft-bearing mice.[95] While they were able to obtain a submillimeter differentiation between tumor tissue and healthy tissue, the SBR was only 1.93 — 2.92 after 6 days of injection.

1.2.4 Aptamer-Based Sensors

One optical imaging modality that is still in its infancy is that based on aptamers as molecular fluorescent beacons. Aptamers are single-stranded ribonucleic acids or deoxyribonucleic acids (RNA or DNA) that adopt unique conformations due to intermolecular forces.[13] Thanks to their extra small size, polyanionic nature, and diminished immunogenicity, aptamers can provide rapid tissue penetration and uptake, high affinity for specific epitopes, shorter residence in blood and non-target organs, and higher target accumulation. Compared to antibodies, they are economical, synthetically reproducible, and can easily be conjugated with signaling molecules without altering their binding affinity or specificity.[96] Because of these properties, aptamers are ideal targets for optical diagnostics and in vivo imaging. Shi et al. produced an always-on aptamer labeled with cyanine 5 (Cy5), denoted as TD05; that were shown to have a strong binding affinity and high specificity for Ramos cells.[96] This Cy5-TD05 aptamer system was found to provide high contrast in vivo in the B-cell lymphoma cell line (Ramos cells) xenografts in mice. After 4 to 5 hours, the unbound, always-on Cy5-TD05 was removed via the blood stream, leaving behind fluorescent probe-enriched tumors. In comparison to a negative control probe that produced a signal-to-background ratio (SBR) of 9.77 in the Ramos xenografts, a SBR of 115.5 was obtained with Cy5-TD05. The same research group

produced an activatable aptamer probe (AAP) for in vivo tumor detection.[13] To alleviate the need for long diagnosis time due to high background signal from imaging with always-on fluorophores, this design utilized an off-on fluorescence system in which the aptamer was essentially nonfluorescent in the unbound state. After binding to a specific marker, the aptamer undergoes conformational change revealing probe fluorescence. This "sgc8" aptamer consisted of three fragments: the cancer-targeting aptamer sequence (A-strand), unreactive poly-T linker (T-strand), and a short DNA recognition sequence (C-strand) complementary to part of the A-strand; this resulted in an aptamer stem-loop hairpin structure that opens up upon specifically binding to the cell membrane protein kinase-7 (PTK7), Figure 1.8.[97]

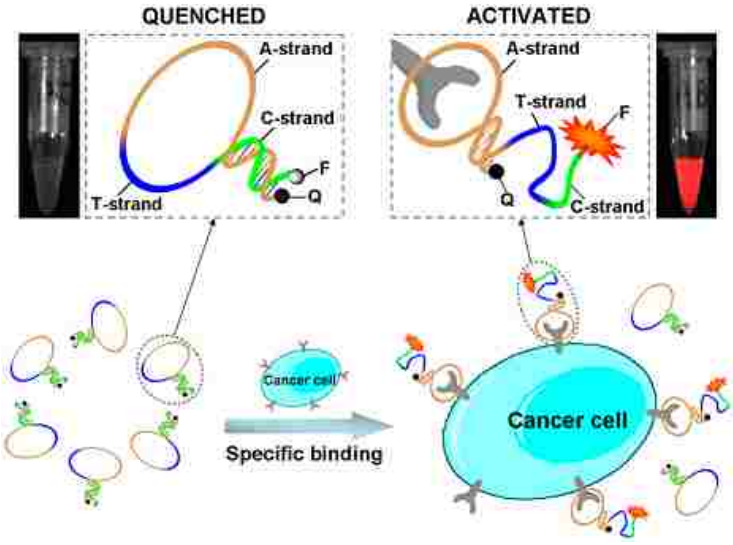

Figure 1.8. Schematic representation of the novel strategy for in vivo cancer imaging using an activatable aptamer probe (AAP) based on cell membrane protein-triggered conformation alteration. The AAP consists of three fragments: a cancer-targeted aptamer sequence (A-strand), a poly-T linker (T-strand), and a short DNA sequence (C-strand) complementary to a part of the A-strand, with a fluorophore and a quencher attached at either terminus. In the absence of a target, the AAP adopts a hairpin structure, resulting in quenched fluorescence. When the probe is bound to membrane receptors of the target cancer cell, its conformation is altered, thus resulting in an activated fluorescence signal; from Shi et al. (2011).[13]

Attached to one terminus is the fluorophore fluorescein-5(6)-carbonyl (FAM) and the other terminus contains the quencher BHQ1, producing a Förster resonance energy transfer

(FRET) quenching mechanism prior to activation binding by PTK7. Though the tumors could be easily observed via fluorescence optical imaging in vivo using xenografts in mice, fluorescence signal was prevalent throughout the entire body after 15 minutes. This leads to one of the downsides of aptamer imaging, which is the instability while circulating in the blood stream. Only after sufficient time has passed to remove the non-specifically activated aptamer probe, can it be possible to obtain high enough contrast for tumor detection. Nonetheless, their studies indicated substantial tumor fluorescence even 120 minutes after injection with minimal signal appearing after 180 minutes.

1.2.5 Peptide Motifs

Another route in the miniaturization of ligands for target-mediated imaging is the use of short peptide sequences labeled with fluorophores. The goal in this model is development of short sequences (10 — 15 amino acids) without losing the specific target affinity of their naturally derived counterparts (antibodies).[27] The positives from this miniaturization process and increased biodistribution and bioavailability, and decreased cost due to fewer steps needed to synthesize the short sequences. However, use of such few amino acids yields a lower number of fluorophores per target recognition moiety, leading to a lower fluorescence signal. As with antibodies, aptamers, and nanocarriers, the epitopes that have been most commonly studied for peptide-mediated imaging are membrane bound and found to be overexpressed in tumor tissues. One of the more commonly studied peptide sequences for in vivo and in vitro analysis is the cyclic tripeptide arginine-glycine-aspartic acid, c(RGD), having been shown to have a high specificity towards the transmembrane glycoprotein $\alpha_v\beta_3$.[62, 98-102] One of the methods used by Jin et al. to improve the contrast capabilites with the c(RGD) peptide sequence is a single species containing multiple copies of the same sequence.[100] Here, they were able to tether four c(RGD)

units to a single Cy5-labeled cyclic decapeptide platform called a regioselectively addressable functionalized template (RAFT), Figure 1.9A. Using cell lines transfected so as to be $\alpha_v\beta_3$-positive or $\alpha_v\beta_3$-negative, they were able to obtain a higher contrast between the cell lines with the RAFT-c(RGD)$_4$ Cy5-labeled unit compared to the single Cy5-labeled c(RGD) sequence. From here, they used the labeling motif in a xenograft model containing both the negative and positive cell lines, where RAFT-c(RGD)$_4$ afforded a SBR of 15.9 at four hours post-injection. After the same time period, the c(RGD) yielded a SBR of 1.4.

Another peptide methodology for optical imaging involves the construct of an activatable cell penetrating peptide (ACPP).[103-105] Cell penetrating peptides (CPPs) were first discovered from the HIV-1 Tat peptide,[106] and it has since been discovered that multicationic oligomers[107] are equally or more effective than Tat. These CPPs are essentially membrane translocation units and can be directly conjugated to materials, which can then enter the cell through a non-receptor mediated process. Though this process is still mostly ambiguous, it is believed the peptides adsorb to the cell surface through electrostatic interactions and enters the cell via endocytosis. Jiang et al. synthesized an ACPP by attaching a CPP to a cleavable linker that was enzymatically removable, Figure 1.9B.[104] This linker neutralized the CPP, preventing it from being taken up intracellularly. The enzyme which they designed this linker to be activated by was a matrix metalloproteinase (MMP), specifically MMP-2 and MMP-9, because they have been the most characterized. MMPs are extracellular proteases that are responsible for invasion, metastasis, and the degradation of the extracellular matrix (ECM).[108-110] To evaluate the ability of the ACPP to label tumors in vivo, they created a xenograft model in mice with a cell line known to contain MMPs and measured the fluorescence intensity at the tumor site from Cy5-labeled ACPPs. After 50 minutes post-injection of the probe, the ACPPs were found to be mildly effective in

labeling the tumors. The contrast index was calculated to be 2.1, while the contrast index for two negative control peptide sequences was 1.3 and 1.5.

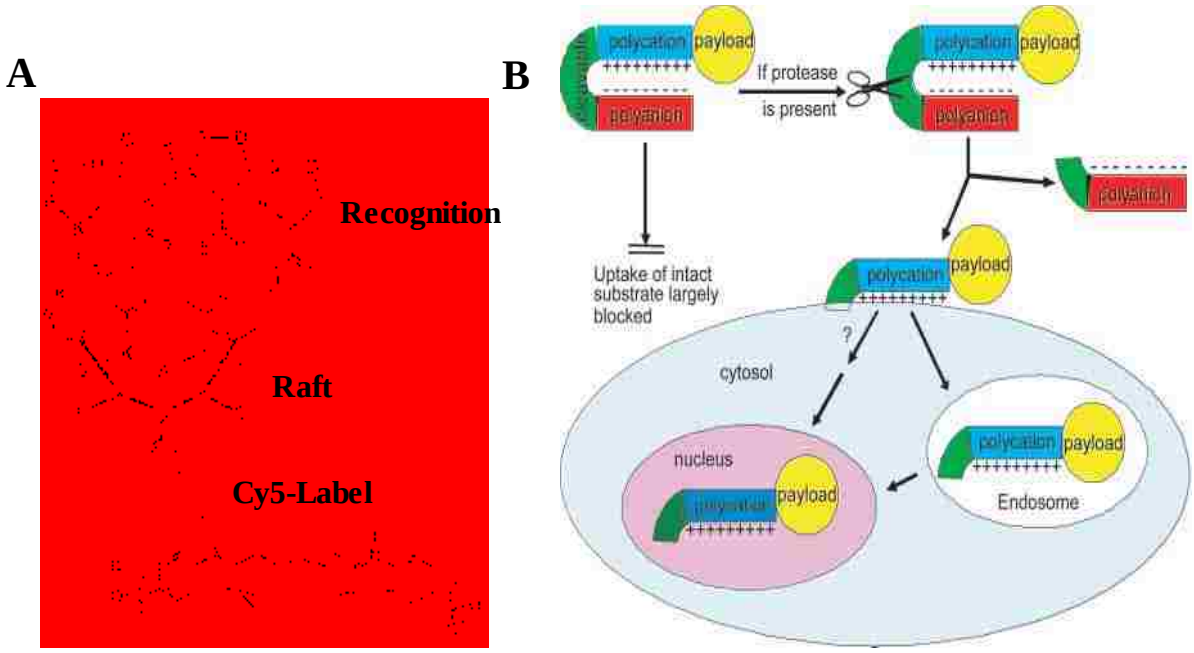

Figure 1.9. Structure of RAFT-c(RGD)$_4$. Schematic diagram of activatable CPPs. Cellular uptake induced by a cationic peptide is blocked by a short stretch of acidic residues attached by a cleavable linker. Once the linker is cleaved, the acidic inhibitory domain drifts away, and the cationic CPP is free to carry its cargo into cells. From Granger et al. (2005) and Jiang et al. (2004).[99, 104]

1.2.6 Small-Molecule Conjugates

An even more simplistic imaging scaffold involves the use of small-molecule targeted probes. From the probes listed above, small molecules are generally more cost effective, easier to make, show better pharmacokinetic properties, higher biodistribution, and are often less immunogenic.[111] For optical imaging, these probes are generally conjugated with always-on NIR fluorophores and target well-known tumor properties, such as prostate-specific membrane antigen (PSMA),[112-113] overexpression of folate receptors,[111] hypoxia,[114] and increased glucose uptake.[115] PSMA has been studied extensively[116] for the detection of prostate cancer, because it is a well-known biomarker (that consists of an extracellular domain) of prostate cancer and

metastatic prostate cancer cells, and it has been detected even in neovasculature of a variety of non-prostatic solid malignancies.[113, 117-118] Chen et al. developed an inhibitor for the enzyme active site of the extracellular domain portion of PSMA and labeled it with the NIR dye IRDye 800CW.[112] To demonstrate this probe's effectiveness, they created a xenograft mouse model containing a cell line known to upregulate PSMA and another cell line that does not express PSMA. In vivo fluorescence imaging revealed substantial retention of the probe in the PSMA-containing cell line after 20.5 hours post-injection and minimal signal from the negative cell line. This positive fluorescent signal was observed 70.5 hours after injection. Tueng et al. synthesized a folic acid-bearing molecule conjugated to an NIR dye for optical detection of ovarian cancer.[111] Previous reports have demonstrated that membrane-bound folic acid receptors are highly overexpressed in ovarian cancer cell lines.[119-121] In this study, they used the probe to determine the fate of the dye in vitro in an ovarian cancer cell line. After 30 minutes of incubating the cultured cells with the probe, it was confirmed the probe was taken up through a receptor-mediated endocytotic process and was localized in endosomes. In vivo analysis was also performed in a xenograft mouse model, where they determined that the probe could be optically imaged one hour after injection, and its signal reached a plateau 24 hours after injection.

1.3 Activatable Fluorophores

Fluorescent probes have become a common tool for sensing biochemical processes, diagnosing diseases, detection of hazardous materials, drug discovery, and sensing biological environments.[122] With intrusive fluorescence being fairly rare amongst most compounds, fluorescence-based sensors are highly sensitive, while being economical, and easy to use. Attachment of specific recognition units on fluorophores that perturb the photophysical properties of the dye allows for the creation of unique probes that can be used to detect specific

analytes. A highly sensitive and selective probe can be created by having a good understanding of the interaction between the recognition unit and the analyte being detected. This receptor-analyte interaction can consist of hydrogen bonding, π-π, donor-acceptor, electrostatic, and hydrophobic/hydrophilic interactions, metal coordination, and chemical or enzymatic reaction.[122-123] Various fluorogenic probes and their applications will be discussed below.

1.3.1 Detection of Metal Ions and pH Changes

One of the common probe types are those for the detection of metal species such as Hg^{2+}, $MeHg^{+}$, Ag^{+}, Pd^{0}, Pd^{2+}, Pt^{2+}, Pt^{4+}, Cu^{+}, Cu^{2+}, Au^{+}, and Au^{3+}.[122] This is in part due to the wide use of metal-containing catalysts in industry that have the potential to leach into soils and water sources as a results of spills and waste disposal. Here, these metal species have the potential to make their way into drinking water and food sources and later into the bodies of people, where they can cause damage to organs and even cause cancer. Having a specific and sensitive probe helps in the detection of polluted water and food and aids in decontamination protocols after industrial spills. Since their inception by de Silva,[124] photoinduced electron transfer (PeT)-based probes have become common place in the fluorescence-based detection arena due to the ease of changing their recognition and signal units. These fluorophores are designed to have a relatively long range interaction between the fluorophore and receptor moieties, and generally are of the structural form fluorophore-linker-receptor.[20] This system generally acts as an off-on (turn-on) type probe. In the quenched state, electron transfer from the non-ionized receptor to the excited fluorophore prevents the fluorophore's excited electronic state from relaxing down via a photon-emitting process. Upon binding of the analyte, the receptor's oxidation potential is perturbed. This prevents the transfer of the electron to the excited fluorophore, thereby dequenching the dye. In a majority of PeT quenching probes using the fluorophore-linker-receptor structure, the

receptor unit contains an aliphatic amine that can readily be protonated and deprotonated so as to cause a shift in the amine oxidation potential. 4-amino-naphthalimide-based fluorophores have become one of the most studied PeT fluorophores, due to their highly fluorescent nature resulting from the "push-pull" internal charge transfer (ICT) mechanism and the aromatic amine that can be easily conjugated with a wide variety of linkers and receptors, Figure 1.10.[125]

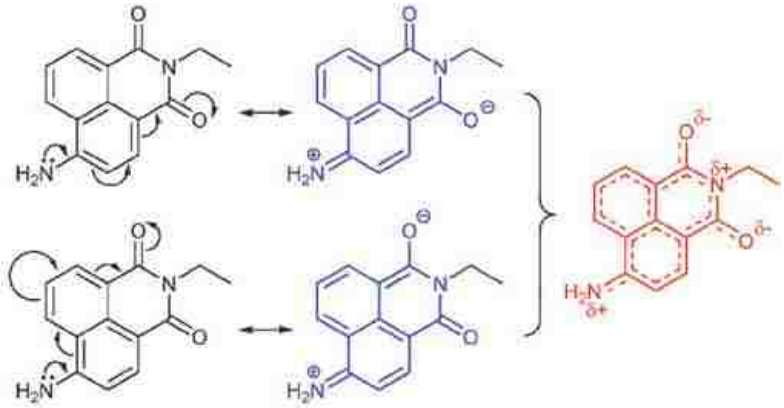

Figure 1.10. 4-amino-1,8-naphthalimide structure and schematic representation of the ICT excited state within the 4-amino-1,8-naphthalimide fluorophore caused by a "push–pull" action. From Duke et al. (2010).[125]

He et al. devised a 4-amino-naphthalimide probe to detect potassium in whole blood and serum using a cryptand as the receptor unit.[126] An ideal probe for detection of any metal cation detector must possess: good selectivity against all other cationic species relative to the one under study, good binding properties to the ligand, and little to no pH interference. Quenching of dye fluorescence through PeT was achieved by its conjugation to the cryptand via a short benzyl linker moiety. Their probe was found to be selective and sensitive to potassium, because smaller cationic metal species are too small to properly bind to the cryptand ligand. However, it was observed that potassium could be displaced by high concentrations of sodium. Also using a 4-amino-naphthalimide PeT quenched probe, it was demonstrated that detecting aqueous/physiological Zn^{2+} was possible, Gunnlaugsson et al.[127] This PeT probe used a simple

aromatic iminodiacetate receptor molecule for the selective detection of Zn^{2+}. While the probe was amenable with PeT type quenching at physiological pH, there was a turn-on effect in fluorescence at lower pH values between 2 and 5 due to the protonation of the tertiary amine of the receptor. With that being the only drawback, the probe was found to be highly selective for Zn^{2+} vs. Mg^{2+}, Ca^{2+}, Hg^{2+}, and Cd^{2+}; none of the latter produced increases in fluorescence.

Recently, another set of fluorogenic probes that exploits naphthalimide dyes are the compounds of ratiometric and colorimetric probes. Rather than turning off and then on, these probes are always fluorescent. However, their emission wavelength shifts in either a red or a blue after binding of the target analyte to the receptor unit. The shift in wavelength is brought on by a perturbation in the ICT mechanism by analyte binding, either through weakening or strengthening of the "push-pull" characteristic.[128] This is useful in that these reporters still contain the sensitivity of off-on probes, but also provide the aesthetic appeal of a colorimetric assay, thereby allowing for quantitative analysis using the ratios of the pre-/post-binding fluorescence.[129] Xu et al. developed this type of dye using a naphthalimide construct for the detection of Zn^{2+}.[129] In a pH 7.0 acetonitrile/water (80/20) solution, it was found that their probe red shifted from 537 nm to 593 nm with excitation at the isosbestic point (λ_{ex} = 470 nm). The quantum yield did decrease from pre-addition to post-addition of zinc, Φ = 0.33 and Φ = 0.14 for λ_{em} = 537 and λ_{em} = 593 nm, respectively. This probe was also found to be quenched by the addition of Cu^{2+}, Co^{2+} and Zn^{2+}, while Li^{+}, Na^{+}, Mg^{2+}, Ca^{2+}, Fe^{3+}, Mn^{2+}, Al^{3+}, Cd^{2+}, Hg^{2+}, Ag^{+} and Pb^{2+} caused no change in the optical properties.[129] Xu et al. also synthesized a Cu^{2+} probe in which the fluorescence was red shifted from 518 nm to 592 nm in an ethanol/water (60/40) solution, with no effect from pH, changes between 2.88 to 12.0.[130] As seen in Figure 1.11, the binding of Cu^{2+} deprotonates the two aromatic nitrogens on the naphthalene system, which in

turn causes the electron-donating ability of the nitrogens to increase thereby shifting the fluorescence to the red. However, the quantum yield for the red-shifted dye was very low, Φ = 0.14.

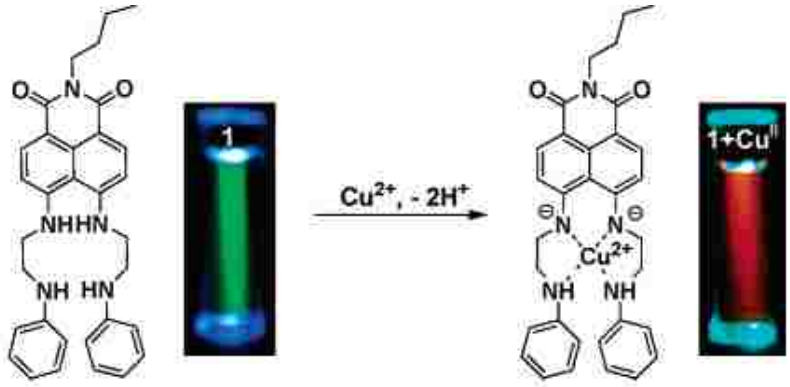

Figure 1.11. Binding of Cu^{2+} and deprotonation of the two aromatic amines. From Xu et al. (2005).[130]

1.3.2 Biologically Relevant Probes

As our knowledge of the biological and biochemical milieu increases, the ability to detect the events and analytes that compose it also increases. A majority of these processes and molecules can be observed using fluorophores, due to the high sensitivity of fluorescent probes. These events can include detection of thiols,[131-133] hypoxia,[134] intracellular hydrogen sulfide,[135] and pH changes to label endosomes and lysosomes for fluorescence microscopy.[128] These probes can be designed based on a variety of mechanisms, from off-on to ratiometric, from structural changes in the fluorophore that induce fluorescence, or altering the ICT of the probe. With glutathione being the most abundant intracellular thiol that plays a major role in regulation, structure, and function of proteins—as well as its association with heart disease, cancer, stroke, and neurological disorders—it has been one of the most studied of the biochemical compounds.[131, 136-138] As with a majority of the thiol-sensing fluorophores, Pires et al. utilized a disulfide bond as the receptor unit for glutathione detection.[131] This probe is of the off-on

variety and consists of a rhodamine-110 base, di-conjugated with two disulfide-containing receptor units. This di-conjugation of both aromatic amines in rhodamine-110 creates a locked form and prevents fluorescence. After reduction of the disulfide bonds by glutathione, both linkers underwent cyclization to leave behind the highly fluorescent rhodamine-110. This probe was found to be specific for glutathione when compared to a second similar probe that contains no disulfide units; minimal change in the fluorescent signal was found when it was incubated with glutathione. Though this cyclization process can be relatively slow, they were able to effectively image cells using confocal microscopy and used flow cytometry to detect the presence of intracellular glutathione.

Tumor environments generally have a lower pH and are hypoxic compared to other physiological environments. Drug resistance, poor progression-free survival, and metastasis have also been linked to hypoxia.[114, 134, 139-141] Recently, work has been performed to produce fluorogenic probes that are selectively activated under hypoxic conditions so as to better understand the tumor microenvironment and to detect tumors using optical imaging. One of the more common methodologies in fluorescent detection of hypoxia involves using a nitro-based receptor group that can be easily reduced under hypoxic conditions. Cui et al. designed a 4-amino-naphthalimide probe with a nitro-benzyl receptor unit.[134] When conjugated to the naphthalimide dye, the receptor weakens the ICT of the fluorophore yielding a blue emission. After reduction of the nitro-group, the receptor undergoes electron-cascade elimination, leaving behind a non-conjugated 4-amino-naphthalimide having a red-shift fluorescence signal. Their irreversible and ratiometric/colorimetric probe was found to be selectively reduced by nitroreductase versus thiol reducing species, such as glutathione, dithiothreitol, cysteine, and

homocysteine. In vitro analysis was performed using the A549 cell line, where it was proven that the probe could differentiate between hypoxic tumors and normal tissues.

1.3.3 Fluorophore Activation by Enzymes

As mentioned above, with a better understanding of the micro-/macroenvironment and biochemistry of diseases come better modalities for detecting and understanding these diseases. One of the more common approaches is to tailor fluorogenic probes to be selectively activated by enzymes that are over-expressed in specific diseases. These probes can be used for in vitro and in vivo analysis, tumor resection, and even aid in drug design. The ability to selectively detect specific enzymes hinges on having in hand a stable receptor substrate that is activated by only the enzyme in question. To be able to relate this probe to in vitro and in vivo work, the enzyme must be highly upregulated in the environment being studied and preferably be non-existent in a majority of other tissues. Coupling this upregulated enzyme with fluorescence-based probes, it is possible to obtain real-time information from the diseased environment. In turn, this leads to better designed enzyme substrates, drug delivery systems, and even fluorophores. Common enzymes being studied include matrix metalloproteinases,[142] γ-glutamyltranspeptidase (GGT),[12] β-galactosidase,[143] aldo-keto reductase,[144-145] cathepsins,[146-147] 3α-hydroxysteroid dehydrogenases,[148] *N*-acetyltransferase 2,[149] cytochrome P450,[19] PSMA,[150] penicillin G acylase (PGA),[151] esterase,[17-18, 152] and caspase-3.[153-154]

The Raines group has performed a significant amount of research in rhodamine110-based latent fluorophores that are activated by esterases[17-18] and cytochrome P450.[19] From this group, multiple "proof-of-concept" type probes have been developed. In one such case, Watkins et al. demonstrated an off-on rhodamine110 fluorophore that is conjugated to an esterase substrate and also with a tag to label a haloalkane dehalogenase (HD) variant.[18] This esterase substrate

contains a trimethyl-lock unit, that after esterase activation, increases the rate at which the activated substrate is cleaved from the fluorophore so as to leave behind the highly fluorescent rhodamine dye. The second unit conjugated to the rhodamine110 is a tag that upon hydrolysis by HD forms a highly reactant species that covalently labels the HD proteins. This probe was able to rapidly (15 minutes) diffuse through the cell membrane, label HD, and become activated by an esterase. In vitro analysis using confocal microscopy and the U2OS cell line demonstrated that when in the quenched state, the probe displayed minimal background signal. This allowed for fluorescence imaging without having to perform time-consuming washing steps. This type of imaging has the potential to play a large part in in vivo and even clinical analysis using fluorogenic probes. Being able to covalently label enzymes with high selectively and using off-on fluorophores that are activated by enzyme prevalent in all tissues could prove to be beneficial in cancer detection by irreversibly labeling overexpressed enzymes with a latent fluorophore, while all un-labeled and activated fluorophores can be rapidly removed from the body.

The Shabat research group has developed latent fluorophores to obtain a better design and understanding of some drug delivery systems (DDSs).[147, 155-158] These types of drugs are activated in a specific target site so as to increase the effectiveness of the drug on the diseased area while reducing harm to healthy tissue. When using off-on fluorescent probes, it is possible to obtain better DDS designs from the trigger system to the linker covalently attaching the trigger to the drug molecule(s). From the sensitivity of fluorescent probes, real-time information can be obtained from the activation and drug release from DDSs when the fluorophore is the pseudo-drug in the DDSs design. This can give information involving pharmacokinetics, pharmacodynamics, cell permeation efficiencies and pathways, and mechanisms of activation.[147] One methodology for obtaining more efficient DDSs is use of a linker that connects the

activatable unit to the drug and subsequently undergoes a rapid elimination; the self-eliminating linker is sufficiently long to separate the activating unit far enough away from any bulky groups that may hinder enzyme activation. Shamis and Shabat developed a dendritic amplification DDS in which six fluorescent probes were attached to a single activating unit.[157] The trigger group in this setup was cleaved by penicillin G acylase (PGA), and the six tryptophan signaling groups were conjugated through an elaborate dendritic self-immolative linker system. From this work, it was observed that it is possible to obtain 100% release of the signaling unit after a single activation event, though release occurred over a 48-hour period.

One of the nascent techniques for the detection of tumors is fluorescence-based optical imaging. By using highly fluorescent markers in vivo, it is possible to rapidly label tumor cells and obtain accurate borders between cancerous tissue and healthy tissue, something that is very difficult to do with small metastatic tumors when using conventional imaging methods. Another drawback to the current clinical imaging techniques is the limited ability to image during surgery, thus not allowing real-time information to be provided to the surgeon resecting the tumors. Current fluorescent-dye cancer imaging applications use always-on probes, and as a result, they require a substantial amount of time to allow for passive accumulatation in the tumor site. Removal of the un-accumulated dye is also essential so as to reduce the amount of background fluorescence (increase the SBR). Urano et al. have developed a rhodamine-based, off-on fluorophore that is selectively activated by γ-glutamyltranspeptidase (GGT).[12] This GGT protein is a membrane-bound enzyme involved in glutathione homeostasis, and it has been found to be expressed in a variety of ovarian cancer cell lines. Using this probe, they were able to within 10 minutes differentiate cell lines containing and devoid of GGT using confocal

microscopy, and after 60 minutes using flow cytometry. It was also possible to detect ovarian tumors in xenograft mouse models using fluorescence imaging.

1.4 NAD(P)H:Quinone Oxidoreductase-1

NAD(P)H:quinone oxidoreductase-1 (NQO1, EC 1.6.99.2, DT-diaphorase) is a flavin-based, two-electron reductase enzyme that is highly upregulated (20- to 80-fold increase with respect to normal tissue) in a wide range of tumor cells, such as lung, colon, melanoma, ovarian, prostate, and breast cancer.[1, 3-4, 159-162] As a result, NQO1 has been the target of studies as a site-specific trigger for quinone-containing prodrugs.[15, 160, 163-165] However, there are no reports demonstrating the use of a real-time, NQO1-activated fluorescent sensor for in vitro analysis or in vivo tumor detection.

1.4.1 Origin and Enzymatic Mechanism

NQO1 was previously discovered in the laboratory of Lars Ernster and visiting professor Franco Navazio in 1957 while they were studying the distribution of intracellular NAD-/NADP-dependent dehydrogenases in soluble fractions of animal tissues.[166-168] This enzyme was first isolated from the cytosolic fractions of rat liver homogenates and was found to oxidize diphosphopyridine nucleotide (DPNH, NADH) and triphosphopyridine nucleotide (TPNH, NADPH) at equal rates, which is how the name "DT-diaphorase" was coined.[169-171] While the first uncharacteristic attribute of NQO1 was that it was nonspecific towards NADH and NADPH, it was also different in that it was cytosolic and more active than diaphorase enzymes associated with the mitochondria and microsomes.[172] In 1962, Ernster et al. published a document detailing NQO1 purification from the soluble fractions of rat-liver cytosol, and the enzymatic properties of NQO1.[173] Of note, it was determined that there was NQO1 activity in the microsomal and mitochondrial centrifugation fractions. However, these activities were 42% for the microsomal

fraction and 28% for the mitochondrial fraction compared to the soluble fraction. It was also speculated that these activities could be due to contamination of the mitochondrial and microsomal fractions. It was mentioned that the quinoid species 2,6-dichlorophenolindolphenol (DCPIP) and coenzyme Q_0 were suitable substrates for NQO1, while its reducing capabilities against vitamin K_1, vitamin K_2, coenzyme Q_{10}, cytochrome *c*, and cytochrome b_5 was negligible. It was also discovered that the rat NQO1 was strongly (and competitively) inhibited by dicumarol, while its activity was enhanced in the presence of bovine serum albumin (BSA), polyvinylpyrrolidone (PVP), certain phospholipids, and certain non-ionic detergents (Tween-20, Tween-60, and Lubrol-W), as well as certain phospholipids. Maximum enzymatic enhancement with added BSA was found to be 3- to 15-fold versus without BSA. While it was found that increased pH also slightly increased enzyme function, there was no defined optimum.

Since the first publication about purification and activity, extensive work has been performed on NQO1 to better understand its structure, activation mechanism, biosynthesis, and its role in humans and animals.[170] It has since been found that the enzyme catalyzes the 2-electron reduction of quinones to hydroquinones, along with other quinoid species to their reduced version. Due to its catalytic mechanism, it has been labeled a detoxifying enzyme as it reduces quinones to hydroquinones, as opposed to quinones being reduced by one electron to the radical-containing semiquinones.[174] NQO-enzymes have been found not only in animals, but also in plants and bacteria.[175] NQO1 and NQO2 are both found in mammals, while NQO3, NQO4, and NQO5 are found in eubacteria, fungi, and archaebacteria, respectively. A mutated version of NQO1 (NQO1*2) has been discovered in which a mutation at position 609 has occurred, causing the enzyme to become inactive.[2] NQO1 is most abundantly found in animal liver tissue, and it is also found in the brain, heart, lung, kidney, small intestine, skeletal muscle,

and mammary glands.[170] But of most importance, NQO1 has been found to be upregulated in cancerous tissues 20- to 80-fold compared to normal tissue of the same origin. [1, 3-4, 159-162] Interestingly, it has been noted that small cell lung carcinomas (SCLCs) have very little NQO1 activity when compared with that of normal tissue, while the difficult to treat non-small cell lung carcinomas (NSCLCs) have been found to have highly elevated NQO1 activity.[159]

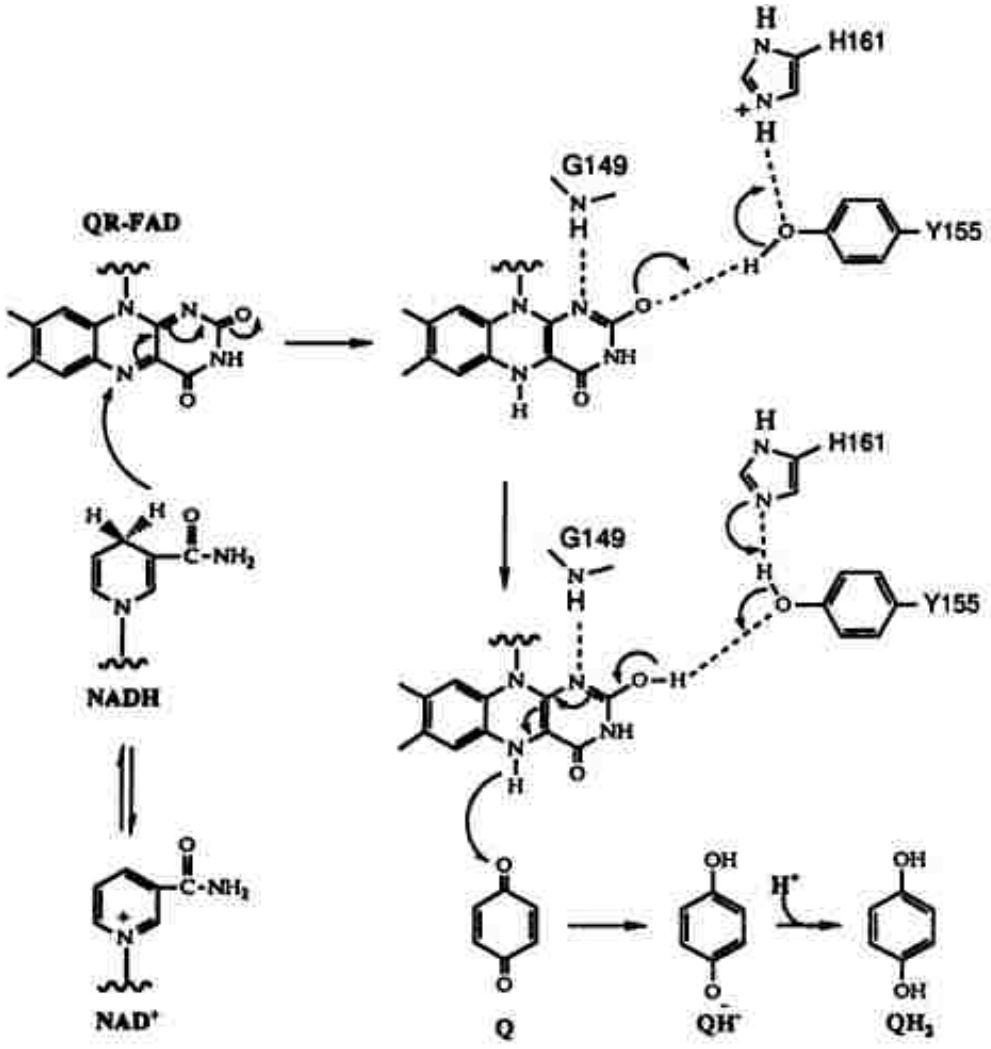

Figure 1.12. Mechanism of the obligatory two-electron reduction of benzoquinone (Q) by rNQO1. The overall reaction is: NADH + Q + H^+ to NAD^+ + QH_2. From Li et al. (1995).

X-ray crystallography has aided in determining the structures of NQO1 from rats (rNQO1), mice (mNQO1), and humans (hNQO1).[176-177] The human enzyme is a roughly 62 kDa interlocking homodimer of 273 residues and contains one flavin adenine dinucleotide (FAD) per monomer. Each NQO1 has two separate domaines, a catalytic domain with an α/β fold and a *C*-terminal domain that forms part of the binding site for the adenosine portion of NAD^+.[176] When reducing the same substrate (vitamin K_3, menadione), the human and mouse version are both slower by a factor of two when compared to the rat version.[176] The FAD units were found to bind tightly in all three enzyme structures (mouse, human, and rat) and did not readily come off in native conditions. Though the residue differences between the three enzymes are only slightly different, there is an 86% similarity between hNQO1 and rNQO1, and 94% similarity between rNQO1 and mNQO1. The proposed reduction mechanism (ping-pong) by Li et al. of rNQO1 reducing benzoquinone is shown in Figure 1.12.[177] Here, the reduced NAD(P)H enters the active site and reduces the FAD^+ to $FADH_2$ via hydride transfer. After NAD^+ leaves, the duroquinone enters the active site and is reduced by the hydride from $FADH_2$.

1.4.2 Intracellular Localization

Previous studies have shown the presence of NQO1 in microsomes (vesicles formed from the smooth/rough endoplasmic reticulum (ER) after cell homogenization), mitochondria, Golgi membranes, plasma membranes, and the largest amount (>90%) in the cytosol, in rat liver cells.[161, 178-181] 40% of the microsomal NQO1 enzyme was found to be in the lumen, while the rest was incorporated into the membrane. NQO1 content was determined by collecting cellular organelles via preparative ultracentrifugation, where the total protein conten—NQO1 and all other proteins—and NQO1 activity were determined for each fraction. Even though this method did provide similar results for all experiments (highest activity was found in the cytosol and

lower activity in the mitochondria, Golgi membrane, plasma membrane, and microsomes), activity caused by cytosolic contamination of the fractions after centrifugation could not be discounted.[178-179, 182] NQO1 movement in rat liver cells was also determined by radioactive labeling of amino acids that were injected into rats.[178] It was found that 5 minutes after injection, the highest enzyme activity was observed in the rough ER. NQO1 was then found to move into the smooth ER after 20 minutes, where it began to leave within minutes.[178] Cytosolic content slowly increased, while mitochondrial NQO1 appeared to reach a maximum after 15 minutes. No other readings were performed after thirty minutes, and the only compartments tested were rough ER, smooth ER, mitochondria, and cytosol. Later, Winski et al. used confocal microscopy and immunohistochemical labeling in fixed cells to determine the location of NQO1 in the cytosol and nucleus of HT-29 (human colorectal adenocarcinoma) and H661 (human non-small cell lung cancer) cells.[183] This group also used immunoelectron microscopy to provide evidence that the enzyme was not located in the mitochondria, Golgi, and endoplasmic reticulum. Along with the electron microscopy data showing a very slight signal in the mitochondria, immunoelectron microscopy has its own drawbacks caused by a loss of antigenicity during the freezing fixative step and also by embedding the cells in resin.[183]

1.4.3 NQO1-Based Prodrugs and Inhibitors for Cancer Treatment

To date, there has been extensive work taking advantage of the upregulated state of hNQO1 in tumor cells with the development of xenobiotics,[1-2, 15, 162, 184-189] prodrugs,[163, 165, 190] and inhibitors.[191-195] After a quinone species undergoes NQO1-catalyzed reduction to its hydroquinone, the compound either becomes activated or deactivated.[188] While NQO1 can deactivate specific quinones to hydroquinones to prevent them from oxidatively damaging cells, it can also activate quinoidal molecules by creating the reduced form that has a higher reactivity,

such as alkylating agents that can damage DNA. This conversion of a quinone to a bioreactive alkylating agent has been essential in the design of a wide variety of xenobiotics for cancer therapy. Tailoring these activating substrates specifically for NQO1 allows for the creation of drug compounds that become cytotoxic in the tumor tissues highly overexpressing the enzyme. The most successful xenobiotic that can be activated by NQO1, is mitomycin C (MMC).[188] MMC has been used as a cytotoxic agent since the 1960s, and has activity against lung, stomach, head and neck, prostate, breast and bladder tumors, and is currently used in cancer therapies.[160] MMC is an indolquinone that, after reduction, forms an alkylating species. This reactive species is cross-linked to DNA, and thereby preventing replication. Though MMC has been clinically used, it is considered a poor substrate for hNQO1. This has led scientists to develop analogs of MMC that are better substrates for hNQO1 and still possess the cytotoxic active nature. One of the more effective analogues is EO9,[15] and it was discovered to be reduced more rapidly by the enzyme when compared to MMC. But this compound failed in clinical trials due to kidney toxicity and rapid plasma clearance. A second type of NQO1-activatable xenobiotic was in the form of an aziridinylbenzoquinone, specifically diaziquone (AZQ).[160, 188] AZQ is also a DNA alkylating agent found to be effective in cancer treatment, but it suffered due to pH-dependent alkylation and poor enzymatic activity, and it failed in clinical trials as it did not supersede therapy agents already in use.[160] Hernick et al. synthesized a series of indolquinone prodrugs containing phosphoramidate at either the 2- or 3-position of the indole ring.[165] After reduction by NQO1, the cytotoxic phosphoramidate was cleaved and could add to DNA. Their work discovered that leaving groups in the 2-position were excellent substrates for NQO1 and could be correlated with cytotoxicity in vitro. While 3-substituted prodrugs were potent inhibitors of the enzyme, there was no correlation found in the cytotoxicity studies.

One of the unique uses of NQO1 has been in the development of mechanism-based inhibitors to aid in the treatment of pancreatic cancer.[194] The reasoning behind this is to remove the ability of NQO1 to use its chemoprotective nature in pancreatic tumor cells. Previous work had shown that NQO1 was a superoxide scavenger and prevented the levels of superoxides in pancreatic cancer cells from elevating.[194, 196] Irreversibly inhibiting the enzyme would allow these levels to increase, causing toxicity. Dicumarol is a well-known potent inhibitor for NQO1, but it lacks solubility in aqueous media, is a reversible inhibitor against NAD(P)H, and is also known to inhibit multiple enzymes.[194] The mechanism-based inhibitor ES936 was developed from an indolquinone that formed a highly reactive iminium ion species after NQO1 reduction.[191, 194] Immediately after activation in the enzyme active site, the hydroquinone undergoes an irreversible alkylation with a tyrosine residue, completely inhibiting the enzyme.

1.4.4 NQO1 Specific Latent Fluorophores

Though NQO1 has been studied extensively for the development and implementation of xenobiotic drugs for cancer therapy due to its high level of overexpression in a large portion of tumors of varying origin, there have never been fluorescent probes synthesized for in vitro and in vivo analysis of NQO1-containing tumor cells. However, there have been two off-on NQO1 activatable latent fluorophores developed by the Huang research group for the detection of glucose in a NQO1-glucose dehydrogenase coupled assay.[197] Thus, their main interest was in analyzing the substrate specificity of the two latent fluorophores with NQO1. The first probe contained a rhodamine110-based dye that was di-conjugated with two trimethyl-locked quinones, similar to that in Scheme 1.1.[197-198] Their analysis of this fluorophore involved performing enzyme assays with NQO1 and relating the increase in fluorescence to a known concentration of rhodamine110, assuming rapid reduction and removal of *both* quinone units.

This assumption is inherently problematic as it does not take into account the fluorescence signal derived from the mono-conjugated rhodamine species that exists after reduction/removal of a single quinone group. This mono-conjugated species has half the fluorescence intensity compared to rhodamine-110.[17] Secondly, having two enzymatic activation steps to achieve the final product is not beneficial in real-time analysis. A second probe was synthesized by conjugating the same trimethyl-locked quinone to an *N*,*N*'-dimethylethylenediamine linker attached to a coumarin dye.[198] This probe, even with a single quinone, lacks real-time analysis due to the linker. Here, it takes two non-enzymatic events to reveal the fluorescent signal of the coumarin dye, removal of the quinone and cyclization/removal of the linker. This cyclization of the diamine linker into an urea species is rather detrimental in obtaining a rapid analysis type assay, as cyclization spacers can be plagued with long half-lives.[199]

1.5 References

(1) Beall, H. D.; Murphy, A. M.; Siegel, D.; Hargreaves, R. H.; Butler, J.; Ross, D., Nicotinamide Adenine Dinucleotide (Phosphate): Quinone Oxidoreductase (DT-diaphorase) as a Target for Bioreductive Antitumor Quinones: Quinone Cytotoxicity and Selectivity in Human Lung and Breast Cancer Cell Lines. *Mol Pharmacol* 1995, *48* (3), 499-504.

(2) Traver, R. D.; Horikoshi, T.; Danenberg, K. D.; Stadlbauer, T. H. W.; Danenberg, P. V.; Ross, D.; Gibson, N. W., NAD(P)H:Quinone Oxidoreductase Gene Expression in Human Colon Carcinoma Cells: Characterization of a Mutation Which Modulates DT-Diaphorase Activity and Mitomycin Sensitivity. *Cancer Res* 1992, *52* (4), 797-802.

(3) Fitzsimmons, S. A.; Workman, P.; Grever, M.; Paull, K.; Camalier, R.; Lewis, A. D., Reductase Enzyme Expression Across the National Cancer Institute Tumor Cell Line Panel: Correlation With Sensitivity to Mitomycin C and EO9. *J Natl Cancer Inst* 1996, *88* (5), 259-269.

(4) Cresteil, T.; Jaiswal, A. K., High Levels of Expression of the NAD(P)H:Quinone Oxidoreductase (NQO1) Gene in Tumor Cells Compared to Normal Cells of the Same Origin. *Biochem Pharmacol* 1991, *42* (5), 1021-1027.

(5) Ueno, T.; Nagano, T., Fluorescent Probes for Sensing and Imaging. *Nat Meth* 2011, *8* (8), 642-645.

(6) Hillman, B. J., Introduction to the Special Issue on Medical Imaging in Oncology. *J Clin Oncol* 2006, *24* (20), 3223-3224.

(7) Ehman, R. L.; Hendee, W. R.; Welch, M. J.; Dunnick, N. R.; Bresolin, L. B.; Arenson, R. L.; Baum, S.; Hricak, H.; Thrall, J. H., Blueprint for Imaging in Biomedical Research. *Radiology* 2007, *244* (1), 12-27.

(8) Siegel, R.; Naishadham, D.; Jemal, A., Cancer Statistics, 2012. *CA Cancer J Clin* 2012, *62* (1), 10-29.

(9) Fass, L., Imaging and Cancer: A Review. *Mol Oncol* 2008, *2* (2), 115-152.

(10) Luo, S.; Zhang, E.; Su, Y.; Cheng, T.; Shi, C., A Review of NIR Dyes in Cancer Targeting and Imaging. *Biomaterials* 2011, *32* (29), 7127-7138.

(11) van den Berg, N. S.; van Leeuwen, F. W.; van der Poel, H. G., Fluorescence Guidance in Urologic Surgery. *Curr Opin Urol* 2012, *22* (2), 109-120.

(12) Urano, Y.; Sakabe, M.; Kosaka, N.; Ogawa, M.; Mitsunaga, M.; Asanuma, D.; Kamiya, M.; Young, M. R.; Nagano, T.; Choyke, P. L.; Kobayashi, H., Rapid Cancer Detection by Topically Spraying a Gamma-Glutamyltranspeptidase-Activated Fluorescent Probe. *Sci Transl Med* 2011, *3* (110), 110-119.

(13) Shi, H.; He, X.; Wang, K.; Wu, X.; Ye, X.; Guo, Q.; Tan, W.; Qing, Z.; Yang, X.; Zhou, B., Activatable Aptamer Probe for Contrast-Enhanced in vivo Cancer Imaging Based on Cell Membrane Protein-Triggered Conformation Alteration. *Proc Natl Acad Sci U S A* 2011, *108* (10), 3900-3905.

(14) Razgulin, A.; Ma, N.; Rao, J., Strategies for in vivo Imaging of Enzyme Activity: An Overview and Recent Advances. *Chem Soc Rev* 2011, *40* (7), 4186-4216.

(15) Phillips, R. M., Bioreductive Activation of a Series of Analogues of 5-aziridinyl-3-hydroxymethyl-1-methyl-2-[1H-indole-4, 7-dione] prop-β-en-α-ol (EO9) by Human DT-Diaphorase. *Biochem Pharmacol* 1996, *52* (11), 1711-1718.

(16) Ong, W.; Yang, Y.; Cruciano, A. C.; McCarley, R. L., Redox-Triggered Contents Release from Liposomes. *J Am Chem Soc* 2008, *130* (44), 14739-14744.

(17) Lavis, L. D.; Chao, T.-Y.; Raines, R. T., Fluorogenic Label for Biomolecular Imaging. *ACS Chem Bio* 2006, *1* (4), 252-260.

(18) Watkins, R. W.; Lavis, L. D.; Kung, V. M.; Los, G. V.; Raines, R. T., Fluorogenic Affinity Label for the Facile, Rapid Imaging of Proteins in Live Cells. *Org Biomol Chem* 2009, *7* (19), 3969-3975.

(19) Yatzeck, M. M.; Lavis, L. D.; Chao, T.-Y.; Chandran, S. S.; Raines, R. T., A Highly Sensitive Fluorogenic Probe for Cytochrome P450 Activity in Live Cells. *Bioorg Med Chem Lett* 2008, *18* (22), 5864-5866.

(20) Bissell, R. A.; de Silva, A. P.; Gunaratne, H. Q. N.; Lynch, P. L. M.; Maguire, G. E. M.; Sandanayake, K. R. A. S., Molecular Fluorescent Signalling with 'Fluor-Spacer-Receptor' Systems: Approaches to Sensing and Switching Devices via Supramolecular Photophysics. *Chem Soc Rev* 1992, *21* (3), 187-195.

(21) Carlson, B. W.; Miller, L. L., Mechanism of the Oxidation of NADH by Quinones - Energetics of One-Electron and Hydride Routes. *J Am Chem Soc* 1985, *107* (2), 479-485.

(22) Ball, E. G., Studies on Oxidation-Reduction XXIII. Ascorbic Acid. *J Biol Chem* 1937, *118* (1), 219-239.

(23) Reipa, V., Direct Spectroelectrochemical Titration of Glutathione. *Bioelectrochem* 2004, *65* (1), 47-49.

(24) Hutchison, R. S.; Ort, D. R., Measurement of Equilibrium Midpoint Potentials of Thiols/Disulfide Regulatory Groups on Thioredoxin-Activated Chloroplast Enzymes. *Biothiols, Pt B* 1995, *252*, 220-228.

(25) Lakowicz, J. R., Mechanisms and Dynamics of Fluorescence Quenching. In *Principles of Fluorescence Spectroscopy*, Third ed.; Springer: 2006; pp 331-351.

(26) Melhuish, W. H., Quantum Efficiencies of Fluorescence of Organic Substances: Effect of Solvent and Concentration of the Fluorescent Solute. *J Phys Chem* 1961, *65* (2), 229-235.

(27) Pierce, M. C.; Javier, D. J.; Richards-Kortum, R., Optical Contrast Agents and Imaging Systems for Detection and Diagnosis of Cancer. *Int J Cancer* 2008, *123* (9), 1979-1990.

(28) de Torres, J. P.; Bastarrika, G.; Wisnivesky, J. P.; Alcaide, A. B.; Campo, A.; Seijo, L. M.; Pueyo, J. C.; Villanueva, A.; Lozano, M. D.; Montes, U.; Montuenga, L.; Zulueta, J. J., Assessing the Relationship Between Lung Cancer Risk and Emphysema Detected on Low-Dose CT of the Chest. *Chest* 2007, *132* (6), 1932-1938.

(29) Lehman, C. D.; Isaacs, C.; Schnall, M. D.; Pisano, E. D.; Ascher, S. M.; Weatherall, P. T.; Bluemke, D. A.; Bowen, D. J.; Marcom, P. K.; Armstrong, D. K.; Domchek, S. M.; Tomlinson, G.; Skates, S. J.; Gatsonis, C., Cancer Yield of Mammography, MR, and US in High-Risk Women: Prospective Multi-Institution Breast Cancer Screening Study. *Radiology* 2007, *244* (2), 381-388.

(30) Paajanen, H., Increasing Use of Mammography Improves the Outcome of Breast Cancer in Finland. *Breast J* 2006, *12* (1), 88-90.

(31) Nelson, S. J.; Huhn, S.; Vigneron, D. B.; Day, M. R.; Wald, L. L.; Prados, M.; Chang, S.; Gutin, P. H.; Sneed, P. K.; Verhey, L.; Hawkins, R. A.; Dillon, W. P., Volume MRI and MRSI Techniques for the Quantitation of Treatment Response in Brain Tumors: Presentation of a Detailed Sase Study. *J Magn Reson Imaging* 1997, *7* (6), 1146-1152.

(32) Kent, M. S.; Port, J. L.; Altorki, N. K., Current State of Imaging for Lung Cancer Staging. *Thorac Surg Clin* 2004, *14* (1), 1-13.

(33) Brink, I.; Schumacher, T.; Mix, M.; Ruhland, S.; Stoelben, E.; Digel, W.; Henke, M.; Ghanem, N.; Moser, E.; Nitzsche, E. U., Impact of [^{18}F]FDG-PET on the Primary Staging of Small-Cell Lung Cancer. *Eur J Nucl Med Mol Imaging* 2004, *31* (12), 1614-1620.

(34) Shim, S. S.; Lee, K. S.; Kim, B.-T.; Chung, M. J.; Lee, E. J.; Han, J.; Choi, J. Y.; Kwon, O. J.; Shim, Y. M.; Kim, S., Non–Small Cell Lung Cancer: Prospective Comparison of Integrated FDG PET/CT and CT Alone for Preoperative Staging. *Radiology* 2005, *236* (3), 1011-1019.

(35) Lee, K. S.; Jeong, Y. J.; Han, J.; Kim, B.-T.; Kim, H.; Kwon, O. J., T1 Non–Small Cell Lung Cancer: Imaging and Histopathologic Findings and Their Prognostic Implications. *Radiographics* 2004, *24* (6), 1617-1636.

(36) Ferme, C.; Vanel, D.; Ribrag, V.; Girinski, T., Role of Imaging to Choose Treatment. *Cancer imaging : the official publication of the International Cancer Imaging Society* 2005, *5 Spec No A*, 113-119.

(37) Ciernik, I. F.; Dizendorf, E.; Baumert, B. G.; Reiner, B.; Burger, C.; Davis, J. B.; Lütolf, U. M.; Steinert, H. C.; Von Schulthess, G. K., Radiation Treatment Planning with an Integrated Positron Emission and Computer Tomography (PET/CT): a Feasibility Study. *Int J Radiat Oncol Biol Phys* 2003, *57* (3), 853-863.

(38) Ashamalla, H.; Rafla, S.; Parikh, K.; Mokhtar, B.; Goswami, G.; Kambam, S.; Abdel-Dayem, H.; Guirguis, A.; Ross, P.; Evola, A., The Contribution of Integrated PET/CT to the Evolving Definition of Treatment Volumes in Radiation Treatment Planning in Lung Cancer. *Int J Radiat Oncol Biol Phys* 2005, *63* (4), 1016-1023.

(39) Neves, A. A.; Brindle, K. M., Assessing Responses to Cancer Therapy Using Molecular Imaging. *Biochim Biophys Acta* 2006, *1766* (2), 242-261.

(40) Stroobants, S.; Goeminne, J.; Seegers, M.; Dimitrijevic, S.; Dupont, P.; Nuyts, J.; Martens, M.; van den Borne, B.; Cole, P.; Sciot, R.; Dumez, H.; Silberman, S.; Mortelmans, L.; van Oosterom, A., ^{18}FDG-Positron Emission Tomography for the Early Prediction of Response in Advanced Soft Tissue Sarcoma Treated with Imatinib Mesylate (Glivec®). *Eur J Cancer* 2003, *39* (14), 2012-2020.

(41) Aboagye, E. O.; Bhujwalla, Z. M., Malignant Transformation Alters Membrane Choline Phospholipid Metabolism of Human Mammary Epithelial Cells. *Cancer Res* 1999, *59* (1), 80-84.

(42) Brindle, K., New Approaches for Imaging Tumour Responses to Treatment. *Nat Rev Cancer* 2008, *8* (2), 94-107.

(43) Keidar, Z.; Haim, N.; Guralnik, L.; Wollner, M.; Bar-Shalom, R.; Ben-Nun, A.; Israel, O., PET/CT Using 18F-FDG in Suspected Lung Cancer Recurrence: Diagnostic Value and Impact on Patient Management. *J Nucl Med* 2004, *45* (10), 1640-1646.

(44) Aldrich, M. B.; Marshall, M. V.; Sevick-Muraca, E. M.; Lanza, G.; Kotyk, J.; Culver, J.; Wang, L. V.; Uddin, J.; Crews, B. C.; Marnett, L. J.; Liao, J. C.; Contag, C.; Crawford, J. M.; Wang, K.; Reisdorph, B.; Appelman, H.; Turgeon, D. K.; Meyer, C.; Wang, T., Seeing it Through: Translational Validation of New Medical Imaging Modalities. *Biomed Opt Express* 2012, *3* (4), 764-776.

(45) Drezek, R.; Brookner, C.; Pavlova, I.; Boiko, I.; Malpica, A.; Lotan, R.; Follen, M.; Richards-Kortum, R., Autofluorescence Microscopy of Fresh Cervical-Tissue Sections Reveals Alterations in Tissue Biochemistry with Dysplasia. *Photochem Photobiol* 2001, *73* (6), 636-641.

(46) Skala, M. C.; Riching, K. M.; Gendron-Fitzpatrick, A.; Eickhoff, J.; Eliceiri, K. W.; White, J. G.; Ramanujam, N., In vivo Multiphoton Microscopy of NADH and FAD Redox States, Fluorescence Lifetimes, and Cellular Morphology in Precancerous Epithelia. *Proc Natl Acad Sci U S A* 2007, *104* (49), 19494-19499.

(47) Trivedi, E. R.; Harney, A. S.; Olive, M. B.; Podgorski, I.; Moin, K.; Sloane, B. F.; Barrett, A. G.; Meade, T. J.; Hoffman, B. M., Chiral Porphyrazine Near-IR Optical Imaging Agent Exhibiting Preferential Tumor Accumulation. *Proc Natl Acad Sci U S A* 2010, *107* (4), 1284-1288.

(48) Zhang, C.; Liu, T.; Su, Y.; Luo, S.; Zhu, Y.; Tan, X.; Fan, S.; Zhang, L.; Zhou, Y.; Cheng, T.; Shi, C., A Near-Infrared Fluorescent Heptamethine Indocyanine Dye with Preferential Tumor Accumulation for in vivo Imaging. *Biomaterials* 2010, *31* (25), 6612-6617.

(49) Xiao, W.; Yao, N.; Peng, L.; Liu, R.; Lam, K. S., Near-Infrared Optical Imaging in Glioblastoma Xenograft with Ligand-Targeting Alpha 3 Integrin. *Eur J Nucl Med Mol Imaging* 2009, *36* (1), 94-103.

(50) Wu, K.; Liu, J.-J.; Adams, W.; Sonn, G. A.; Mach, K. E.; Pan, Y.; Beck, A. H.; Jensen, K. C.; Liao, J. C., Dynamic Real-time Microscopy of the Urinary Tract Using Confocal Laser Endomicroscopy. *Urology* 2011, *78* (1), 225-231.

(51) Sonn, G. A.; Jones, S. N.; Tarin, T. V.; Du, C. B.; Mach, K. E.; Jensen, K. C.; Liao, J. C., Optical Biopsy of Human Bladder Neoplasia with in vivo Confocal Laser Endomicroscopy. *J Urol* 2009, *182* (4), 1299-1305.

(52) Tobis, S.; Knopf, J.; Silvers, C.; Yao, J.; Rashid, H.; Wu, G.; Golijanin, D., Near Infrared Fluorescence Imaging with Robotic Assisted Laparoscopic Partial Nephrectomy: Initial Clinical Experience for Renal Cortical Tumors. *The Journal of urology* 2011, *186* (1), 47-52.

(53) Kobayashi, H.; Ogawa, M.; Alford, R.; Choyke, P. L.; Urano, Y., New Strategies for Fluorescent Probe Design in Medical Diagnostic Imaging. *Chemical reviews* 2010, *110* (5), 2620-2640.

(54) Son, J. H.; Lim, C. S.; Han, J. H.; Danish, I. A.; Kim, H. M.; Cho, B. R., Two-Photon Lysotrackers for in vivo Imaging. *J Org Chem* 2011, *76* (19), 8113-8116.

(55) Robinson, J. T.; Hong, G.; Liang, Y.; Zhang, B.; Yaghi, O. K.; Dai, H., In Vivo Fluorescence Imaging in the Second Near-Infrared Window with Long Circulating Carbon Nanotubes Capable of Ultrahigh Tumor Uptake. *J Am Chem Soc* 2012, *134* (25), 10664-10669.

(56) Miyashiro, I.; Miyoshi, N.; Hiratsuka, M.; Kishi, K.; Yamada, T.; Ohue, M.; Ohigashi, H.; Yano, M.; Ishikawa, O.; Imaoka, S., Detection of Sentinel Node in Gastric Cancer Surgery by Indocyanine Green Fluorescence Imaging: Comparison with Infrared Imaging. *Ann Surg Oncol* 2008, *15* (6), 1640-1643.

(57) Kejík, Z.; Bříza, T.; Králová, J.; Martásek, P.; Král, V., Selective Recognition of a Saccharide-type Tumor Marker with Natural and Synthetic Ligands: a New Trend in Cancer Diagnosis. *Anal Bioanal Chem* 2010, *398* (5), 1865-1870.

(58) Olivo, M.; Fu, C.; Raghavan, V.; Lau, W., New Frontier in Hypericin-Mediated Diagnosis of Cancer with Current Optical Technologies. *Ann Biomed Eng* 2012, *40* (2), 460-473.

(59) Lee, D. A.; Knight, M. M.; F. Bolton, J.; Idowu, B. D.; Kayser, M. V.; Bader, D. L., Chondrocyte Deformation Within Compressed Agarose Constructs at the Cellular and Sub-Cellular Levels. *J Biomech* 2000, *33* (1), 81-95.

(60) Lustbader, J. W.; Cirilli, M.; Lin, C.; Xu, H. W.; Takuma, K.; Wang, N.; Caspersen, C.; Chen, X.; Pollak, S.; Chaney, M.; Trinchese, F.; Liu, S.; Gunn-Moore, F.; Lue, L. F.; Walker, D. G.; Kuppusamy, P.; Zewier, Z. L.; Arancio, O.; Stern, D.; Yan, S. S.; Wu, H., ABAD Directly Links Abeta to Mitochondrial Toxicity in Alzheimer's Disease. *Science* 2004, *304* (5669), 448-452.

(61) Watson, P.; Jones, A. T.; Stephens, D. J., Intracellular Trafficking Pathways and Drug Delivery: Fluorescence Imaging of Living and Fixed Cells. *Advanced drug delivery reviews* 2005, *57* (1), 43-61.

(62) Lucie, S.; Elisabeth, G.; Stephanie, F.; Guy, S.; Amandine, H.; Corinne, A.-R.; Didier, B.; Catherine, S.; Alexei, G.; Pascal, D.; Jean-Luc, C., Clustering and Internalization of Integrin [alpha]v[beta]3 With a Tetrameric RGD-Synthetic Peptide. *Mol Ther* 2009, *17* (5), 837-843.

(63) Jean, F.; Bourg-Heckly, G.; Viellerobe, B., Fibered Confocal Spectroscopy and Multicolor Imaging System for in vivo Fluorescence Analysis. *Optics express* 2007, *15* (7), 4008-4017.

(64) Thiberville, L.; Moreno-Swirc, S.; Vercauteren, T.; Peltier, E.; Cave, C.; Bourg Heckly, G., In vivo Imaging of the Bronchial Wall Microstructure Using Fibered Confocal Fluorescence Microscopy. *American journal of respiratory and critical care medicine* 2007, *175* (1), 22-31.

(65) Tearney, G. J.; Wang, T. D.; Society of Photo-optical Instrumentation Engineers., *Endoscopic microscopy III : 20-21 January 2008, San Jose, California, USA*. SPIE: Bellingham, Wash., 2008.

(66) Hsiung, P.-L.; Hardy, J.; Friedland, S.; Soetikno, R.; Du, C. B.; Wu, A. P.; Sahbaie, P.; Crawford, J. M.; Lowe, A. W.; Contag, C. H.; Wang, T. D., Detection of Colonic Dysplasia in vivo Using a Targeted Heptapeptide and Confocal Microendoscopy. *Nat Med* 2008, *14* (4), 454-458.

(67) Christensen, D. J.; Nedergaard, M., Two-Photon in vivo Imaging of Cells. *Pediatr Nephrol* 2011, *26* (9), 1483-1489.

(68) Brown, E. B.; Campbell, R. B.; Tsuzuki, Y.; Xu, L.; Carmeliet, P.; Fukumura, D.; Jain, R. K., In vivo Measurement of Gene Expression, Angiogenesis and Physiological Function in Tumors Using Multiphoton Laser Scanning Microscopy. *Nat Med* 2001, *7* (7), 864-868.

(69) Runnels, J. M.; Zamiri, P.; Spencer, J. A.; Veilleux, I.; Xunbin, W.; Bogdanov, A.; Lin, C. P., Imaging Molecular Expression on Vascular Endothelial Cells by In Vivo Immunofluorescence Microscopy. *Mol Imaging* 2006, *5* (1), 31-40.

(70) Huland, D. M.; Brown, C. M.; Howard, S. S.; Ouzounov, D. G.; Pavlova, I.; Wang, K.; Rivera, D. R.; Webb, W. W.; Xu, C., In vivo Imaging of Unstained Tissues Using Long Gradient Index Lens Multiphoton Endoscopic Systems. *Biomed Opt Express* 2012, *3* (5), 1077-1085.

(71) Bird, D.; Gu, M., Fibre-Optic Two-Photon Scanning Fluorescence Microscopy. *J Microsc* 2002, *208* (1), 35-48.

(72) Tang, S.; Jung, W.; McCormick, D.; Xie, T.; Su, J.; Ahn, Y. C.; Tromberg, B. J.; Chen, Z., Design and Implementation of Fiber-Based Multiphoton Endoscopy with

Microelectromechanical Systems Scanning. *Journal of biomedical optics* 2009, *14* (3), 1-17.

(73) Sevick-Muraca, E. M.; Sharma, R.; Rasmussen, J. C.; Marshall, M. V.; Wendt, J. A.; Pham, H. Q.; Bonefas, E.; Houston, J. P.; Sampath, L.; Adams, K. E.; Blanchard, D. K.; Fisher, R. E.; Chiang, S. B.; Elledge, R.; Mawad, M. E., Imaging of Lymph Flow in Breast Cancer Patients after Microdose Administration of a Near-Infrared Fluorophore: Feasibility Study1. *Radiology* 2008, *246* (3), 734-741.

(74) Tagaya, N.; Yamazaki, R.; Nakagawa, A.; Abe, A.; Hamada, K.; Kubota, K.; Oyama, T., Intraoperative Identification of Sentinel Lymph Nodes by Near-Infrared Fluorescence Imaging in Patients with Breast Cancer. *American journal of surgery* 2008, *195* (6), 850-853.

(75) Troyan, S. L.; Kianzad, V.; Gibbs-Strauss, S. L.; Gioux, S.; Matsui, A.; Oketokoun, R.; Ngo, L.; Khamene, A.; Azar, F.; Frangioni, J. V., The FLARE Intraoperative Near-Infrared Fluorescence Imaging System: A First-in-Human Clinical Trial in Breast Cancer Sentinel Lymph Node Mapping. *Ann Surg Oncol* 2009, *16* (10), 2943-2952.

(76) Tanaka, E.; Choi, H.; Fujii, H.; Bawendi, M.; Frangioni, J., Image-Guided Oncologic Surgery Using Invisible Light: Completed Pre-Clinical Development for Sentinel Lymph Node Mapping. *Ann Surg Oncol* 2006, *13* (12), 1671-1681.

(77) Ogasawara, Y.; Ikeda, H.; Takahashi, M.; Kawasaki, K.; Doihara, H., Evaluation of Breast Lymphatic Pathways with Indocyanine Green Fluorescence Imaging in Patients with Breast Cancer. *World J Surg* 2008, *32* (9), 1924-1929.

(78) Mieog, J.; Troyan, S.; Hutteman, M.; Donohoe, K.; van der Vorst, J.; Stockdale, A.; Liefers, G.-J.; Choi, H.; Gibbs-Strauss, S.; Putter, H.; Gioux, S.; Kuppen, P.; Ashitate, Y.; Löwik, C.; Smit, V.; Oketokoun, R.; Ngo, L.; van de Velde, C.; Frangioni, J.; Vahrmeijer, A., Toward Optimization of Imaging System and Lymphatic Tracer for Near-Infrared Fluorescent Sentinel Lymph Node Mapping in Breast Cancer. *Ann Surg Oncol* 2011, *18* (9), 2483-2491.

(79) Unno, N.; Inuzuka, K.; Suzuki, M.; Yamamoto, N.; Sagara, D.; Nishiyama, M.; Konno, H., Preliminary Experience with a Novel Fluorescence Lymphography Using Indocyanine Green in Patients with Secondary Lymphedema. *J Vasc Surg* 2007, *45* (5), 1016-1021.

(80) Frimberger, D.; Zaak, D.; Stepp, H.; Knüchel, R.; Baumgartner, R.; Schneede, P.; Schmeller, N.; Hofstetter, A., Autofluorescence Imaging to Optimize 5-ALA-Induced Fluorescence Endoscopy of Bladder Carcinoma. *Urology* 2001, *58* (3), 372-375.

(81) van der Poel, H. G.; Buckle, T.; Brouwer, O. R.; Valdes Olmos, R. A.; van Leeuwen, F. W., Intraoperative Laparoscopic Fluorescence Guidance to the Sentinel Lymph Node in Prostate Cancer Patients: Clinical Proof of Concept of an Integrated Functional Imaging Approach Using a Multimodal Tracer. *Eur Urol* 2011, *60* (4), 826-33.

(82) Shen, Y. J.; Zhu, Y. P.; Ye, D. W.; Yao, X. D.; Zhang, S. L.; Dai, B.; Zhang, H. L.; Zhu, Y., Narrow-Band Imaging Flexible Cystoscopy in the Detection of Primary Non-Muscle Invasive Bladder Cancer: A "Second Look" Matters? *International urology and nephrology* 2012, *44* (2), 451-457.

(83) Mérian, J.; Gravier, J.; Navarro, F.; Texier, I., Fluorescent Nanoprobes Dedicated to in Vivo Imaging: From Preclinical Validations to Clinical Translation. *Molecules* 2012, *17* (5), 5564-5591.

(84) Rzigalinski, B. A.; Strobl, J. S., Cadmium-Containing Nanoparticles: Perspectives on Pharmacology and Toxicology of Quantum Dots. *Toxicology and applied pharmacology* 2009, *238* (3), 280-288.

(85) Oberdörster, G.; Oberdörster, E.; Oberdörster, J., Nanotoxicology: An Emerging Discipline Evolving from Studies of Ultrafine Particles. *Environ Health Perspect* 2005, *113* (7).

(86) Gao, X.; Cui, Y.; Levenson, R. M.; Chung, L. W. K.; Nie, S., In vivo Cancer Targeting and Imaging with Semiconductor Quantum Dots. *Nat Biotech* 2004, *22* (8), 969-976.

(87) Schädlich, A.; Caysa, H.; Mueller, T.; Tenambergen, F.; Rose, C.; Göpferich, A.; Kuntsche, J.; Mäder, K., Tumor Accumulation of NIR Fluorescent PEG–PLA Nanoparticles: Impact of Particle Size and Human Xenograft Tumor Model. *ACS Nano* 2011, *5* (11), 8710-8720.

(88) Cai, W.; Shin, D.-W.; Chen, K.; Gheysens, O.; Cao, Q.; Wang, S. X.; Gambhir, S. S.; Chen, X., Peptide-Labeled Near-Infrared Quantum Dots for Imaging Tumor Vasculature in Living Subjects. *Nano Lett* 2006, *6* (4), 669-676.

(89) Sahoo, S. K.; Parveen, S.; Panda, J. J., The Present and Future of Nanotechnology in Human Health Care. *Nanomedicine : nanotechnology, biology, and medicine* 2007, *3* (1), 20-31.

(90) Wagner, V.; Dullaart, A.; Bock, A. K.; Zweck, A., The Emerging Nanomedicine Landscape. *Nat Biotechnol* 2006, *24* (10), 1211-1217.

(91) Sandanaraj, B. S.; Gremlich, H.-U.; Kneuer, R.; Dawson, J.; Wacha, S., Fluorescent Nanoprobes as a Biomarker for Increased Vascular Permeability: Implications in Diagnosis and Treatment of Cancer and Inflammation. *Bioconjug Chem* 2009, *21* (1), 93-101.

(92) Portnoy, E.; Lecht, S.; Lazarovici, P.; Danino, D.; Magdassi, S., Cetuximab-Labeled Liposomes Containing Near-Infrared Probe for in vivo Imaging. *Nanomedicine : nanotechnology, biology, and medicine* 2011, *7* (4), 480-488.

(93) Soukos, N. S.; Hamblin, M. R.; Keel, S.; Fabian, R. L.; Deutsch, T. F.; Hasan, T., Epidermal Growth Factor Receptor-targeted Immunophotodiagnosis and Photoimmunotherapy of Oral Precancer in Vivo. *Cancer Res* 2001, *61* (11), 4490-4496.

(94) Rosenthal, E. L.; Kulbersh, B. D.; King, T.; Chaudhuri, T. R.; Zinn, K. R., Use of Fluorescent Labeled Anti-Epidermal Growth Factor Receptor Antibody to Image Head and Neck Squamous Cell Carcinoma Xenografts. *Molecular cancer therapeutics* 2007, *6* (4), 1230-1238.

(95) Terwisscha van Scheltinga, A. G. T.; van Dam, G. M.; Nagengast, W. B.; Ntziachristos, V.; Hollema, H.; Herek, J. L.; Schröder, C. P.; Kosterink, J. G. W.; Lub-de Hoog, M. N.; de Vries, E. G. E., Intraoperative Near-Infrared Fluorescence Tumor Imaging with Vascular Endothelial Growth Factor and Human Epidermal Growth Factor Receptor 2 Targeting Antibodies. *J Nucl Med* 2011, *52* (11), 1778-1785.

(96) Shi, H.; Tang, Z.; Kim, Y.; Nie, H.; Huang, Y. F.; He, X.; Deng, K.; Wang, K.; Tan, W., In vivo Fluorescence Imaging of Tumors using Molecular Aptamers Generated by Cell-SELEX. *Chem Asian J* 2010, *5* (10), 2209-2213.

(97) Shangguan, D.; Cao, Z.; Meng, L.; Mallikaratchy, P.; Sefah, K.; Wang, H.; Li, Y.; Tan, W., Cell-Specific Aptamer Probes for Membrane Protein Elucidation in Cancer Cells. *J Proteome Res* 2008, *7* (5), 2133-2139.

(98) Haubner, R.; Gratias, R.; Diefenbach, B.; Goodman, S. L.; Jonczyk, A.; Kessler, H., Structural and Functional Aspects of RGD-Containing Cyclic Pentapeptides as Highly Potent and Selective Integrin αVβ3 Antagonists. *J Am Chem Soc* 1996, *118* (32), 7461-7472.

(99) Garanger, E.; Boturyn, D.; Jin, Z.; Dumy, P.; Favrot, M.-C.; Coll, J.-L., New Multifunctional Molecular Conjugate Vector for Targeting, Imaging, and Therapy of Tumors. *Mol Ther* 2005, *12* (6), 1168-1175.

(100) Zhao-Hui, J.; Josserand, V.; Razkin, J.; Garanger, E.; Boturyn, D.; Favrot, M.-C.; Dumy, P.; Coll, J.-L., Noninvasive Optical Imaging of Ovarian Metastases Using Cy5-labeled RAFT-c(-RGDfK-)4. *Mol Imaging* 2006, *5* (3), 188-197.

(101) Jin, Z. H.; Josserand, V.; Foillard, S.; Boturyn, D.; Dumy, P.; Favrot, M. C.; Coll, J. L., In vivo Optical Imaging of Integrin Alpha(v)-Beta(3) in Mice Using Multivalent or Monovalent cRGD Targeting Vectors. *Molecular cancer therapeutics* 2007, *6*.

(102) Themelis, G.; Harlaar, N. J.; Kelder, W.; Bart, J.; Sarantopoulos, A.; van Dam, G. M.; Ntziachristos, V., Enhancing Surgical Cision by Using Real-Time Imaging of Alpha(V)-Beta(3)-Integrin Targeted Near-Infrared Fluorescent Agent. *Ann Surg Oncol* 2011, *18* (12), 3506-3513.

(103) Nguyen, Q. T.; Olson, E. S.; Aguilera, T. A.; Jiang, T.; Scadeng, M.; Ellies, L. G.; Tsien, R. Y., Surgery with Molecular Fluorescence Imaging Using Activatable Cell-Penetrating Peptides Decreases Residual Cancer and Improves Survival. *Proc Natl Acad Sci U S A* 2010, *107* (9), 4317-4322.

(104) Jiang, T.; Olson, E. S.; Nguyen, Q. T.; Roy, M.; Jennings, P. A.; Tsien, R. Y., Tumor Imaging by Means of Proteolytic Activation of Cell-Penetrating Peptides. *Proc Natl Acad Sci U S A* 2004, *101* (51), 17867-17872.

(105) Olson, E. S.; Jiang, T.; Aguilera, T. A.; Nguyen, Q. T.; Ellies, L. G.; Scadeng, M.; Tsien, R. Y., Activatable Cell Penetrating Peptides Linked to Nanoparticles as Dual Probes for in vivo Fluorescence and MR Imaging of Proteases. *Proc Natl Acad Sci U S A* 2010, *107* (9), 4311-4316.

(106) Vivès, E.; Brodin, P.; Lebleu, B., A Truncated HIV-1 Tat Protein Basic Domain Rapidly Translocates through the Plasma Membrane and Accumulates in the Cell Nucleus. *J Biol Chem* 1997, *272* (25), 16010-16017.

(107) Rothbard, J. B.; Kreider, E.; VanDeusen, C. L.; Wright, L.; Wylie, B. L.; Wender, P. A., Arginine-Rich Molecular Transporters for Drug Delivery: Role of Backbone Spacing in Cellular Uptake. *J Med Chem* 2002, *45* (17), 3612-3618.

(108) Talvensaari-Mattila, A.; Paakko, P.; Turpeenniemi-Hujanen, T., Matrix Metalloproteinase-2 (MMP-2) is Associated with Survival in Breast Carcinoma. *Br. J. Cancer* 2003, *89* (7), 1270-1275.

(109) Bremer, C.; Bredow, S.; Mahmood, U.; Weissleder, R.; Tung, C.-H., Optical Imaging of Matrix Metalloproteinase–2 Activity in Tumors: Feasibility Study in a Mouse Model. *Radiology* 2001, *221* (2), 523-529.

(110) Rocca, G. L.; Pucci-Minafra, I.; Marrazzo, A.; Taormina, P.; Minafra, S., Zymographic Detection and Clinical Correlations of MMP-2 and MMP-9 in Breast Cancer Sera. *Br J Cancer* 2004, *90* (7), 1414-1421.

(111) Tung, C.-H.; Lin, Y.; Moon, W. K.; Weissleder, R., A Receptor-Targeted Near-Infrared Fluorescence Probe for In Vivo Tumor Imaging. *ChemBioChem* 2002, *3* (8), 784-786.

(112) Chen, Y.; Dhara, S.; Banerjee, S. R.; Byun, Y.; Pullambhatla, M.; Mease, R. C.; Pomper, M. G., A Low Molecular Weight PSMA-based Fluorescent Imaging Agent for Cancer. *Biochem Biophys Res Commun* 2009, *390* (3), 624-629.

(113) Liu, T.; Wu, L. Y.; Hopkins, M. R.; Choi, J. K.; Berkman, C. E., A Targeted Low Molecular Weight Near-Infrared Fluorescent Probe for Prostate Cancer. *Bioorg Med Chem Lett* 2010, *20* (23), 7124-7126.

(114) Okuda, K.; Okabe, Y.; Kadonosono, T.; Ueno, T.; Youssif, B. G. M.; Kizaka-Kondoh, S.; Nagasawa, H., 2-Nitroimidazole-Tricarbocyanine Conjugate as a Near-Infrared Fluorescent Probe for in Vivo Imaging of Tumor Hypoxia. *Bioconjug Chem* 2012, *23* (3), 324-329.

(115) Levi, J.; Cheng, Z.; Gheysens, O.; Patel, M.; Chan, C. T.; Wang, Y.; Namavari, M.; Gambhir, S. S., Fluorescent Fructose Derivatives for Imaging Breast Cancer Cells. *Bioconjug Chem* 2007, *18* (3), 628-634.

(116) Elfriede, S., Biological and Chemical Sensors for Cancer Diagnosis. *Meas Sci Technol* 2010, *21* (11), 112002-112026.

(117) Chang, S. S.; Reuter, V. E.; Heston, W. D. W.; Gaudin, P. B., Metastatic Renal Cell Carcinoma Neovasculature Expresses Prostate-Specific Membrane Antigen. *Urology* 2001, *57*, 801-805.

(118) Chang, S. S.; O'Keefe, D. S.; Bacich, D. J.; Reuter, V. E.; Heston, W. D. W.; Gaudin, P. B., Prostate-specific Membrane Antigen Is Produced in Tumor-associated Neovasculature. *Clin Cancer Res* 1999, *5* (10), 2674-2681.

(119) Konda, S. D.; Aref, M.; Wang, S.; Brechbiel, M.; Wiener, E. C., Specific Targeting of Folate-Dendrimer MRI Contrast Agents to the High Affinity Folate Receptor Expressed in Ovarian Tumor Xenografts. *Magn. Reson. Mat. Phys. Biol. Med.* 2001, *12* (2-3), 104-113.

(120) Toffoli, G.; Cernigoi, C.; Russo, A.; Gallo, A.; Bagnoli, M.; Boiocchi, M., Overexpression of Folate Binding Protein in Ovarian Cancers. *Int J Cancer* 1997, *74* (2), 193-198.

(121) Miotti, S.; Bagnoli, M.; Ottone, F.; Tomassetti, A.; Colnaghi, M. I.; Canevari, S., Simultaneous Activity of Two Different Mechanisms of Folate Transport in Ovarian Carcinoma Cell Lines. *J Cell Biochem* 1997, *65* (4), 479-491.

(122) Eun Jun, M.; Roy, B.; Han Ahn, K., "Turn-On" Fluorescent Sensing With "Reactive" Probes. *Chem Comm* 2011, *47* (27), 7583-7601.

(123) Yoon, Z. S.; Noh, S. B.; Cho, D.-G.; Sessler, J. L.; Kim, D., Evaluation of Planarity and Aromaticity in Sapphyrin and Inverted Sapphyrin Using a Bidirectional NICS (Nucleus-Independent Chemical Shift) Scan Method. *Chem Comm* 2007, (23), 2378-2380.

(124) de Silva, A. P.; Gunaratne, H. Q. N.; Habib-Jiwan, J.-L.; McCoy, C. P.; Rice, T. E.; Soumillion, J.-P., New Fluorescent Model Compounds for the Study of Photoinduced Electron Transfer: The Influence of a Molecular Electric Field in the Excited State. *Angew Chem, Int Ed* 1995, *34* (16), 1728-1731.

(125) Duke, R. M.; Veale, E. B.; Pfeffer, F. M.; Kruger, P. E.; Gunnlaugsson, T., Colorimetric and Fluorescent Anion Sensors: An Overview of Recent Developments in the Use of 1,8-naphthalimide-Based Chemosensors. *Chem Soc Rev* 2010, *39* (10), 3936-3953.

(126) He, H.; Mortellaro, M. A.; Leiner, M. J. P.; Fraatz, R. J.; Tusa, J. K., A Fluorescent Sensor with High Selectivity and Sensitivity for Potassium in Water. *J Am Chem Soc* 2003, *125* (6), 1468-1469.

(127) Gunnlaugsson, T.; Lee, T. C.; Parkesh, R., A Highly Selective and Sensitive Fluorescent PET (Photoinduced Electron Transfer) Chemosensor for Zn(II). *Org Biomol Chem* 2003, *1* (19), 3265-3267.

(128) Qian, X.; Xiao, Y.; Xu, Y.; Guo, X.; Qian, J.; Zhu, W., "Alive" Dyes as Fluorescent Sensors: Fluorophore, Mechanism, Receptor and Images in Living Cells. *Chem Commun* 2010, *46* (35), 6418-6436.

(129) Xu, Z.; Qian, X.; Cui, J.; Zhang, R., Exploiting the Deprotonation Mechanism for the Design of Ratiometric and Colorimetric Zn^{2+} Fluorescent Chemosensor with a Large Red-Shift in Emission. *Tetrahedron* 2006, *62* (43), 10117-10122.

(130) Xu, Z.; Qian, X.; Cui, J., Colorimetric and Ratiometric Fluorescent Chemosensor with a Large Red-Shift in Emission: Cu(II)-Only Sensing by Deprotonation of Secondary Amines as Receptor Conjugated to Naphthalimide Fluorophore. *Org Lett* 2005, *7* (14), 3029-3032.

(131) Pires, M. M.; Chmielewski, J., Fluorescence Imaging of Cellular Glutathione Using a Latent Rhodamine. *Org Lett* 2008, *10* (5), 837-840.

(132) Lee, M. H.; Han, J. H.; Kwon, P.-S.; Bhuniya, S.; Kim, J. Y.; Sessler, J. L.; Kang, C.; Kim, J. S., Hepatocyte-Targeting Single Galactose-Appended Naphthalimide: A Tool for Intracellular Thiol Imaging in Vivo. *J Am Chem Soc* 2011, *134* (2), 1316-1322.

(133) Zhu, B.; Zhang, X.; Li, Y.; Wang, P.; Zhang, H.; Zhuang, X., A Colorimetric and Ratiometric Fluorescent Probe for Thiols and its Bioimaging Applications. *Chem Comm* 2010, *46* (31), 5710-5712.

(134) Cui, L.; Zhong, Y.; Zhu, W.; Xu, Y.; Du, Q.; Wang, X.; Qian, X.; Xiao, Y., A New Prodrug-Derived Ratiometric Fluorescent Probe for Hypoxia: High Selectivity of Nitroreductase and Imaging in Tumor Cell. *Org Lett* 2011, *13* (5), 928-931.

(135) Lippert, A. R.; New, E. J.; Chang, C. J., Reaction-Based Fluorescent Probes for Selective Imaging of Hydrogen Sulfide in Living Cells. *J Am Chem Soc* 2011, *133* (26), 10078-10080.

(136) Wu, G.; Fang, Y.-Z.; Yang, S.; Lupton, J. R.; Turner, N. D., Glutathione Metabolism and Its Implications for Health. *J Nutr* 2004, *134* (3), 489-492.

(137) Deneke, S. M., Thiol-based antioxidants. In *Current Topics in Cellular Regulation*, Earl, R. S.; Chock, P. B., Eds. Academic Press: 2001; Vol. Volume 36, pp 151-180.

(138) Cole, S. P. C.; Deeley, R. G., Transport of Glutathione and Glutathione Conjugates by MRP1. *Trends Pharmacol Sci* 2006, *27* (8), 438-446.

(139) Williams, K. J.; Albertella, M. R.; Fitzpatrick, B.; Loadman, P. M.; Shnyder, S. D.; Chinje, E. C.; Telfer, B. A.; Dunk, C. R.; Harris, P. A.; Stratford, I. J., In vivo Activation of the Hypoxia-targeted Cytotoxin AQ4N in Human Tumor Xenografts. *Mol Cancer Thera* 2009, *8* (12), 3266-3275.

(140) Höckel, M.; Schlenger, K.; Aral, B.; Mitze, M.; Schäffer, U.; Vaupel, P., Association Between Tumor Hypoxia and Malignant Progression in Advanced Cancer of the Uterine Cervix. *Cancer Res* 1996, *56* (19), 4509-4515.

(141) Rofstad, E. K.; Rasmussen, H.; Galappathi, K.; Mathiesen, B.; Nilsen, K.; Graff, B. A., Hypoxia Promotes Lymph Node Metastasis in Human Melanoma Xenografts by Up-Regulating the Urokinase-Type Plasminogen Activator Receptor. *Cancer Res* 2002, *62* (6), 1847-1853.

(142) Weissleder, R.; Tung, C.-H.; Mahmood, U.; Bogdanov, A., In vivo Imaging of Tumors with Protease-Activated Near-Infrared Fluorescent Probes. *Nat Biotech* 1999, *17* (4), 375-378.

(143) Kamiya, M.; Kobayashi, H.; Hama, Y.; Koyama, Y.; Bernardo, M.; Nagano, T.; Choyke, P. L.; Urano, Y., An Enzymatically Activated Fluorescence Probe for Targeted Tumor Imaging. *J Am Chem Soc* 2007, *129* (13), 3918-3929.

(144) Halim, M.; Yee, D. J.; Sames, D., Imaging Induction of Cytoprotective Enzymes in Intact Human Cells: Coumberone, a Metabolic Reporter for Human AKR1C Enzymes Reveals Activation by Panaxytriol, an Active Component of Red Ginseng. *J Am Chem Soc* 2008, *130* (43), 14123-14128.

(145) Yee, D. J.; Balsanek, V.; Bauman, D. R.; Penning, T. M.; Sames, D., Fluorogenic Metabolic Probes for Direct Activity Readout of Redox Enzymes: Selective Measurement of Human AKR1C2 in Living Cells. *Proc Natl Acad Sci U S A* 2006, *103* (36), 13304-13309.

(146) Abd-Elgaliel, W. R.; Cruz-Monserrate, Z.; Logsdon, C. D.; Tung, C.-H., Molecular Imaging of Cathepsin E-Positive Tumors in Mice Using a Novel Protease-Activatable Fluorescent Probe. *Molecular BioSystems* 2011, *7* (12), 3207-3213.

(147) Weinstain, R.; Segal, E.; Satchi-Fainaro, R.; Shabat, D., Real-Time Monitoring of Drug Release. *Chem Commun* 2010, *46* (4), 553-555.

(148) Yee, D. J.; Balsanek, V.; Sames, D., New Tools for Molecular Imaging of Redox Metabolism: Development of a Fluorogenic Probe for 3α-Hydroxysteroid Dehydrogenases. *J Am Chem Soc* 2004, *126* (8), 2282-2283.

(149) Cui, L.; Zhong, Y.; Zhu, W.; Xu, Y.; Qian, X., Selective and Sensitive Detection and Quantification of Arylamine N-acetyltransferase 2 by a Ratiometric Fluorescence Probe. *Chem Commun* 2010, *46* (38), 7121-7123.

(150) Jones, G. B.; Crasto, C. F.; Mathews, J. E.; Xie, L.; Mitchell, M. O.; El-Shafey, A.; D'Amico, A. V.; Bubley, G. J., An Image Contrast Agent Selectively Activated by Prostate Specific Antigen. *Bioorg Med Chem Lett* 2006, *14* (2), 418-425.

(151) Meyer, Y.; Richard, J.-A.; Delest, B.; Noack, P.; Renard, P.-Y.; Romieu, A., A Comparative Study of the Self-Immolation of Para-aminobenzylalcohol and Hemithioaminal-Based Linkers in the Context of Protease-Sensitive Fluorogenic Probes. *Org Biomol Chem* 2010, *8* (8), 1777-1780.

(152) Mangold, S. L.; Carpenter, R. T.; Kiessling, L. L., Synthesis of Fluorogenic Polymers for Visualizing Cellular Internalization. *Org Lett* 2008, *10* (14), 2997-3000.

(153) Richard, J.-A.; Meyer, Y.; Jolivel, V. r.; Massonneau, M.; Dumeunier, R.; Vaudry, D.; Vaudry, H.; Renard, P.-Y.; Romieu, A., Latent Fluorophores Based on a Self-Immolative Linker Strategy and Suitable for Protease Sensing. *Bioconjug Chem* 2008, *19* (8), 1707-1718.

(154) Wang, Z.-Q.; Liao, J.; Diwu, Z., N-DEVD-N′-morpholinecarbonyl-rhodamine 110: Novel Caspase-3 Fluorogenic Substrates for Cell-Based Apoptosis Assay. *Bioorg Med Chem Lett* 2005, *15* (9), 2335-2338.

(155) Erez, R.; Shabat, D., The Azaquinone-methide Elimination: Comparison Study of 1,6- and 1,4-eliminations Under Physiological Conditions. *Org Biomol Chem* 2008, *6* (15), 2669-2672.

(156) Amir, R. J.; Popkov, M.; Lerner, R. A.; Barbas, C. F.; Shabat, D., Prodrug Activation Gated by a Molecular "OR" Logic Trigger. *Angew Chem Int Ed Engl* 2005, *44* (28), 4378-4381.

(157) Shamis, M.; Shabat, D., Single-Triggered AB6 Self-Immolative Dendritic Amplifiers. *Chemistry – A Euro J* 2007, *13* (16), 4523-4528.

(158) Haba, K.; Popkov, M.; Shamis, M.; Lerner, R. A.; Barbas, C. F.; Shabat, D., Single-Triggered Trimeric Prodrugs. *Angew Chem Int Ed Engl* 2005, *44* (5), 716-720.

(159) Malkinson, A. M.; Siegel, D.; Forrest, G. L.; Gazdar, A. F.; Oie, H. K.; Chan, D. C.; Bunn, P. A.; Mabry, M.; Dykes, D. J.; Harrison, S. D.; Ross, D., Elevated DT-diaphorase Activity and Messenger RNA Content in Human Non-Small Cell Lung Carcinoma: Relationship to the Response of Lung Tumor Xenografts to Mitomycin C. *Cancer Res* 1992, *52* (17), 4752-4757.

(160) Danson, S.; Ward, T. H.; Butler, J.; Ranson, M., DT-Diaphorase: A Target for New Anticancer Drugs. *Cancer Treat Rev* 2004, *30* (5), 437-449.

(161) Ernster, L.; Danielson, L.; Ljunggren, M., Dt Diaphorase I. Purification from the Soluble Fraction of Rat-Liver Cytoplasm, and Properties. *Biochim Biophys Acta* 1962, *58* (2), 171-188.

(162) Smitskamp-Wilms, E.; Hendriks, H. R.; Peters, G. J., Development, Pharmacology, Role of DT-Diaphorase and Prospects of the Indoloquinone EO9. *Gen Pharmacol* 1996, *27* (3), 421-429.

(163) Volpato, M.; Abou-Zeid, N.; Tanner, R. W.; Glassbrook, L. T.; Taylor, J.; Stratford, I.; Loadman, P. M.; Jaffar, M.; Phillips, R. M., Chemical Synthesis and Biological Evaluation of a NAD(P)H:quinone Oxidoreductase-1 Targeted Tripartite Quinone Drug Delivery System. *Molecular cancer therapeutics* 2007, *6* (12 Pt 1), 3122-3130.

(164) Buffinton, G. D.; Ollinger, K.; Brunmark, A.; Cadenas, E., DT-Diaphorase-Catalysed Reduction of 1,4-naphthoquinone Derivatives and Glutathionyl-Quinone Conjugates. Effect of Substituents on Autoxidation Rates. *Biochem J* 1989, *257* (2), 561-571.

(165) Hernick, M.; Flader, C.; Borch, R. F., Design, Synthesis, and Biological Evaluation of Indolequinone Phosphoramidate Prodrugs Targeted to DT-Diaphorase. *J Med Chem* 2002, *45* (16), 3540-3548.

(166) Ernster, L.; Navazio, F., Studies on TPN-Linked Oxidations: I. Pathways of Isocitrate Oxidation in Rat Liver Mitochondria. *Biochimica et Biophysica Acta* 1957, *26* (2), 408-415.

(167) Navazio, F.; Ernster, B. B.; Ernster, L., Studies on TPN-Linked Oxidations: II. The Quantitative Significance of Liver Lactic Dehydrogenase as a Catalyzer of TPNH-Oxidation. *Biochimica et Biophysica Acta* 1957, *26* (2), 416-421.

(168) Ernster, L., DT-Diaphorase: A Historical Review. *Chemica Scripta* 1987, *27A*, 1-13.

(169) Ernster, L.; Navazio, F., Soluble Diaphorase in Animal Tissues. *Acta Chemica Scandinavica* 1958, *12* (3), 595-595.

(170) Lind, C.; Cadenas, E.; Hochstein, P.; Ernster, L., [30] DT-diaphorase: Purification, Properties, and Function. In *Methods in Enzymology*, Lester Packer, A. N. G., Ed. Academic Press: 1990; Vol. Volume 186, pp 287-301.

(171) Ernster, L.; Ljunggren, M.; Danielson, L., Purification and Some Properties of a Highly Dicumarol-sensitive Liver Diaphorase. *Biochem Biophys Research Comm* 1960, *2* (2), 88-92.

(172) Ernster, L., Structural Factors Involved in the Diaphorase and Cytochrome c-Reductase Activities of Mitochondria and Microsomes. *Acta Chemica Scandinavica* 1958, *12* (3), 600-602.

(173) Ernster, L.; Ljunggren, M.; Danielson, L., DT Diaphorase 1. Purification From Soluble Fraction of Rat-Liver Cytoplasm, and Properties. *Biochim Biophys Acta* 1962, *58* (2), 171-188.

(174) Dinkova-Kostova, A. T.; Talalay, P., Persuasive Evidence that Quinone Reductase Type 1 (DT Diaphorase) Protects Cells Against the Toxicity of Electrophiles and Reactive Forms of Oxygen. *Free Radical Biology and Medicine* 2000, *29* (3–4), 231-240.

(175) Vasiliou, V.; Ross, D.; Nebert, D. W., Update of the NAD(P)H:Quinone Oxidoreductase (NQO) Gene Family. *Hum Genomics* 2006, *2* (5), 329-335.

(176) Faig, M.; Bianchet, M. A.; Talalay, P.; Chen, S.; Winski, S.; Ross, D.; Amzel, L. M., Structures of Recombinant Human and Mouse NAD(P)H:Quinone Oxidoreductases:

Species Comparison and Structural Changes with Substrate Binding and Release. *Proc Natl Acad Sci U S A* 2000, *97* (7), 3177-3182.

(177) Li, R.; Bianchet, M. A.; Talalay, P.; Amzel, L. M., The Three-Dimensional Structure of NAD(P)H:Quinone Reductase, a Flavoprotein Involved in Cancer Chemoprotection and Chemotherapy: Mechanism of the Two-Electron Reduction. *Proc Natl Acad Sci U S A* 1995, *92* (19), 8846-8850.

(178) Edlund, C.; Elhammer, A.; Dallner, G., Distribution of Newly Synthesized DT-Diaphorase in Rat Liver. *Biosci Rep* 1982, *2* (11), 861-865.

(179) Nakamura, M.; Hayashi, T., One- and Two-Electron Reduction of Quinones by Rat Liver Subcellular Fractions. *J Biochem* 1994, *115* (6), 1141-1147.

(180) Das, M.; Rastogi, S.; Khanna, S. K., Mechanism to Study 1:1 Stoichiometry of NADPH and Alkoxyphenoxazones Metabolism Spectrophotometrically in Subcellular Biological Preparations. *Biochim Biophys Acta* 2004, *1675* (1–3), 1-11.

(181) Vaes, G., Cell-to-Cell Interactions in the Secretion of Enzymes of Connective Tissue Breakdown, Collagenase and Proteoglycan-Degrading Neutral Proteases. A Review. *Inflammation Research* 1980, *10* (6), 474-485.

(182) Das, M.; Rastogi, S.; Khanna, S. K., Mechanism to Study 1 : 1 Stoichiometry of NADPH and Alkoxyphenoxazones Metabolism Spectrophotometrically in Subcellular Biological Preparations. *Biochim Biophys Acta* 2004, *1675* (1-3), 1-11.

(183) Winski, S. L.; Koutalos, Y.; Bentley, D. L.; Ross, D., Subcellular Localization of NAD(P)H:Quinone Oxidoreductase 1 in Human Cancer Cells. *Cancer Res* 2002, *62* (5), 1420-1424.

(184) Winski, S. L.; Hargreaves, R. H.; Butler, J.; Ross, D., A New Screening System for NAD(P)H:quinone Oxidoreductase (NQO1)-directed Antitumor Quinones: Identification of a New Aziridinylbenzoquinone, RH1, as a NQO1-directed Antitumor Agent. *Clin Cancer Res* 1998, *4* (12), 3083-3088.

(185) Beall, H. D.; Winski, S.; Swann, E.; Hudnott, A. R.; Cotterill, A. S.; O'Sullivan, N.; Green, S. J.; Bien, R.; Siegel, D.; Ross, D.; Moody, C. J., Indolequinone Antitumor Agents: Correlation Between Quinone Structure, Rate of Metabolism by Recombinant Human NAD(P)H:Quinone Oxidoreductase, and in Vitro Cytotoxicity. *J Med Chem* 1998, *41* (24), 4755-4766.

(186) Everett, S. A.; Naylor, M. A.; Patel, K. B.; Stratford, M. R. L.; Wardman, P., Bioreductively-Activated Prodrugs for Targetting Hypoxic Tissues: Elimination of Aspirin from 2-nitroimidazole Derivatives. *Bioorg Med Chem Lett* 1999, *9*, 1267-1272.

(187) Newsome, J. J.; Swann, E.; Hassani, M.; Bray, K. C.; Slawin, A. M. Z.; Beall, H. D.; Moody, C. J., Indolequinone Antitumour Agents: Correlation Between Quinone Structure and Rate of Metabolism by Recombinant Human NAD(P)H:Quinone Oxidoreductase. *Org Biomol Chem* 2007, *5* (10), 1629-1640.

(188) Ross, D.; Kepa, J. K.; Winski, S. L.; Beall, H. D.; Anwar, A.; Siegel, D., NAD(P)H : Quinone Oxidoreductase 1 (NQO1): Chemoprotection, Bioactivation, Gene Regulation and Genetic Polymorphisms. *Chem Biol Interact* 2000, *129* (1-2), 77-97.

(189) Gibson, N. W.; Hartley, J. A.; Butler, J.; Siegel, D.; Ross, D., Relationship Between DT-Diaphorase-Mediated Metabolism of a Series of Aziridinylbenzoquinones and DNA Damage and Cytotoxicity. *Mol Pharm* 1992, *42* (3), 531-536.

(190) Skelly, J. V.; Sanderson, M. R.; Suter, D. A.; Baumann, U.; Read, M. A.; Gregory, D. S. J.; Bennett, M.; Hobbs, S. M.; Neidle, S., Crystal Structure of Human DT-Diaphorase: A Model for Interaction with the Cytotoxic Prodrug 5-(Aziridin-1-yl)-2,4-dinitrobenzamide (CB1954). *J Med Chem* 1999, *42* (21), 4325-4330.

(191) Winski, S. L.; Faig, M.; Bianchet, M. A.; Siegel, D.; Swann, E.; Fung, K.; Duncan, M. W.; Moody, C. J.; Amzel, L. M.; Ross, D., Characterization of a Mechanism-Based Inhibitor of NAD(P)H:Quinone Oxidoreductase 1 by Biochemical, X-ray Crystallographic, and Mass Spectrometric Approaches. *Biochem* 2001, *40* (50), 15135-15142.

(192) Phillips, R. M., Inhibition of DT-Diaphorase (NAD(P)H:Quinone Oxidoreductase, ec (1.6.99.2) by 5,6-dimethylxanthenone-4-acetic acid (DMXAA) and Flavone-8-acetic acid (FAA): Implications for Bioreductive Drug Development. *Biochem Pharmacol* 1999, *58* (2), 303-310.

(193) Lee, Y. Y.; Westphal, A. H.; de Haan, L. H. J.; Aarts, J. M. M. J. G.; Rietjens, I. M. C. M.; van Berkel, W. J. H., Human NAD(P)H:Quinone Oxidoreductase Inhibition by Flavonoids in Living Cells. *Free Radic Biol Med* 2005, *39* (2), 257-265.

(194) Colucci, M. A.; Reigan, P.; Siegel, D.; Chilloux, A.; Ross, D.; Moody, C. J., Synthesis and Evaluation of 3-Aryloxymethyl-1,2-dimethylindole-4,7-diones as Mechanism-Based Inhibitors of NAD(P)H:Quinone Oxidoreductase 1 (NQO1) Activity. *J Med Chem* 2007, *50* (23), 5780-5789.

(195) Reigan, P.; Colucci, M. A.; Siegel, D.; Chilloux, A.; Moody, C. J.; Ross, D., Development of Indolequinone Mechanism-Based Inhibitors of NAD(P)H:Quinone Oxidoreductase 1 (NQO1): NQO1 Inhibition and Growth Inhibitory Activity in Human Pancreatic MIA PaCa-2 Cancer Cells. *Biochem* 2007, *46* (20), 5941-5950.

(196) Siegel, D.; Gustafson, D. L.; Dehn, D. L.; Han, J. Y.; Boonchoong, P.; Berliner, L. J.; Ross, D., NAD(P)H:Quinone Oxidoreductase 1: Role as a Superoxide Scavenger. *Molecular Pharmacology* 2004, *65* (5), 1238-1247.

(197) Huang, S. T.; Lin, Y. L., New Latent Fluorophore for DT Diaphorase. *Org Lett* 2006, *8* (2), 265-268.

(198) Huang, S.-T.; Peng, Y.-X.; Wang, K.-L., Synthesis of a New Long-Wavelength Latent Fluorimetric Indicator for Analytes Determination in the DT-Diaphorase Coupling Dehydrogenase Assay System. *Biosens Bioelectron* 2008, *23* (12), 1793-1798.

(199) de Groot, F. M. H.; Loos, W. J.; Koekkoek, R.; van Berkom, L. W. A.; Busscher, G. F.; Seelen, A. E.; Albrecht, C.; de Bruijn, P.; Scheeren, H. W., Elongated Multiple Electronic Cascade and Cyclization Spacer Systems in Activatible Anticancer Prodrugs for Enhanced Drug Release. *J Org Chem* 2001, *66* (26), 8815-8830.

CHAPTER 2

SHEDDING LIGHT BY CANCER REDOX—HUMAN NAD(P)H:QUINONE OXIDOREDUCTASE-1 ACTIVATION OF A CLOAKED FLUOROPHORE DYE *

2.1 Introduction

Reductase enzymes associated with cancer have become an active area of research due to their presence being used to understand the cellular machinery of the disease and their potential for activation of prodrugs for disease therapies. NQO1 (DT-diaphorase, EC 1.6.99.2) is highly upregulated in cancer cells[1-3] and is found in the cytosol, Golgi complex, nucleus, mitochondria, cellular membrane, and endoplasmic reticulum, as well as extracellularly.[4-11] NQO1 catalyzes the 2-electron reduction of quinones to their hydroquinones using NADH or NADPH as an electron donor.[12-13] As a result, NQO1 is a focal point for cancer therapies utilizing bioactivatable prodrug quinones, including those that undergo rearrangement reactions[14-15] and quinones that are cleaved from a target drug upon reduction, thereby releasing the active drug target.[16-17] The lack of information on the effects of local environment on quinone prodrug activation and target drug release has slowed progress in this arena.[18-19] Thus, it is of great importance to develop and understand the behavior of triggerable reporter molecules that may allow for selective and sensitive detection of NQO1 activity and provide temporal and spatial feedback on quinone reduction and target release. Of the various routes to measure enzyme activity, cloaked or latent fluorophores are particularly attractive due to their triggerable off-on fluorescence.[20-22] This off-on activation mechanism provides superior signal-to-background ratio due to the low amount of signal the cloaked fluorophore gives off.[23-24] Discussed here is the delineation, synthesis, successful, and even unsuccessful use of a new cloaked reporter whose fluorescence is vastly increased upon its efficient human NQO1-catalyzed reductive de-cloaking.

* Portions of this chapter appear previously as Silvers, W.; Payne, A; McCarley, R., Chem. Comm. 2011, 47 (40), 11264-11266. Reproduced by permission of The Royal Society of Chemistry. Article.

Possible reasons for the unsuccessful use of this cloaked fluorophore in relation to in vitro analysis of NQO1 are analyzed and discussed, so as to provide insight for the future design and selection of fluorophores that may be created for cellular-based sensing.

2.2 Experimental Section

2.2.1 Materials and Methods

3-(3',6'-dioxo-2',4',5'-trimethylcyclohexa-1',4'-diene)-3,3-dimethylpropionic acid (Q_3PA, **1**) and rhodamine$_{110}$-morpholino urea (Rho-Morph) were prepared according to literature procedures.[21, 25] All chemicals were purchased from Sigma-Aldrich or Fisher Scientific and used as received. For column chromatography, a Biotage FlashMaster Personal (Biotage) was used with pre-packed 10 g silica gel columns. Fluorescence-based activity, quantum yield determination, and stability studies were performed on a Perkin Elmer LS55 fluorescence spectrometer in quartz cuvettes. Enzyme assays were performed using black plastic 96-well plates (BD Falcon brand) on a FLUOstar OPTIMA from BMG LABTECH. ^{1}H-NMR spectra were collected in $CDCl_3$ on a Bruker AV-400 spectrometer and ^{13}C-NMR spectra were collected in $CDCl_3$ on a Varian system 700 spectrometer. All NMR experiments were performed in deuterated solvents and the chemical shifts are reported in standard δ notation as parts per million using tetramethylsilane as an internal standard.

2.2.2 Cell Culture

HT-29 (human colorectal adenocarcinoma), A549 (human non-small cell lung cancer (NSCLC)), and H596 (human NSCLC) were all purchased from American Type Cell Culture. HT-29 cells were cultured in McCoy's 5A medium supplemented with 10% fetal bovine serum (FBS) and 100 IU/mL penicillin-streptomycin. A549 cells were cultured in F-12K medium supplemented with 10% FBS and 100 IU/mL penicillin-streptomycin. H596 cells were cultured

in RPMI-1640 supplemented with 10% FBS and 100 IU/mL penicillin-streptomycin. Cells were incubated at 37 °C in a humidified incubator containing 5% wt/vol carbon dioxide (CO_2).

2.2.3 Synthesis of Q_3-Rho-Morph

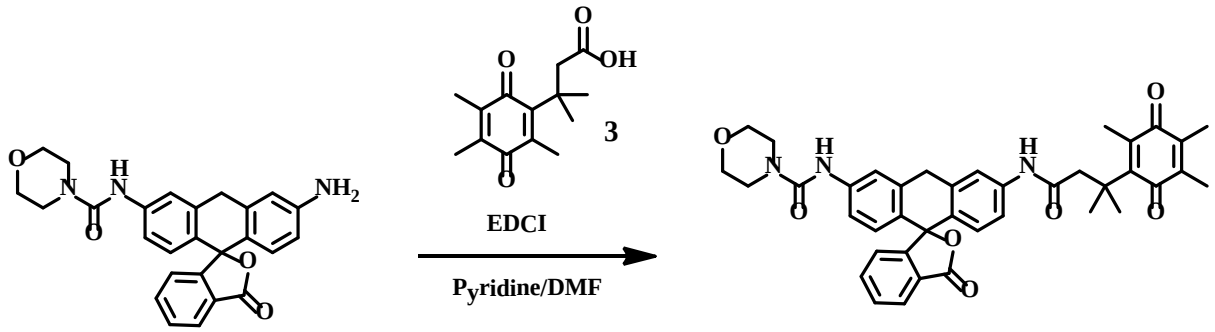

Scheme 2.1. Synthesis of Q_3-Rho-Morph (**1**).

Rho-Morph **2** (53.6 mg, 0.121 mmol) was dissolved in anhydrous DMF (0.9 mL) and anhydrous pyridine (0.6 mL) under Ar. To this was added EDCI (43.72 mg, 0.228 mmol) and Q_3PA **3** (74.91 mg, 0.299 mmol). This solution was stirred at room temperature for 24 hr. Solvent was removed under reduced pressure and the resulting residue was purified using column chromatography (1:1 DCM:ethyl acetate, R_f = 0.43) to give probe **1** as a yellow solid (27.8 mg, 34 %). ^{1}H-NMR (400 MHz, $CDCl_3$) δ (ppm): 1.51 (d, 4H, J = 4.2 Hz), 1.99 (d, 4H, J = 4.2 Hz), 2.18 (s, 3H), 3.05 (s, 3H), 3.53 (d, 4H, J = 2.5 Hz), 3.75 (d, 4H, J = 2.4 Hz), 6.61 (m, 2H), 6.95 (d, 1H, J = 4.8 Hz), 7.02 (m, 3H), 7.39 (d, 1H, J = 4.9 Hz), 7.60 (m, 2H), 7.88 (s, 1H), 7.98 (d, 1H, J = 4.2 Hz). ^{13}C-NMR (175 MHz, $CDCl_3$) δ (ppm): 12.2, 12.8, 14.3, 29.0, 38.4, 44.4, 50.2, 66.6, 83.4, 107.8, 107.8, 112.8, 114.0, 115.5, 115.8, 124.2, 125.0, 126.2, 128.2, 128.3, 129.9, 135.4, 138.1, 138.3, 139.9, 141.4, 143.4, 151.6, 151.7, 153.1, 154.9, 170.1, 170.9, 187.6, 191.5. ESI-MS: For $C_{39}H_{37}N_3O_8$: calculated m/z = 676.2659 $[M+H]^+$; observed m/z = 676.2656 $[M+H]^+$; 0.4 ppm error.

2.2.4 Stability of Q_3-Rho-Morph Against Biological Reductants

Stability studies against biological reductants were performed with a final concentration of probe **1** being 5.0×10^{-6} M, using quartz cuvettes (final volume of 3.0 mL) and a Perkin Elmer LS55 spectrophotometer (λ_{ex} = 490 nm and λ_{em} = 520 nm). The buffer used was 0.1 M PBS (pH = 7.4, 0.007% BSA, 0.1 M KCl). Stability against NADH was performed in a 100×10^{-6} M solution of NADH, with and without the presence of human NQO1 (5×10^{-5} g); the fluorescence intensity was monitored every 40 sec for 2.2 hr. Stability against biological reductants was tested by adding enough reductant to achieve a 1.0×10^{-3} M concentration for glutathione, ascorbic acid, and dithiothreitol, and 0.4 mM sodium dithionite, in a 5.0×10^{-6} M solution of compound **1** in buffer. The fluorescence intensity was monitored every 0.5 min for 6 hr.

2.2.5 NQO1 Assay of Compound Q_3-Rho-Morph

NQO1 assays for the conversion of probe **1** to dye **2** were performed by following fluorescence intensity (excitation at 485 nm and emission at 520 nm) every minute for at least 20 minutes using a FLUOstar OPTIMA instrument and Falcon 96-well plates (black with clear bottoms). Recombinant human NQO1 (Sigma-Aldrich) in pH 7.4, 0.1 M PBS and supplemented with 0.007% bovine serum albumin (BSA) was used. Stock solutions of compound **1** were prepared in ethanol and diluted in buffer to a final concentration between 2.5×10^{-6} and 60×10^{-6} M. Total volume per well was 200×10^{-6} L with a final NQO1 content of 1×10^{-5} g. Assays were initiated by the instrument-injection of NADH so as to yield a final NADH concentration of 100×10^{-6} M. The concentration of released **2** at any given time was determined from a fluorescence intensity vs. concentration calibration curve (Figure 2.1) for dye **2** in pH 7.4, 0.1 M PBS and 0.007% BSA. Rate versus [**1**] curves were fitted with a non-linear

least-squares algorithm so as to obtain K_m and V_{max} values using the computer program from Cleland.[26]

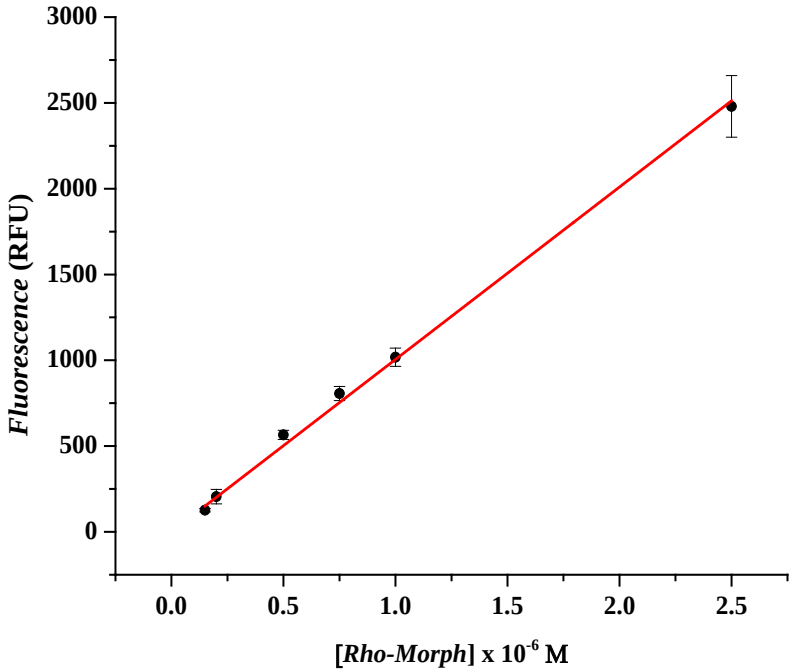

Figure 2.1. Calibration curve of Rho-Morph in pH 7.4, 0.1 M PBS supplemented with 0.007% BSA. Calibration was performed in a black clear bottom Falcon 96-well plate while exciting at λ_{ex} = 485 nm and observing the emission at λ_{em} = 520 nm.

2.2.6 Q_3-Rho-Morph Incubation in Cells and Post Incubation Analysis

A549, HT-29, and H596 cells were plated in sterile black plastic Falcon 96-well plates overnight to allow the cells to adhere to the bottom of the wells. Each cell line was plated in 4 different wells at ~95% confluency. The next day, the medium was removed and replaced with 10 μM Q_3-Rho-Morph in DMEM/F-12K medium supplemented with 10% FBS. Fluorescence analysis was performed using a FLUOStar Optima (BMG Labtech) at 37.0 °C scanning every 15 minutes for 16 hours, λ_{ex} = 485 and λ_{em} = 520 nm.

Post-analysis of the culture medium and cells was performed using the FLUOStar Optima, λ_{ex} = 485 and λ_{em} = 520 nm. The old medium from the experiment was removed and placed into

empty wells and fresh medium with no probe was added to the wells containing cells to analyze the fluorescence intensities from the cells and medium separately.

2.2.7 Live Cell Confocal Imaging

Confocal fluorescence images were acquired with a Leica TCS SP2 tandem scanning laser scanning microscope. Experiments were performed using a 40x oil immersion objective lens (1.25 NA). Imaging of DRAQ5 (nuclear stain) and Q_3-Rho-Morph—loaded cells was accomplished using a sequential scanning method with excitation via a 488 nm laser and collecting emitted light between 500 and 555 nm with a PMT voltage of 790 V. DRAQ5 was excited using a 633 nm laser and emitted light collected between 650 to 750 nm with a PMT voltage of 513 V. Images were frame averaged 6 times. HT-29, A549, and H596 cells were incubated overnight in black 35 x 10 mm, 22 mm well glass bottom dishes (Chemglass Life Sciences) in its complete growth medium at 37 °C with 5% CO_2. Prior to imaging, the medium was removed and replaced with F-12K medium (containing no phenol red) maintained at 37 °C. From a concentrated solution of Q_3-Rho-Morph in DMSO, the probe was added directly to the dish to give a concentration of 10 μM (while ensuring approximately 1% or less DMSO with respect to medium). Cells were incubated with Q_3-Rho-Morph for varying amounts of time. Five minutes prior to imaging, DRAQ5 was added from a stock solution in DMSO to give a concentration of 3.0 μM. Background for all images was removed in the same fashion using the Leica software LAS LF Lite. Image analysis was performed using ImageJ.

2.2.8 Formation of Dihydro-Rho-Morph

The reduction of Rho-Morph to Dihydro-Rho-Morph was carried out by mixing a 5 μM solution of Rho-Morph in 0.1 M PBS with 7 mg NADH (final concentration of 3.3 mM) and

observing the change in absorbance over time. Spectra were collected every hour for 6 hours between 400 and 600 nm on a Cary 50 Bio UV-Visible Spectrophotometer.

2.3 Results and Discussion

2.3.1 De-Cloaking of Q_3-Rho-Morph

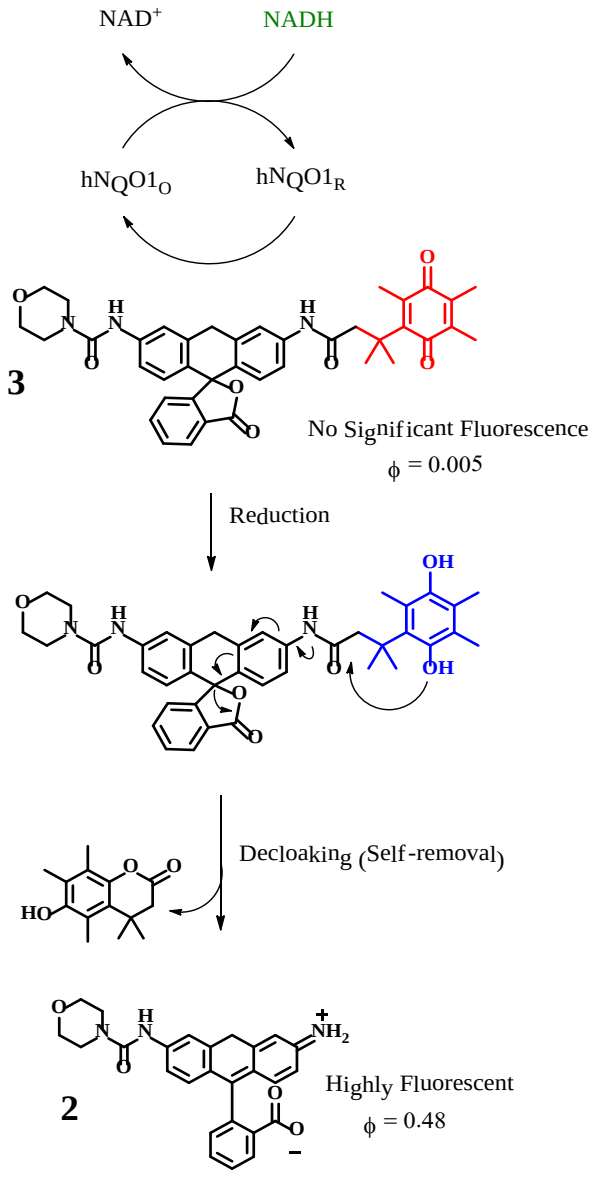

Figure 2.2. Activation of cloaked fluorophore **1** by human NQO1 to yield the highly fluorescent dye **2**.

The cloaked reporter Q_3-Rho-Morph is based on two fundamental units, namely an *N*-morpholino-capped rhodamine **2**[21] and a quinone propionic acid trigger group (Q_3PA),[27] Figure 2.2. Formation of the de-cloaked Rho-Morph occurs by Q_3PA trigger group removal, which is composed of two steps. Reductive activation of the Q_3PA trigger group of **1** can be initiated via chemical[27] or enzymatic routes to yield the trimethyl-locked[25] hydroquinone that subsequently undergoes self-removal to form the lactone and highly fluorescent **2**. As previously reported, the rate of lactone formation for the Q_3PA trigger group is relatively fast in buffered aqueous media, with a $t_{1/2}$ in the minutes time domain.[28] We designed the cloaked reporter **1** such that there are no concerns over removal of two trigger groups to yield the active reporter,[29-30] nor are there issues regarding additional slow chemical steps[31] to signal the presence of hNQO1 activity.

To ensure an off-on cloaked reporter system was produced, the emission spectra and quantum yield (Φ) values of probe Q_3-Rho-Morph and dye Rho-Morph were obtained in aqueous media at physiological pH (0.1 M phosphate-buffered saline, PBS, pH = 7.4) using Equation 2.1:

$$\Phi_F = \Phi_S \left(\frac{\int F_{em,F}}{\int F_{em,S}} \right) \qquad \textbf{Equation 2.1}$$

where Φ_F is the quantum yield of the dye, Φ_S is the quantum yield of the standard, $F_{em,F}$ is the integration of the fluorescence spectrum of the dye, and $F_{em,S}$ is the integration of the fluorescence spectrum for the standard.[32] Fluorescein was used as the standard with a quantum yield of Φ = 0.95.[21] Q_3-Rho-Morph exhibits little in the way of fluorescence emission as noted by its spectrum in Figure 2.3 and quantum yield of 0.005. However, Rho-Morph is strongly fluorescent with a quantum yield of 0.48, leading to a 96-fold difference in quantum efficiencies. This significant difference in quantum yields is quite sufficient to classify this reporter system as being off-on in nature.

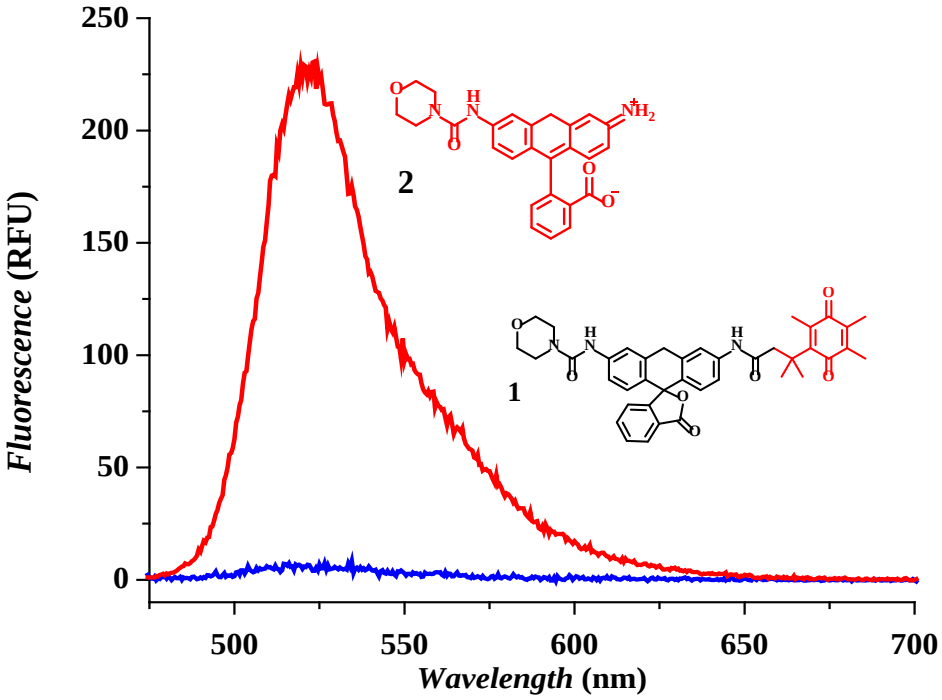

Figure 2.3. Fluorescence spectra of Q_3-Rho-Morph **1** (blue line) and Rho-Morph **2** (red line) in pH 7.4, 0.1 M PBS; concentrations of each were such so as to provide an absorbance of 0.047 at 465 nm. Excitation wavelength = 490 nm and emission wavelength = 520 nm.

2.3.2 Stability of Q_3-Rho-Morph

To assess the selectivity of the de-cloaking of probe Q_3-Rho-Morph, we investigated its stability under physiological solution conditions in the presence of various adventitious, potential reducing agents. Upon inspection of Figure 2.4, it is clear that probe **1** (5.0×10^{-6} M) is relatively unaffected while in the presence of high concentrations (1×10^{-3} M, 100-fold excess) of various reductants: ascorbic acid (AA, $E_{1/2}$ = 0.051 vs. SHE),[33] glutathione (GSH, $E_{1/2}$ = -0.22 V),[34] and dithiothreitol (DTT, $E_{1/2}$ = -0.33 V).[35] As a control, a strong reducing agent (sodium dithionite, 4×10^{-4} M final concentration) known to efficiently reduce the Q_3PA trigger group was added to a 5.0×10^{-6} M solution of probe **1** to provide a signal for ~100% activation of the probe. GSH and AA are found to have minimal effect (~3–4% activation at 8 min), while DTT caused a slightly higher (~8%) increase in fluorescence. Based on these results, cloaked probe **1** is highly stable

toward activation by possible biological interferents, such as glutathione that is known to be present at millimolar concentrations within cells and micromolar levels in the blood stream.[36-37]

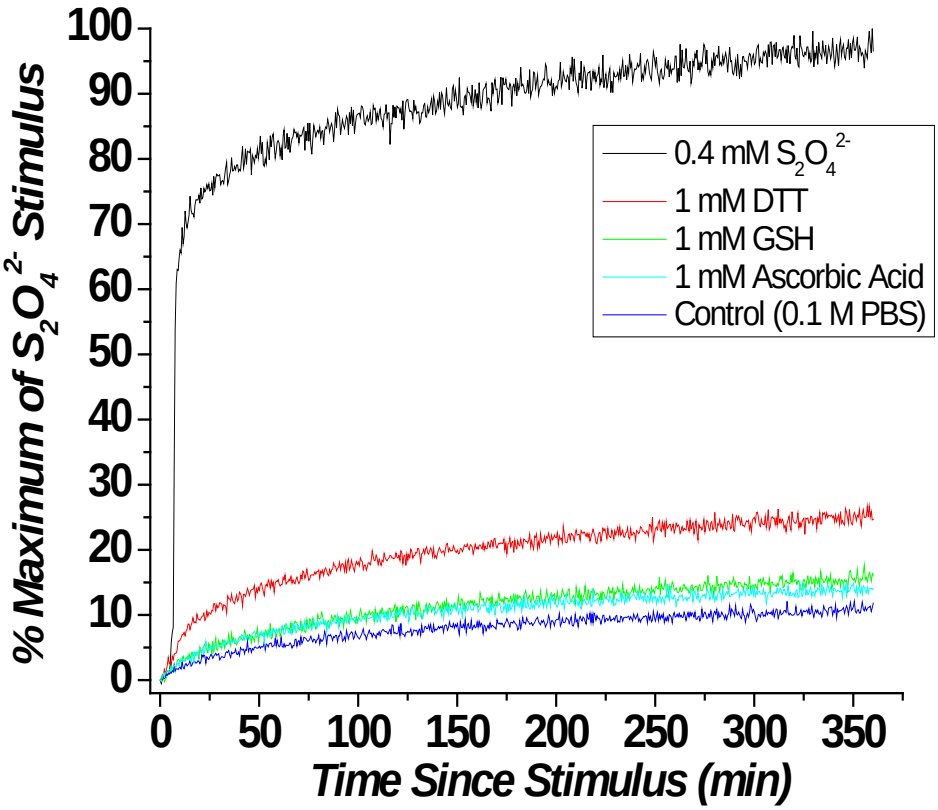

Figure 2.4. Fluorescence response of probe **1** (5.0×10^{-6} M) in pH 7.4, 0.1 M PBS while in the presence of 1×10^{-3} M DTT, AA, and GSH relative to the complete activation of **1** by 4×10^{-4} M sodium dithionite.

We determined the ability of hNQO1 to de-cloak **1** to yield dye **2** upon activation of the Q_3PA trigger group ($E_{p,c}$ = -0.28 V vs. SHE). Solutions of probe **1** exhibited a rapid increase in fluorescence after hNQO1 (5.0×10^{-5} g) was added (Figure 2.5), pointing to efficient de-cloaking of the dye by hNQO1. Under the same conditions in the absence of hNQO1, i.e. an aqueous solution containing only β-NADH cofactor (1×10^{-4} M; $E_{1/2}$ = -0.31 V)[38] in 0.1 M PBS, there was no evidence for hydrolytic or NADH-based activation of cloaked reporter **1**. Thus, cloaked reporter **1** can be used to quickly detect hNQO1 activity.

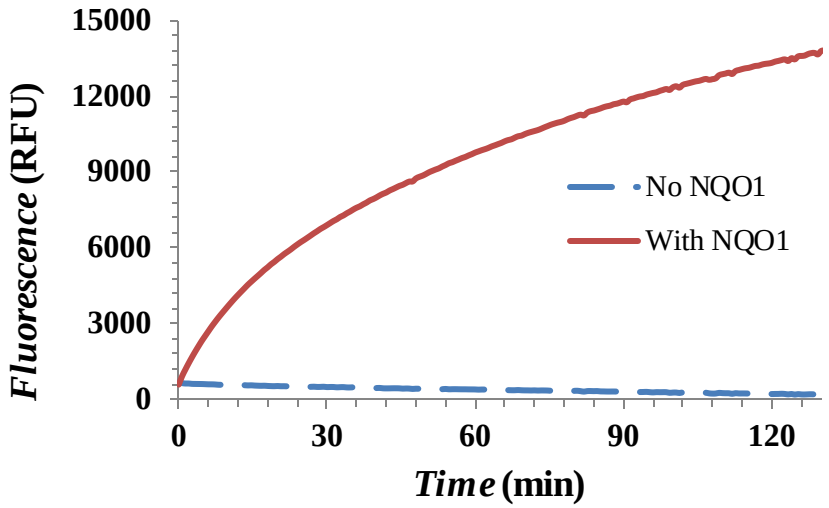

Figure 2.5. Fluorescent signal from the activation of 5.0 × 10^{-6} M **1** in a 1 × 10^{-4} M solution of NADH in the presence and absence of recombinant human NQO1 (5 × 10^{-5} g, 8 × 10^{-6} M) in pH 7.4, 0.1 M PBS with 0.007% bovine serum albumin. Excitation wavelength = 490 nm and emission wavelength = 520 nm.

2.3.3 Q_3-Rho-Morph Substrate Analysis With hNQO1

In order to quantitatively evaluate the ability of hNQO1 to activate **1** with time, kinetic parameters were obtained for hNQO1 based on the release of **2**. The amount of **2** present was obtained by observing the intensity of its fluorescence (λ_{ex} = 485 nm and λ_{em} = 520 nm) and converting this to a concentration by use of a calibration curve for **2**, which was linear over the concentration ranges studied. Monitoring fluorescent product formation is a common approach for enzymatic activation of cloaked fluorophores.[22, 39] The initial rate of product formation V was obtained for **2** concentrations of 2.5–60 × 10^{-6} M and then plotted as a function of [**1**], as presented in Figure 2.6. Kinetic parameters were determined by non-linear, least-squares fitting of the data in Figure 2.6 to the Michaelis–Menten equation.[26] The Michaelis constant (K_m) value was determined to be 23.7 ± 3.5 μM, maximum velocity (V_{max}) was 0.00214 ± 0.00013 μmol min^{-1} mg·$NQO1^{-1}$, catalytic activity (k_{cat}) was 0.00110 ± 0.00007 $sec,^{-1}$ catalytic efficiency (k_{cat}/K_m) was 46.4 ± 7.4 M^{-1} sec^{-1}, and the error from fitting was χ^2 =5.6 × 10^{-9},. Based on the values for V_{max}, k_{cat}, and k_{cat}/K_m, it can be concluded that Q_3-Rho-Morph is a good substrate

(though not the best) for hNQO1 when compared to substrates containing the same Q_3PA activatable group.[17, 29, 31] The cause for lower catalytic efficiency could be in part due to the bulky rhodamine$_{110}$ species to which the Q_3PA is directly conjugated. This steric hindrance would potentially slow the rate at which Q_3-Rho-Morph moves into the active site in hNQO1.

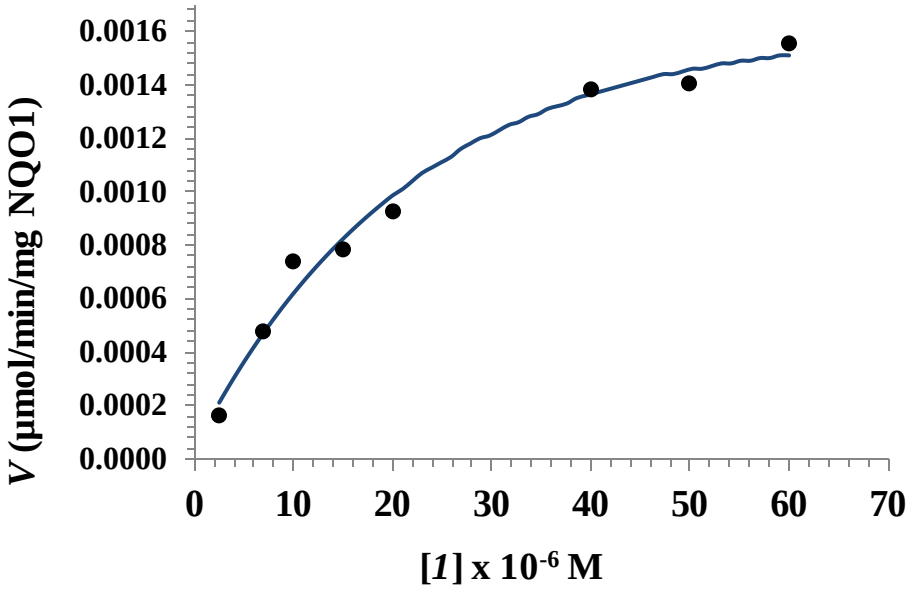

Figure 2.6. Kinetic plot for recombinant human NQO1 (1×10^{-5} g) towards **1** in pH 7.4, 0.1 M PBS, and 0.007% bovine serum albumin. Solid blue line indicates best fit to Michaelis–Menten equation.

2.3.4 hNQO1 Sensor Using Q_3-Rho-Morph

With the evidence that Q_3-Rho-Morph is activated by hNQO1, is stable towards certain biological reductants, and has a large 96-fold fluorescence enhancement (FE), we set out to determine if the dye could be used as an hNQO1 sensor in cancer cells. First, a simple test was used to determine if cells known to contain hNQO1 could significantly activate Q_3-Rho-Morph when compared to cells devoid of hNQO1. The three cell lines used had been previously studied for hNQO1 activity and are: HT-29 (colorectal carcinoma, hNQO1-positive), A549 (NSCLC, hNQO1-positive), and H596 (NSCLC, hNQO1-negative).[14, 40] When in the presence of 10 μM Q_3-Rho-Morph, an almost linear increasing fluorescence was found for not only the two positive

cells lines, but also the negative cell and even the medium (though only a 1.5-fold increase), Figure 2.7.

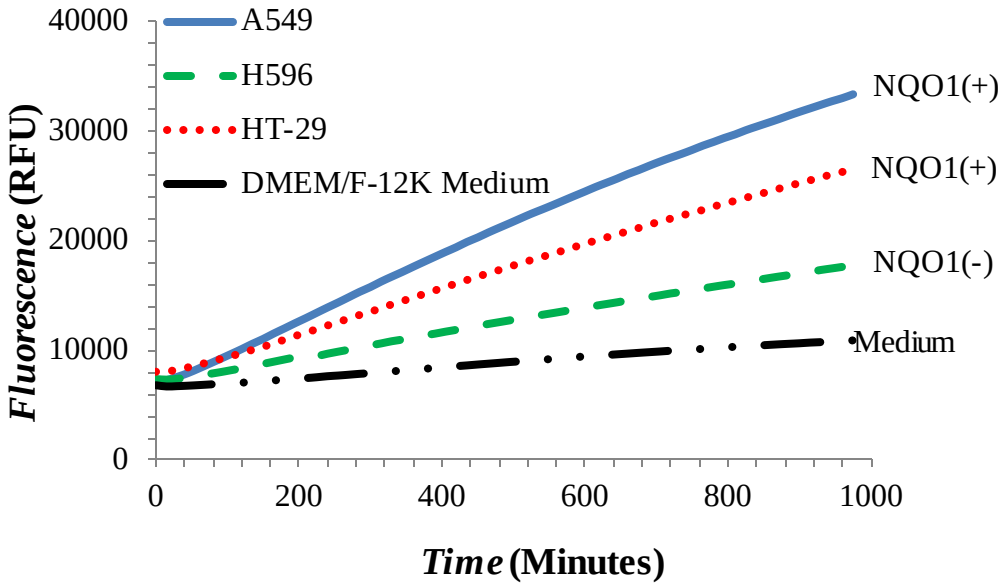

Figure 2.7. Following the fluorescence in HT-29 cells (red, dot), A549 cells (blue, solid), H596 cells (green, dash), and DMEM/F-12K with 10% fetal bovine serum (black, dot-dot, dash) when in the presence of 10 μM Q_3-Rho-Morph. Samples were scanned every 15 minutes over a 16 hour period with λ_{ex} = 485 nm and λ_{em} = 520 nm.

Based on the fact that there was a significant increase in signal over 16 hours for A549 (4.8-fold increase) and HT-29 (3.3-fold increase), it is believed that the increase is due to conversion of Q_3-Rho-Morph to Rho-Morph. Over the same time period, an increase in fluorescence was also found for the negative cell line H596 (2.6-fold increase) and also the dye in complete DMEM/F-12K growth medium (1.6-fold increase).

To again assess the applicability of Q_3-Rho-Morph as a rapid sensor for hNQO1 in cancer cells, confocal imaging was performed on HT-29, A549, and H596 cells lines after incubation with the probe. Cells were always cultured overnight and plated at ~80% confluency in the imaging dishes to allow for adhesion of the cells to the glass bottom. To simplify the imaging process, the culture medium containing dye was never removed from the wells and the cells were never washed prior to observing the cells under the confocal microscope. The first

complication was found to be the amount of weak signal arising intracellularly. It was found that the only way to achieve usable images was to use a high (790 V) PMT detector voltage, which also produced signal from the probe in the medium. Secondly, there was no differentiation between the two cell lines (HT-29 and A549) known to contain hNQO1 and the cell line (H596) which is devoid of the enzyme. As seen in Figure 2.8, all three cell lines essentially look the same (with minimal background removed using the imaging software) with respect to the amount of green signal, which is derived from the excitation at 488 nm. The nuclei are blue in each image. Using the program ImageJ, the relative average cytosolic intensities for each cell line were determined from the images in Figure 2.8. HT-29 (**A**) was found to have an average intensity at 11.4, A549 (**B**) at 22.5, and H596 (**C**) at 17.1. These values confirm the fact that A549 and HT-29 cannot be distinguished from H596. This type of experiment was performed multiple times with varying concentrations of Q_3-Rho-Morph and varying incubation times, all leading to similar images where no cell line could be labeled as "hNQO1-positive" or "hNQO1-negative".

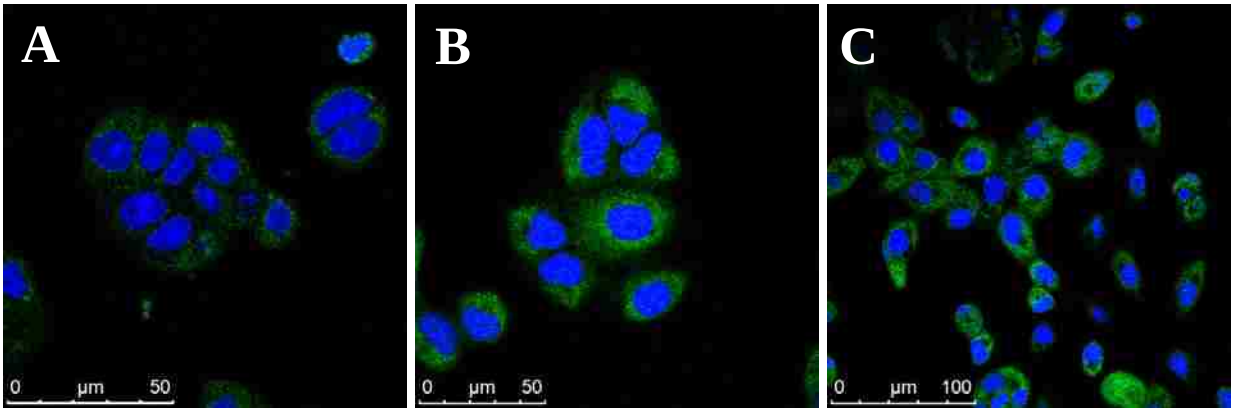

Figure 2.8. Confocal imaging of HT-29 (A), A549 (B), and H596 (C) cells after a one hour incubation with 10 μM Q_3-Rho-Morph (green). Cells were all stained with 3.0 μM DRAQ5, which is labeled in blue. Cells were imaged using 488 nm and 633 nm lasers to excite Rho-Morph and DRAQ5, respectively.

It was next illustrated that changing certain variables, such as incubation time, would lead to similar results as seen in Figure 2.8. To do this, we incubated A549 and H596 cells with Q_3-Rho-Morph for 24 and 72 hours and obtained fluorescence images at each time period, Figure 2.9.

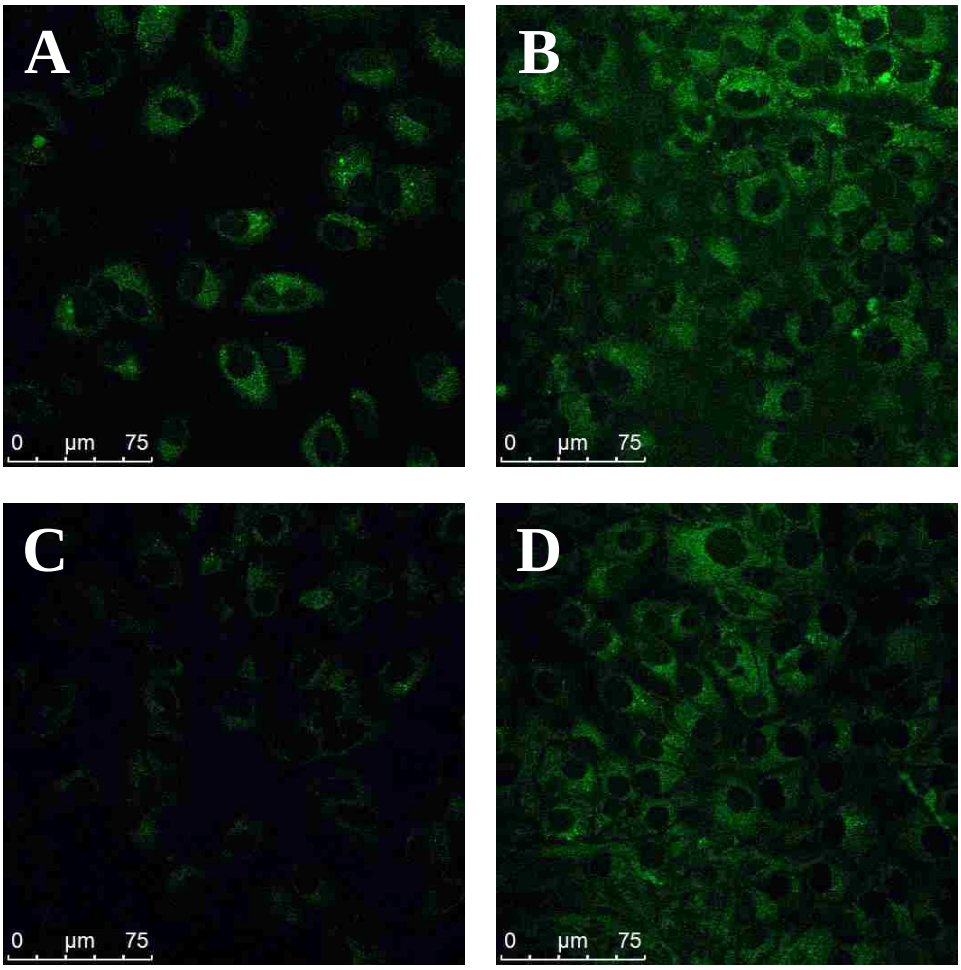

Figure 2.9. Confocal imaging of A549 cells after 24 and 72 hours of incubating with Q_3-Rho-Morph, A and B respectively, and H596 cells after 24 and 72 hours of incubating with Q_3-rho-Morph, C and D respectively. Cells were imaged while exciting at 488 nm, represented by green in each image.

It is clearly visible that the intensities in both cell lines increase from 24 to 72 hours, but A549 never obtains substantially more signal than H596. Using ImageJ to analyze the cytosolic signal of each image, values for A549 at 24 hours and 72 hours were found to be 18.0 and 32.9,

respectively. Values for H596 at 24 hours and 72 hours were found to be 11.3 and 23.2, respectively. Also of note, the PMT detector voltage was left the same between the two incubation periods which indicates a lack of formation or accumulation of Rho-Morph in the cells. This lack of intense signal leads me to believe there is either no (or very little) activation to Rho-Morph, degradation of Q_3-Rho-Morph, or efflux/quenching of Rho-Morph in the hNQO1 positive cell lines.

2.3.5 Elucidating the Negatives of Q_3-Rho-Morph

To try and elucidate the mechanism(s) for which Q_3-Rho-Morph failed to be used as an in vitro hNQO1 sensor, several experiments were performed involving stability of Q_3-Rho-Morph and Rho-Morph. First, the stability of Q_3-Rho-Morph was tested at a low pH (4.0) to determine if there was any degradation due to the low pH of acidic compartments in cells. A 10 μM solution of Q_3-Rho-Morph was made in pH 4.0, 0.1 M PBS and fluorescence was checked for 16 hours while exciting at 485 nm and following the emission at 520 nm. As seen in Figure 2.10, there is no significant change in fluorescence. In fact, the change that does occur is similar to the results in Figure 2.4. Over the first 15 minutes, an increase of 4% is seen and 14% over the first hour. This provides evidence that low intracellular pH would not degrade the sensor and thus lead to little gain in fluorescence when imaging.

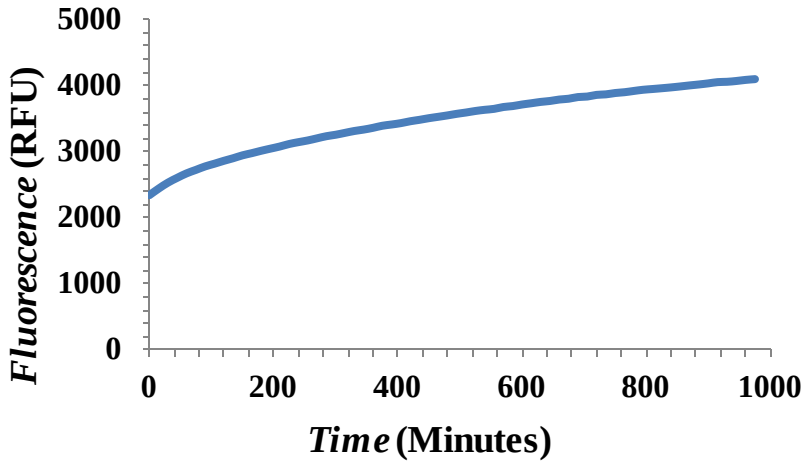

Figure 2.10. Following the fluorescence of Q_3-Rho-Morph over time while in pH 4.0, 0.1 M PBS. λ_{ex} = 485 nm and λ_{em} = 520, scanning every 15 minutes for 16 hours.

The next goal was to try and determine the fate of Rho-Morph after its production in the hNQO1-positive cell lines. Though Q_3-Rho-Morph was found to be stable towards biological reductants, Rho-Morph was tested against one of the more prevalent intracellular reducing species, NADH. NADH has a reduction potential of -0.31 V and the concentration in human breast cancer cells has been calculated to be 168 ± 49 μM.[38, 41] A 5 μM solution of Rho-Morph was made up in pH 7.4, 0.1 M PBS, and NADH was added to give a concentration of 100 μM. From this, fluorescence intensity was followed over time. In Figure 2.11, it is seen that NADH rapidly reduces the signal from Rho-Morph. One hour after the addition of NADH, Rho-Morph produces 30% less fluorescence. This is a significant reduction in signal with a relatively low NADH concentration, as compared to intracellular concentrations.

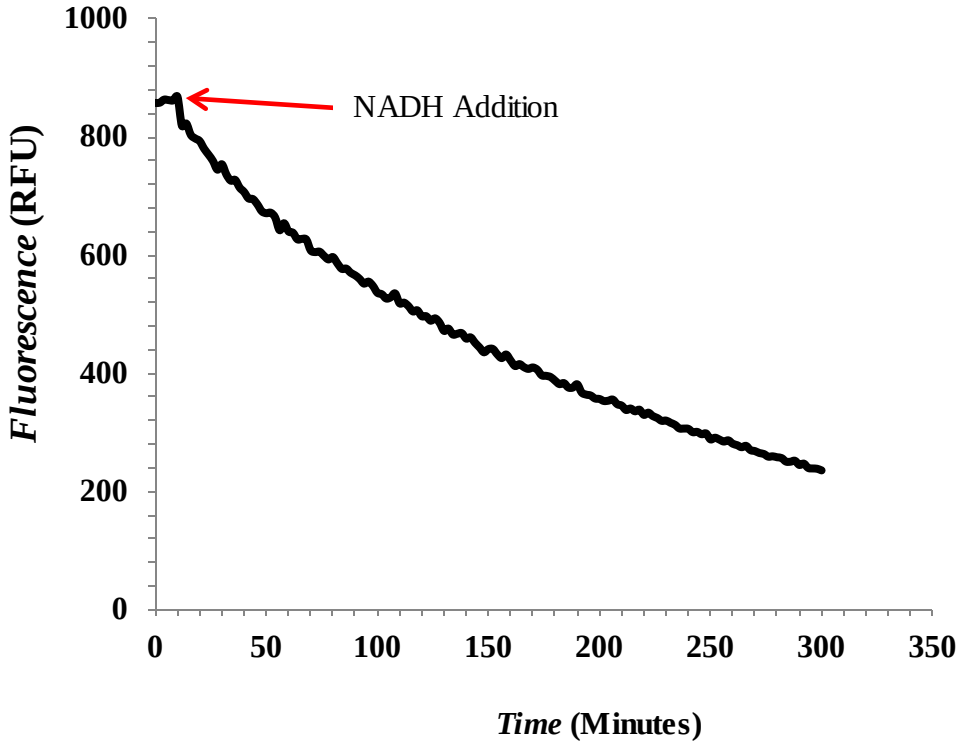

Figure 2.11. Observing the signal reduction of a 5 μM solution of Rho-Morph in pH 7.4, 0.1 M PBS with 100 μM NADH. Sample was scanned every 5 minutes over 5 hours, λ_{ex} = 490 nm and λ_{em} = 520 nm.

Observing that the signal decreases over time after NADH is introduced also shows the reduction of fluorescence of Rho-Morph is most likely not a photophysical property, but rather a chemical interaction between the two compounds. Similar nonfluorescent "dihydro" forms of rhodamine and fluorescein dyes were found to have been patented and are currently commercially available for the detection of intracellular reactive oxygen species.[42] These dyes were synthesized by the reduction of the parent dye via sodium borohydride in buffer until no absorption band (λ = 490 nm) appeared, after which the dye was diluted as is and used immediately in cell studies. After being re-oxidized, these sensors regained their fluorescence. It was postulated Rho-Morph was undergoing a similar reduction by NADH, Scheme 2.2.

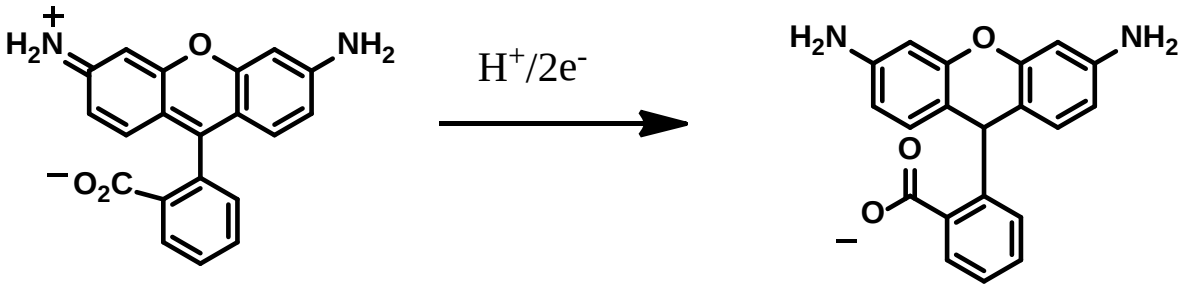

Scheme 2.2. Possible conversion of the quinoid version of Rho-Morph to a Dihydro-Rho-Morph species via reduction by NADH.

To test this theory, a 5 μM solution of Rho-Morph in pH 7.4, 0.1 M PBS was added sufficient NADH to give a final concentration of 3.3 mM. The absorbance spectrum was scanned over a 6 hour period in one hour intervals in the region where Rho-Morph is excited (400-600 nm), Figure 2.12. As seen below, the absorbance diminished to 3% of its original absorbance at λ = 485. After the first hour, the absorbance at λ = 485 nm had dropped by 43%, and 71% after the first 2 hours. This observation of reduction and absorbance decrease leads to the conclusion that the Dihydro-Rho-Morph is not be fluorescent, similar to the commercially available dyes.

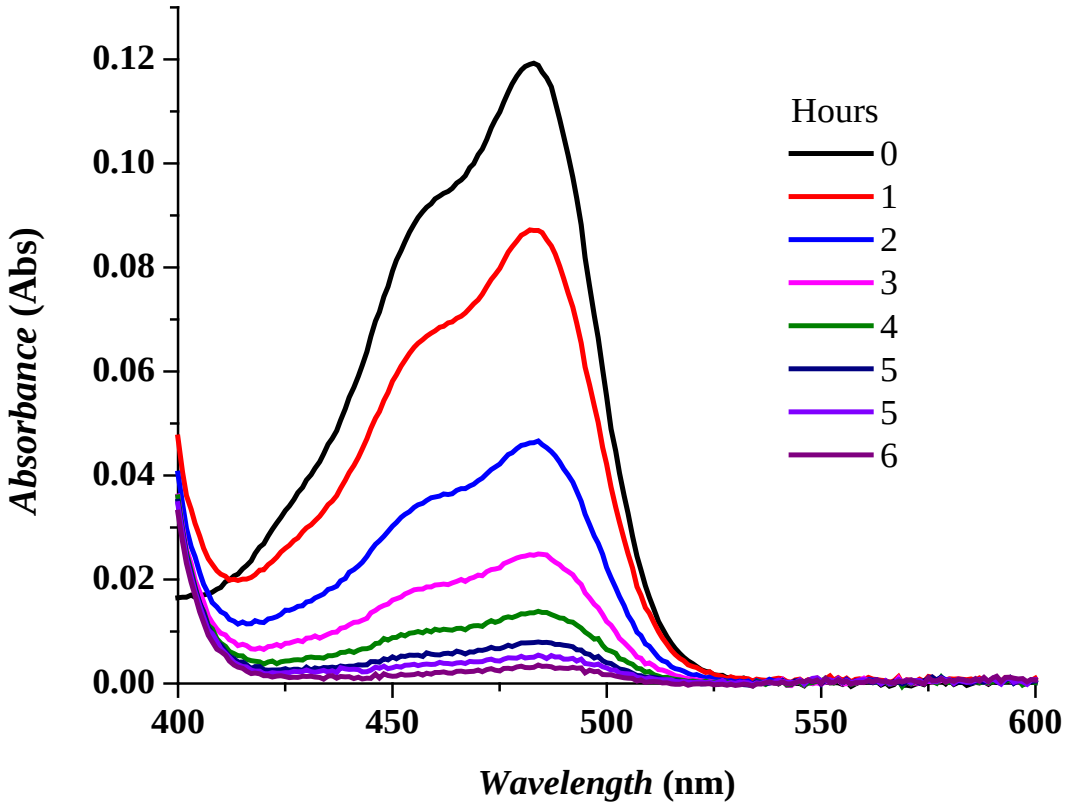

Figure 2.12. Observing the reduction and change in absorbance of Rho-Morph to Dihydro-Rho-Morph via reduction in a 3.3 mM solution of NADH.

Though NADH is not as strong as a reducing agent as sodium borohydride, we speculated the electron withdrawing urea group on Rho-Morph would sufficiently lower the reduction potential of the dye allowing Rho-Morph to be reduced by NADH at higher concentrations. This formation of Dihydro-Rho-Morph intracellularly would be in competition with the formation of Rho-Morph from Q_3-Rho-Morph and the re-oxidation of Dihydro-Rho-Morph into its fluorescent form.

A reason why Q_3-Rho-Morph possibly failed as an in vitro sensor could be due to the specific form that Rho-Morph exists while being intracellular that was published by Watkins et al.[43] Their group discovered a perturbation in the equilibrium of the rhodamine quinoid and lactone species when rhodamine was mono-conjugated with an electron withdrawing group, such

as a urea bond, Scheme 2.3. This created a shift towards the cell membrane permeant/non-fluorescent lactone form. This issue explains the lack of dye accumulation in the hNQO1-positive cell lines and the need to image with a high PMT detector voltage. This theory was tested by removing the medium from the wells after the end of experiment in Figure 2.7 and measuring the fluorescence of the medium and cells and comparing the two values to determine if a majority of the dye signal was present in medium. At the end of that experiment, wells containing A549 cells and the used medium had an average intensity of 33,347; HT-29 had 26,541, and 17,758 relative fluorescence units (RFU). After removing the old medium and placing it in an empty well, the signal arising from the cells with fresh medium and also the old medium by itself was measured, with the results in Table 2.1. From the data collected, it was found that the intensity of A549 cells was only 3.4% of that from the used medium. Similar results were found for HT-29 and H596 cells, 7.4% and 6.0% respectively. First observations were that the intensities were higher when measuring the fluorescence from the old medium with no cells compared to the values obtained at the end of the incubation period with the cells. This can be attributed to the bottom-read nature of the FLUOStar Optima and that the cell layer was most likely acting as a filter between the detector and medium. It is also clear that the signal attributed to the cells with fresh medium was low for all cell lines, demonstrating the lack of accumulation of Rho-Morph in each cell line. While the signal from the old A549 medium is significantly higher (55%) than that derived from the H596 cells, the HT-29 medium signal was only 15% higher than that of H596. These old medium intensities are similar to what was seen in Figure 2.7, leading to a very plausible efflux mechanism to which Rho-Morph shifts to the lactone form and moves from intracellular to extracellular.

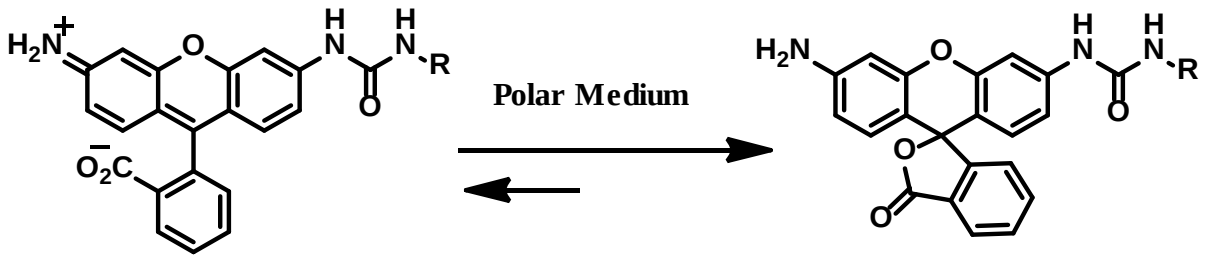

Scheme 2.3. Shift in equilibrium from the fluorescent quinoid form to the non-fluorescent/membrane permeable lactone form.

Table 2.1. Summary of fluorescence intensities in cells and culture medium after incubating in culture medium containing 10 μM Q_3-Rho-Morph for 16 hours. λ_{ex} = 485 and λ_{em} = 520 nm. Units are in RFU.

Cells Only			Old Medium		
A549	**H596**	**HT-29**	**A549**	**H596**	**HT-29**
1804	1275	1835	46888	21184	24890

2.4 Conclusions

Based on the data presented here, we have clearly demonstrated that the turning on (de-cloaking) of the new cloaked fluorophore Q_3-Rho-Morph under physiological solution conditions is sensitive to the presence of hNQO1, while the de-cloaking is sufficiently selective with regard to the presence of potential interferents. Importantly, Q_3-Rho-Morph was designed to utilize ‘‘single-hit’’ enzyme activation; in other words, only a single stimulus is required to cause signal transduction (the release of Rho-Morph). In addition, the signal revealing process for the activated species is efficient, as it requires only one step (hydroquinone lactonization). Though the biological stability of Q_3-Rho-Morph and the photophysical properties of Rho-Morph were promising as an in vitro sensor, there were unforeseen pitfalls with the Rho-Morph scaffold that led to the inability to use Q_3-Rho-Morph in cellular studies. One shortcoming was

found to be the formation of a nonfluorescent Dihydro-Rho-Morph species following the reduction of Rho-Morph by NADH. Another issue with Rho-Morph was published by Watkins et al.[43] and leads to the postulation that in the presence of polar media, Rho-Morph favors a nonfluorescent/cell membrane permeable lactone form over the fluorescent quinoid form. This is due to the electron withdrawing urea group on one side of the xanthene ring system. Though Q_3-Rho-Morph is not suitable for intracellular hNQO1 sensing, it is quite useful for enzymology studies with hNQO1 due to the single-hit activation mechanism and the large FE from the quenched dye to the de-quenched dye. It also has provided invaluable information in regards to the future design of cloaked fluorescent sensors, regardless of the specific activation mechanism.

2.5 References

(1) Cresteil, T.; Jaiswal, A. K., High Levels of Expression of the NAD(P)H:Quinone Oxidoreductase (NQO1) Gene in Tumor Cells Compared to Normal Cells of the Same Origin. *Biochem Pharmacol* 1991, *42* (5), 1021-1027.

(2) Fitzsimmons, S. A.; Workman, P.; Grever, M.; Paull, K.; Camalier, R.; Lewis, A. D., Reductase Enzyme Expression Across the National Cancer Institute Tumor Cell Line Panel: Correlation With Sensitivity to Mitomycin C and EO9. *J Natl Cancer Inst* 1996, *88* (5), 259-269.

(3) Malkinson, A. M.; Siegel, D.; Forrest, G. L.; Gazdar, A. F.; Oie, H. K.; Chan, D. C.; Bunn, P. A.; Mabry, M.; Dykes, D. J.; Harrison, S. D.; Ross, D., Elevated DT-diaphorase Activity and Messenger RNA Content in Human Non-Small Cell Lung Carcinoma: Relationship to the Response of Lung Tumor Xenografts to Mitomycin C. *Cancer Res* 1992, *52* (17), 4752-4757.

(4) Das, M.; Rastogi, S.; Khanna, S. K., Mechanism to Study 1:1 Stoichiometry of NADPH and Alkoxyphenoxazones Metabolism Spectrophotometrically in Subcellular Biological Preparations. *Biochim Biophys Acta* 2004, *1675* (1–3), 1-11.

(5) Edlund, C.; Elhammer, A.; Dallner, G., Distribution of Newly Synthesized DT-Diaphorase in Rat Liver. *Biosci Rep* 1982, *2* (11), 861-865.

(6) Winski, S. L.; Koutalos, Y.; Bentley, D. L.; Ross, D., Subcellular Localization of NAD(P)H:Quinone Oxidoreductase 1 in Human Cancer Cells. *Cancer Res* 2002, *62* (5), 1420-1424.

(7) Nakamura, M.; Hayashi, T., One- and Two-Electron Reduction of Quinones by Rat Liver Subcellular Fractions. *J Biochem* 1994, *115* (6), 1141-1147.

(8) Appelt, L. C.; Reicks, M. M., Soy Induces Phase II Enzymes but Does Not Inhibit Dimethylbenz[a]anthracene-Induced Carcinogenesis in Female Rats. *J Nutr* 1999, *129* (10), 1820-1826.

(9) Prochaska, H. J.; Fernandes, C. L., Elevation of Serum Phase-III Enzymes by Anticarcinogenic Enzyme Inducers - Markers for a Chemoprotected State. *Carcinogenesis* 1993, *14* (12), 2441-2445.

(10) Siegel, D.; McGuinness, S. M.; Winski, S. L.; Ross, D., Genotype-Phenotype Relationships in Studies of a Polymorphism in NAD(P)H : Quinone Oxidoreductase 1. *Pharmacogenetics* 1999, *9* (1), 113-121.

(11) Sreerama, L.; Hedge, M. W.; Sladek, N. E., Identification of a Class 3 Aldehyde Dehydrogenase in Human Saliva and Increased Levels of This Enzyme, Glutathione S-transferases, and DT-Diaphorase in the Saliva of Subjects Who Continually Ingest Large Quantities of Coffee or Broccoli. *Clin Cancer Res* 1995, *1* (10), 1153-1163.

(12) Ernster, L.; Ljunggren, M.; Danielson, L., DT Diaphorase 1. Purification From Soluble Fraction of Rat-Liver Cytoplasm, and Properties. *Biochim Biophys Acta* 1962, *58* (2), 171-188.

(13) Ross, D.; Kepa, J. K.; Winski, S. L.; Beall, H. D.; Anwar, A.; Siegel, D., NAD(P)H : Quinone Oxidoreductase 1 (NQO1): Chemoprotection, Bioactivation, Gene Regulation and Genetic Polymorphisms. *Chem Biol Interact* 2000, *129* (1-2), 77-97.

(14) Beall, H. D.; Murphy, A. M.; Siegel, D.; Hargreaves, R. H.; Butler, J.; Ross, D., Nicotinamide Adenine Dinucleotide (Phosphate): Quinone Oxidoreductase (DT-diaphorase) as a Target for Bioreductive Antitumor Quinones: Quinone Cytotoxicity and Selectivity in Human Lung and Breast Cancer Cell Lines. *Mol Pharmacol* 1995, *48* (3), 499-504.

(15) Danson, S.; Ward, T. H.; Butler, J.; Ranson, M., DT-Diaphorase: A Target for New Anticancer Drugs. *Cancer Treat Rev* 2004, *30* (5), 437-449.

(16) Flader, C.; Liu, J. W.; Borch, R. F., Development of Novel Quinone Phosphorodiamidate Prodrugs Targeted to DT-Diaphorase. *J Med Chem* 2000, *43* (16), 3157-3167.

(17) Volpato, M.; Abou-Zeid, N.; Tanner, R. W.; Glassbrook, L. T.; Taylor, J.; Stratford, I.; Loadman, P. M.; Jaffar, M.; Phillips, R. M., Chemical Synthesis and Biological Evaluation of a NAD(P)H:quinone Oxidoreductase-1 Targeted Tripartite Quinone Drug Delivery System. *Molecular cancer therapeutics* 2007, *6* (12 Pt 1), 3122-3130.

(18) Chen, Y.; Hu, L., Design of Anticancer Prodrugs for Reductive Activation. *Medicinal Research Reviews* 2009, *29* (1), 29-64.

(19) Wilson, W. R.; Hay, M. P., Targeting Hypoxia in Cancer Therapy. *Nat Rev Cancer* 2011, *11* (6), 393-410.

(20) Johnsson, N.; Johnsson, K., Chemical Tools for Biomolecular Imaging. *ACS Chemical Biology* 2007, *2* (1), 31-38.

(21) Lavis, L. D.; Chao, T.-Y.; Raines, R. T., Fluorogenic Label for Biomolecular Imaging. *ACS Chem Bio* 2006, *1* (4), 252-260.

(22) Beija, M.; Afonso, C. A. M.; Martinho, J. M. G., Synthesis and Applications of Rhodamine Derivatives as Fluorescent Probes. *Chem Soc Rev* 2009, *38* (8), 2410-2433.

(23) Qian, X.; Xiao, Y.; Xu, Y.; Guo, X.; Qian, J.; Zhu, W., "Alive" Dyes as Fluorescent Sensors: Fluorophore, Mechanism, Receptor and Images in Living Cells. *Chem Commun* 2010, *46* (35), 6418-6436.

(24) Razgulin, A.; Ma, N.; Rao, J., Strategies for in vivo Imaging of Enzyme Activity: An Overview and Recent Advances. *Chem Soc Rev* 2011, *40* (7), 4186-4216.

(25) Carpino, L. A.; Triolo, S. A.; Berglund, R. A., Reductive Lactonization of Strategically Methylated Quinone Propionic Acid Esters and Amides. *J Org Chem* 1989, *54* (14), 3303-3310.

(26) Cleland, W. W., Computer Programmes for Processing Enzyme Kinetic Data. *Nature* 1963, *198* (487), 463-465.

(27) Ong, W.; Yang, Y.; Cruciano, A. C.; McCarley, R. L., Redox-Triggered Contents Release from Liposomes. *J Am Chem Soc* 2008, *130* (44), 14739-14744.

(28) Ong, W.; McCarley, R. L., Chemically and Electrochemically Mediated Release of Dendrimer End Groups. *Macromolecules* 2006, *39* (21), 7295-7301.

(29) Huang, S. T.; Lin, Y. L., New Latent Fluorophore for DT Diaphorase. *Org Lett* 2006, *8* (2), 265-268.

(30) Chandran, S. S.; Dickson, K. A.; Raines, R. T., Latent Fluorophore Based on the Trimethyl Lock. *J Am Chem So* 2005, *127* (6), 1652-1653.

(31) Huang, S.-T.; Peng, Y.-X.; Wang, K.-L., Synthesis of a New Long-Wavelength Latent Fluorimetric Indicator for Analytes Determination in the DT-Diaphorase Coupling Dehydrogenase Assay System. *Biosens Bioelectron* 2008, *23* (12), 1793-1798.

(32) Fery-Forgues, S.; Lavabre, D., Are Fluorescence Quantum Yields So Tricky to Measure? A Demonstration Using Familiar Stationery Products. *J Chem Ed* 1999, *76* (9), 1260.

(33) Ball, E. G., Studies on Oxidation-Reduction XXIII. Ascorbic Acid. *J Biol Chem* 1937, *118* (1), 219-239.

(34) Reipa, V., Direct Spectroelectrochemical Titration of Glutathione. *Bioelectrochem* 2004, *65* (1), 47-49.

(35) Hutchison, R. S.; Ort, D. R., Measurement of Equilibrium Midpoint Potentials of Thiols/Disulfide Regulatory Groups on Thioredoxin-Activated Chloroplast Enzymes. *Biothiols, Pt B* 1995, *252*, 220-228.

(36) Meister, A.; Anderson, M. E., Glutathione. *Annual Review of Biochemistry* 1983, *52*, 711-760.

(37) Pacsial-Ong, E. J.; McCarley, R. L.; Wang, W.; Strongin, R. M., Electrochemical Detection of Glutathione Using Redox Indicators. *Anal Chem* 2006, *78* (21), 7577-7581.

(38) Carlson, B. W.; Miller, L. L., Mechanism of the Oxidation of NADH by Quinones - Energetics of One-Electron and Hydride Routes. *J Am Chem Soc* 1985, *107* (2), 479-485.

(39) Weinstain, R.; Segal, E.; Satchi-Fainaro, R.; Shabat, D., Real-Time Monitoring of Drug Release. *Chem Commun* 2010, *46* (4), 553-555.

(40) Smitskamp-Wilms, E.; Hendriks, H. R.; Peters, G. J., Development, Pharmacology, Role of DT-Diaphorase and Prospects of the Indoloquinone EO9. *Gen Pharmacol* 1996, *27* (3), 421-429.

(41) Yu, Q.; Heikal, A. A., Two-Photon Autofluorescence Dynamics Imaging Reveals Sensitivity of Intracellular NADH Concentration and Conformation to Cell Physiology at the Single-Cell Level. *J Photochem Photobiol B* 2009, *95* (1), 46-57.

(42) Tolleshaug, H. Fluorescent Contrast Agents. 22 June 2006, 2006.

(43) Watkins, R. W.; Lavis, L. D.; Kung, V. M.; Los, G. V.; Raines, R. T., Fluorogenic Affinity Label for the Facile, Rapid Imaging of Proteins in Live Cells. *Org Biomol Chem* 2009, *7* (19), 3969-3975.

CHAPTER 3

NAPHTHALIMIDE-BASED CLOAKED FLUOROPHORE FOR THE RAPID AND FACILE DETECTION OF HUMAN NAD(P)H:QUINONE OXIDOREDUCTASE-1 IN TUMOR CELLS

3.1 Introduction

To obtain the best prognosis possible in dealing with cancer, it is desirable to have an accurate and early diagnosis and resect as much tumor(s) as possible.[1-2] This is conceivable by having a highly sensitive and selective probe that has the ability to detect circulating cancer cells or rapidly give proof-positive results from a biopsy of ex vivo tumors. By providing real-time information on the tumor microenvironment, a better determination of pharmacodynamic effect of drugs on the specific tumor cells can be obtained. This will lead to better prediction and evaluation of which therapy should be undertaken.[3] With complete resection of tumors correlating to "curing" patients, it is highly important to determine small tumor locations and accurate borders between tumors and healthy tissues.[2, 4-5] Fluorescence-guided surgical resection has been of great interest recently with the production of several varieties of activatable fluorophores ranging from cell penetrating peptides, aptamers, enzyme catalyzed fluorophores, and biosynthetically produced fluorophores.[6-9] Previously reported enzyme activatable probes for tumor detection are primarily activated by: cathepsin, caspase, γ-glutamyltranspeptidase, and matrix metalloproteinase.[8, 10-12] By selecting a specific enzyme biomarker with unique properties that is highly upregulated in tumor cells from a wide range of origin, it is possible to produce a single sensor with multifunctional capabilities.

Multifunctional fluorescent-based sensors have recently become a powerful tool in the treatment and diagnosis of cancer, given their specific and sensitive nature.[13] The use of smart off-on sensors, where the fluorescence is quenched and only revealed after a specific stimulus,

provide a more ideal system due to the sensitivity, low signal-to-background ratio, specificity, more economical when using fewer synthetic steps and inexpensive starting materials, and stability in biological environments.[13-14] This strategy can utilize the upregulation of specific enzymes in tumor cells with respect to normal tissue. Enzymatically cleavable groups can be conjugated directly to fluorophores causing a quenching effect of the fluorescent signal, with the subsequent generation of the fluorescent species upon the removal of the cleavable group. This enzyme catalyzed off-on sensor is more advantageous than receptor-mediated diagnosis, which commonly employs "always-on" probes containing high background signal and require considerable time to achieve a desirable background-to-signal ratio.[8, 15] Ideally, the sensor would be of low molecular weight (<1000 Da) and be hydrophobic in nature to facilitate diffusion and retention in tumor cells.[13]

One of the more prolific upregulated cytosolic enzymes present in a wide variety of tumor cells is NAD(P)H:quinone oxidoreductase-1 (NQO1), which is widely distributed and found to be over-expressed 2- to 50-fold (with respect to normal tissue) in human tumors ranging from colon, breast, lung (small cell and non-small cell lung cancers), liver, stomach, kidney, head/neck, to ovarian carcinomas.[16-17] This flavoprotein catalyzes the two-electron reduction of quinones and quinoid species, preventing the formation of reactive oxygen species (ROS) from the single-electron reduction of quinones to semiquinones. Given its over-expression in tumor cells and its enzyme catalyzing reaction, NQO1 has been previously studied as a bioactivator for chemotherapeutics.[18-19] Outside of its enzymatic characterization, NQO1 is a multitasking enzyme and has also been associated as being a gatekeeper for the 20S proteasome pathway and, though the exact mechanism is still unclear, stabilizing the tumor suppressors p53, p73α, and p33.[20] The suppressor p53 is activated under conditions of stress which initiates cell cycle arrest,

DNA repair, and apoptosis and is also important in suppressing tumor initiation and growth. More than half of all human cancers have been known to have lost p53 function.[21]

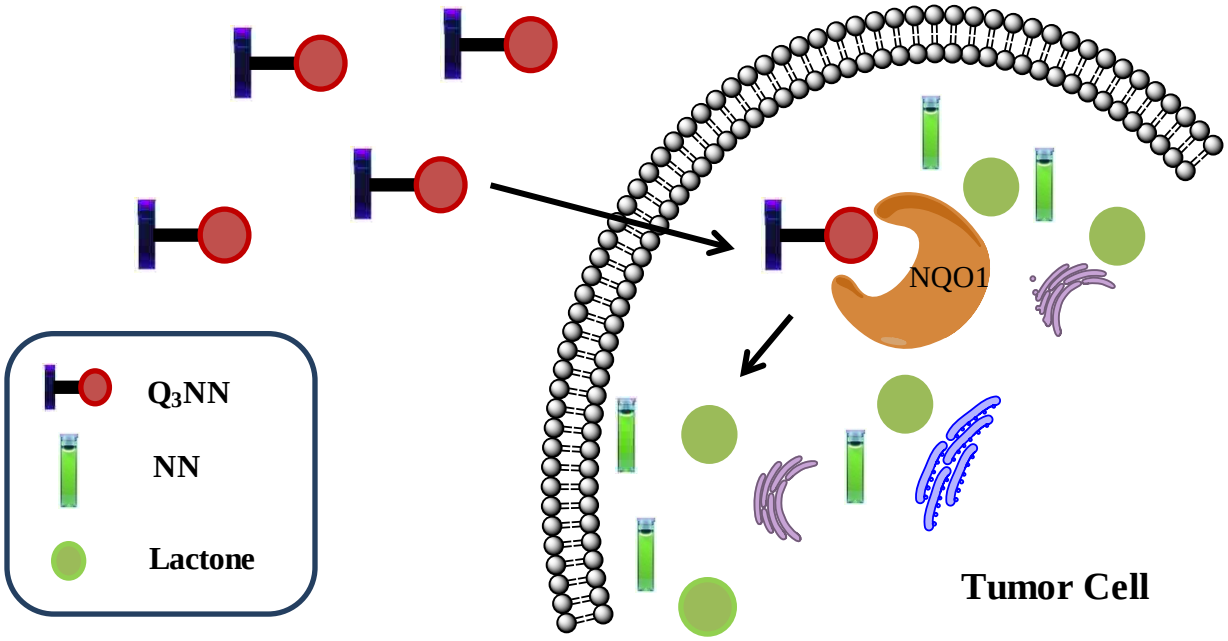

Figure 3.1. Passive diffusion of the hNQO1 sensor (Q_3NN) across the cell membrane, followed by enzymatic activation with subsequent release of the fluorescent dye NN.

3.2 Experimental Section

Here, the design, characterization, and utilization of a first generation activatable cloaked fluorophore enzymatically activated by NQO1 is reported. This fluorophore contains an activatable trimethyl-locked quinone subunit that, after reduction, rapidly cyclizes leaving behind the reporter fluorophore. This sensor employs a unique two-step quenching mechanism of photoinduced electron transfer (PeT), allowing it to be highly sensitive and specific for NQO1 activity. This two-step PeT exploits the two-electron reduction from NQO1 and only reveals its fluorescence after quinone elimination, circumventing false activation from non-specific single-electron reduction of the quinone unit. The sensor is hydrophobic, small in molecular weight, and neutral in charge, allowing it to easily passively diffuse into the cytosol of tumor cells,

Figure 3.1. The product dye contains a naphthalimide scaffold and is fluorescent via a push-pull internal charge transfer (ICT) mechanism. The dye was found to be highly fluorescent in aqueous media and is cationic at neutral pH. Given its rapid activation mechanism, it provides real-time tumor cell analysis and allows for quick tumor cell differentiation with respect to NQO1.

3.2.1 Materials and Methods

3-(3',6'-dioxo-2',4',5'-trimethylcyclohexa-1',4'-diene)-3,3-propionic acid (Q_1PA, **6A**) and 3-(3',6'-dioxo-2',4',5'-trimethylcyclohexa-1',4'-diene)-3,3-dimethylpropionic acid (Q_3PA, **6B**) were prepared according to literature procedures.[22] All chemicals were purchased from Sigma-Aldrich or Fisher Scientific and used as received. For column chromatography, a Biotage FlashMaster Personal was used with 50 g SNAP silica columns (Biotage). Thin layer chromatography was performed on aluminum-backed 60 F254 silica plates from EMD Chemicals, INC. ^{1}H- and ^{13}C-NMR spectra were collected at room temperature on a Bruker AV-400 or a Varian system 700 spectrometer. All NMR experiments were performed in deuterated solvents and the chemical shifts are reported in standard δ notation as parts per million using tetramethylsilane as an internal standard. Peaks in NMR are listed as either, singlet (s), doublet (d), doublet of doublets (dd) triplet (t), multiplet (m), two triplets (2t) while coupling constants (J) are reported in Hertz (Hz). Mass spectral analyses were carried out using an Agilent 6210 ESI-TOF.

3.2.2 Cell Culture

HT-29 (human colorectal adenocarcinoma), A549 (human NSCLC), H596 (human NSCLC), and H446 (human small cell lung cancer) were all purchased from American Type Cell Culture. HT-29 cells were cultured in McCoy's 5A medium supplemented with 10% fetal

bovine serum (FBS) and 100 IU/mL penicillin-streptomycin. A549 cells were cultured in F-12K medium supplemented with 10% FBS and 100 IU/mL penicillin-streptomycin. H596 were cultured in RPMI-1640 supplemented with 10% FBS and 100 IU/mL penicillin-streptomycin. H446 were cultured in RPMI-1640 supplemented with 10% FBS and 100 IU/mL penicillin-streptomycin. Cells were incubated at 37 °C in a humidified incubator containing 5% wt/vol carbon dioxide (CO_2).

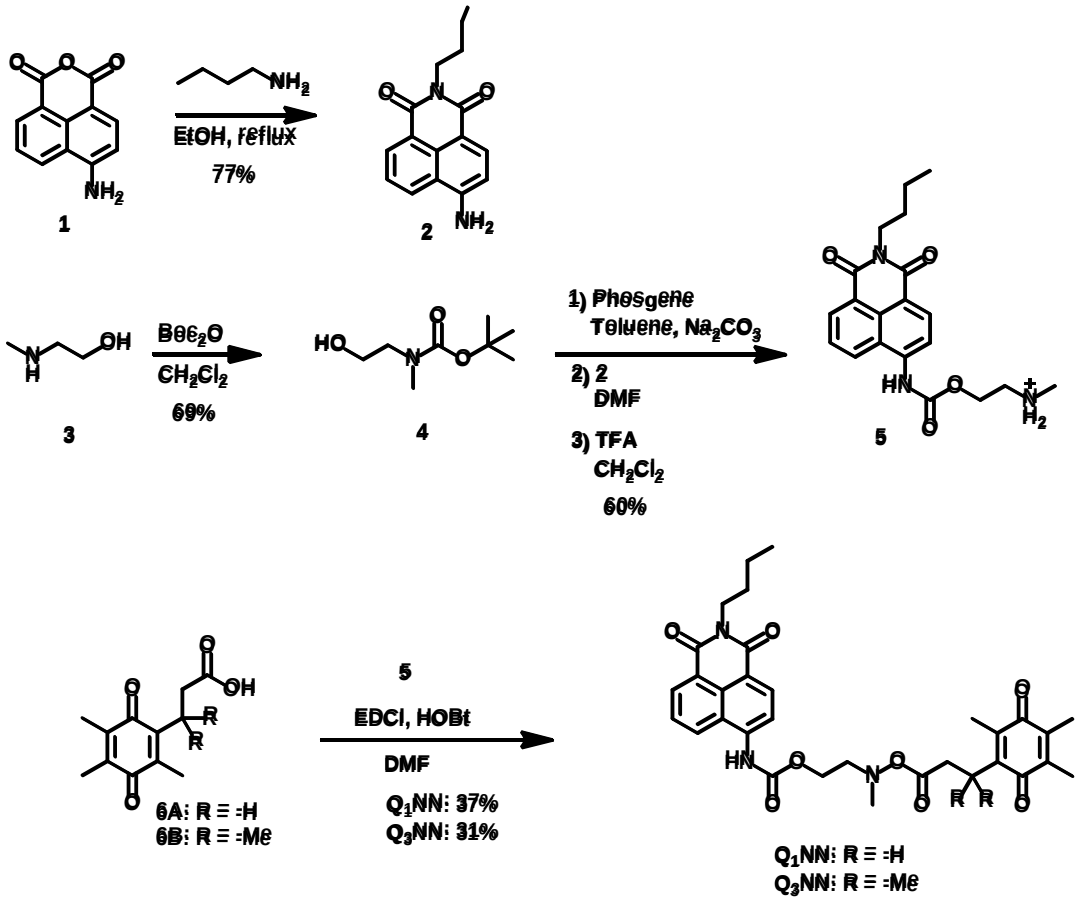

Scheme 3.1. Synthetic route for Q_3NN and Q_1NN.

3.2.3 4-Amino-9-(*N*-butyl)-1,8-naphthalimide Synthesis

4-amino-1,8-napthalic anhydride **1** (0.99 g, 4.64 mmol) was dissolved in 250 mL 200 proof ethanol under a nitrogen atmosphere and brought to reflux. To this solution was added 1-butylamine (1.84 mL, 18.56 mmol), after which the reaction was left to reflux for 14 hours.

After cooling to room temperature, the solvent was removed under reduced pressure and the crude product was collected and purified using silica gel column chromatography (2:1 DCM:EtOAc, R_f = 0.38). Product was collected, solvent removed, and the solid was placed under high vacuum yielding **2** as a yellow solid (0.95 g, 77%). ^{1}H-NMR (DMSO-d_6, 400 MHz): δ 8.57 (1H, d, J = 8.3 Hz), 8.39 (1H, d, J = 7.2 Hz), 8.15 (1H, d, J = 8.3 Hz), 7.62 (1H, t, J = 7.5 Hz), 7.41 (2H, s), 6.81 (1H, d, J = 8.7 Hz), 3.98 (2H, t, J = 7.1 Hz), 1.55 (2H, m, J = 7.4 Hz), 1.30 (2H, m, J = 7.4 Hz), and 0.89 (3H, t, J = 7.3 Hz). ^{13}C-NMR (DMSO-d_6, 100 MHz): δ 164.2, 163.4, 153.1, 134.4, 131.4, 130.1, 129.7, 124.4, 122.3, 119.8, 108.6, 108.0, 30.3, 20.3, 14.2. ESI-MS: for $C_{16}H_{16}N_2O_{12}$: calculated m/z = 291.1104 $[M + Na]^+$; observed m/z = 291.1111 $[M + Na]^+$; 2.4 ppm error.

3.2.4 *tert*-Butyl-2-hydroxyethyl(methyl)carbamate Synthesis

N-(methylamino)ethanol **3** (4.41 g, 55.1 mmol) was dissolved in dry THF under nitrogen atmosphere and chilled using an ice bath. Di-*tert*-butyl dicarbonate (35.8 mL of a 2 M solution in THF, 71.7 mmol) was added slowly to the reaction mixture and left to stir for 2 hours. The solvent was removed under vacuum and the crude product was purified using silica gel chromatography (1:1 Hexanes:EtOAc, R_f = 0.37). Product was collected and after a night on high vacuum afforded **4** as a slight yellow to colorless oil (6.67 g, 69%). ^{1}H-NMR ($CDCl_3$, 400 MHz): δ 3.63 (2H, t, J = 5.6 Hz), 3.27 (2H, t, J = 6.1 Hz), 2.83 (3H, s), 1.36 (9H, s). ^{13}C-NMR ($CDCl_3$, 100 MHz): δ 154.0, 79.6, 60.8, 60.0, 51.1, 35.3, and 28.2. ESI-MS: for $C_{16}H_{16}N_2O_{12}$: calculated m/z = 198.1101 $[M + H]^+$; observed m/z = 198.1101 $[M + H]^+$; 0.0 ppm error.

3.2.5 NN Synthesis

To a dry round bottom flask under argon atmosphere was added 120 mL dry toluene and sodium carbonate (4.65 g, 0.044 mol). To the toluene suspension was added phosgene (28.5 mL

from a 20% solution in toluene, 53.5 mmol) and 100 μL dry DMF, after which the solution was chilled in an ice bath. **4** (1.9 g, 10.7 mmol) was dissolved in 20 mL dry toluene and slowly added to the phosgene solution over a 10 minute period. After 2 hours, nitrogen was rapidly bubbled through the reaction for 30 minutes to remove excess phosgene. Reaction was then filtered and solvent removed under reduced pressure. The colorless oil product was dissolved in 15 mL dry DMF under a nitrogen atmosphere and **2** (0.36 g, 1.34 mmol) was added. After stirring for 20 hours the DMF was removed using a rotary evaporator. Product was partially purified using silica gel column chromatography (2:1 DCM:EtOAc), leaving a yellow solid after removal of the solvent.

The partially purified product was dissolved in 15 mL dry DCM under nitrogen atmosphere to which 10 mL trifluoroacetic acid was added slowly. After one hour, the solvent was removed and the product was purified using silica gel column chromatography (1:5 DCM:EtOAc, R_f = 0.22). Removal of the solvent yielded **5** as a yellow solid (0.298 g, 60%). ^{1}H-NMR (DMSO-d_6, 400 MHz): δ 8.70 (1H, d, J = 8.4 Hz), 8.51 (2H, dd, J = 7.4 Hz), 8.17 (1H, d, J = 8.2 Hz), 7.86 (1H, t, J = 7.5 Hz), 4.44 (2H, t, J = 4.9 Hz), 4.03 (2H, t, J = 7.4 Hz), 3.30 (2H, t, J = 5.2 Hz), 2.65 (3H, s), 1.60 (2H, m, J = 7.6 Hz), 1.33 (2H, m, J = 7.5 Hz), 0.91 (3H, t, J = 7.4 Hz). ^{13}C-NMR (DMSO-d_6, 100 MHz): δ 163.9, 163.4, 158.5, 158.2, 154.2, 140.9, 132.1, 131.5, 129.7, 128.8, 126.9, 124.4, 122.8, 119.2, 119.0, 117.8, 116.2, 61.1, 47.9, 33.4, 31.2, 30.1, 20.3, 14.2. ESI-MS: for $C_{16}H_{16}N_2O_{12}$: calculated m/z = 370.1761 $[M + H]^+$; observed m/z = 370.1760 $[M + H]^+$; 0.3 ppm error.

3.2.6 Q_1NN Synthesis

5 (55.2 mg, 0.15 mmol) was dissolved in 4 mL DMF under a nitrogen atmosphere, to which 60 μL triethylamine was added. To DMF was added HOBt (41.0 mg, 0.30 mmol) and

EDCI (58.0 mg, 0.30 mmol), and **6A** (33.0 mg, 0.15 mmol). Reaction was left to stir for 12 hours, after which the solvent was removed under high vacuum. Product was purified using silica gel column chromatography (1:1 DCM:EtOAc, R_f = 0.29). Removal of the solvent afforded Q_1NN as a yellow solid (31.8 mg, 37%). ^{1}H-NMR (DMSO-d_6, 400 MHz): δ 8.66 (1H, dd, *J* = 7.7 Hz), 8.49 – 8.37 (2H, m, *J* = 8.2 Hz), 8.11 (1H, dd, *J* = 8.2 Hz), 7.82 (1H, m, *J* = 9.0 Hz), 4.34 & 4.28 (2H, 2t, *J* = 5.9 Hz), 4.03 (2H, t, *J* = 4.2 Hz), 3.63 (2H, t, 5.8 Hz), 3.02 – 2.89 (3H, m), 2.55 (2H, m, *J* = 8.2 Hz), 2.35 (2H, m, *J* = 8.4 Hz), 1.90 (5H, m), 1.80 – 1.72 (4H, m), 1.59 (2H, m, *J* = 8.0 Hz), 1.34 (2H, m, *J* = 7.7 Hz), and 0.91 (3H, t). ^{13}C-NMR (DMSO-d_6, 175 MHz): δ 186.9, 186.6, 186.4, 186.2, 171.4, 171.1, 163.4, 162.9, 154.0, 142.6, 140.7, 140.5, 140.3, 140.1, 139.9, 139.8, 139.7, 131.6, 130.9, 129.4, 128.3, 126.4, 124.0, 122.2, 118.5, 118.3, 117.1, 72.0, 70.1, 62.5, 62.3, 48.2, 46.4, 35.8, 33.1, 31.6, 30.9, 29.7, 22.3, 22.1, 19.8, 13.7, 12.1, 12.0, 11.9, 11.7, and 11.6. ESI-MS: for $C_{16}H_{16}N_2O_{12}$: calculated *m/z* = 574.2548 $[M + H]^+$; observed *m/z* = 574.2556 $[M + H]^+$; 1.4 ppm error.,

3.2.7 Q_3NN Synthesis

5 (113 mg, 0.31 mmol) was dissolved in 5 mL DMF under a nitrogen atmosphere, to which 400 μL triethylamine was added. To DMF was added HOBt (83.8 mg, 0.62 mmol) and EDCI (118.9 mg, 0.61 mmol), and **6B** (77.5 mg, 0.31 mmol). Reaction was left to stir for 12 hours, after which the solvent was removed under high vacuum. Product was purified using silica gel column chromatography (1:1 DCM:EtOAc, R_f = 0.61). Removal of the solvent afforded Q_3NN as a yellow solid (57.8 mg, 31%). ^{1}H-NMR (DMSO-d_6, 400 MHz): δ 8.68 (1H, t, *J* = 9.4 Hz), 8.49 (2H, m, *J* = 6.6 Hz), 8.14 (1H, m, *J* = 8.2 Hz), 7.84 (1H, m, *J* = 5.4 Hz), 4.37 & 4.20 (2H, 2t, *J* = 5.6 Hz), 4.03 (2H, t, *J* = 7.3 Hz), 3.66 & 3.54 (2H, 2t, *J* = 5.3 Hz), 3.05 – 2.80 (5H, m, *J* = 22.4 Hz), 1.97 (3H, d, *J* = 5.3 Hz), 1.83 – 1.77 (6H, m, *J* = 9.8 Hz), 1.60 (2H,

m, J = 6.5 Hz), 1.35 – 1.29 (8H, m, J = 7.4 Hz), and 0.91 (3H, t). ^{13}C-NMR (DMSO-d_6, 175 MHz): δ 190.3, 186.8, 171.9, 171.5, 163.5, 162.9, 155.3, 153.9, 143.2, 140.6, 136.5, 134.6, 131.6, 128.3, 124.0, 122.3, 117.3, 62.5, 46.2, 45.7, 37.3, 37.2, 33.2, 29.7, 27.9, 19.8, 13.7, 12.5, and 11.6. ESI-MS: for $C_{16}H_{16}N_2O_{12}$: calculated m/z = 602.2861 $[M + H]^+$; observed m/z = 602.2872 $[M + H]^+$; 1.8 ppm error.

3.2.8 Acetyl-NN Synthesis

5 (63.5 mg, 0.17 mmol) was dissolved in 2 mL dry DMF under a nitrogen atmosphere. From a 1 M solution in DCM, 0.8 mL acetyl chloride (0.8 mmol) and 0.2 mL triethylamine was added to the DMF solution. Reaction was left to stir for 4 hours, after which the solvent was removed using a rotary evaporator. Product was purified using silica gel chromatography (1:4 DCM:EtOAc, R_f = 0.13). Solvent was removed and Acetyl-NN collected as a yellow solid (28.4 mg, 40%). ^{1}H-NMR (DMSO-d_6, 400 MHz): δ 8.61 (1H, m), 8.49 (2H, m, J = 7.3 Hz), 8.11 (1H, m, J = 2.6 Hz), 7.83 (1H, m, J = 7.4 Hz), 4.35 – 4.27 (2H, 2t), 4.02 (2H, t, J = 7.3 Hz), 2.63 (2H, m, J = 12.6 Hz), 3.05 – 2.86 (3H, 2s), 2.04 – 1.99 (3H, 2s), 1.60 (2H, t, J = 7.4 Hz), 1.35 (2H, t, J = 7.5 Hz), and 0.91 (3H, t, J = 7.6 Hz). ESI-MS: for $C_{16}H_{16}N_2O_{12}$: calculated m/z = 412.1867 $[M + H]^+$; observed m/z = 412.1872 $[M + H]^+$; 1.2 ppm error.

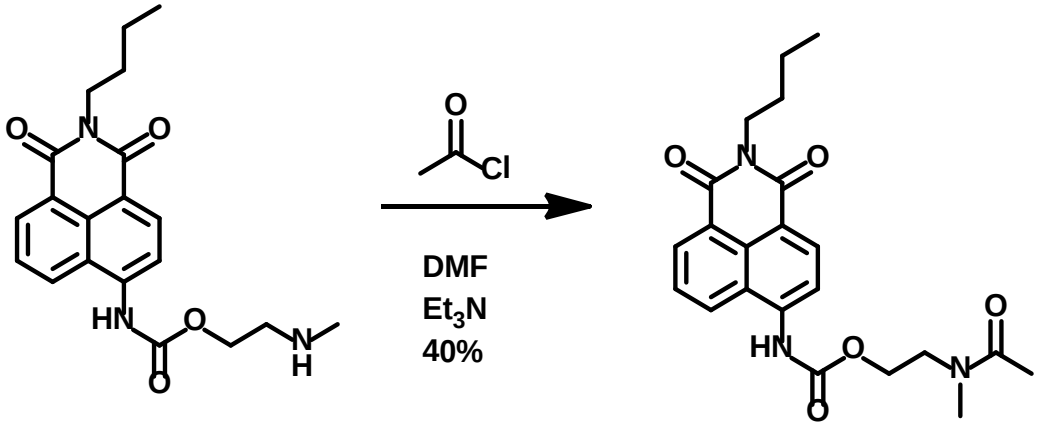

Scheme 3.2. Synthesis of Acetyl-NN.

3.2.9 Cyclic Voltammetry

Cyclic voltammetry was performed on NN and Q_3PA in dry acetonitrile and 0.1 M tetrabutylammonium perchlorate. Princeton applied research potentiostat/galvanostat model 273A was used along with the program Power suite-2.53. Voltammograms were collected at room temperature after degassing the solution with nitrogen for 20 minutes. A glassy-carbon electrode (pretreated for ten minutes) was used as the working electrode, platinum wire as the counter electrode, and a silver (Ag/Ag^+) reference electrode was used. To obtain the oxidation peak for NN, the solution was cycled from 0.5 to 2.0 back to 0.5 V at 100 mV/second and the reduction peak was collected by cycling from 0.0 to -1.8 back to 0.0 V at 100 mV/second. Quinone reduction and oxidation peaks were determined after cycling from -0.25 to -2.0 back to -0.25 at 100 mV/second. Afterwards, ferrocenecarboxylic acid was run from 0.0 V to 0.8 V and back to 0.0 V at 100 mV/second in 0.1 M tetrabutylammonium perchlorate in ACN using a 3.0 M KCl Ag/AgCl reference electrode and again with the Ag/Ag^+ electrode. From this, the half-wave potential was determined for both reference electrodes. To convert the $E_{1/2}$ to a standard hydrogen electrode (SHE) value, 0.21 V was added to the $E_{1/2}$ value for the Ag/AgCl electrode sample value.[23] The difference between the two reference electrode $E_{1/2}$ values was used to convert all values to SHE.

3.2.10 Enzyme Kinetics

Kinetic measurements were performed using a PerkinElmer LS55 fluorescence spectrometer. All measurements were collected at room temperature in pH 7.4, 0.1 M PBS with 0.1 M KCl and supplemented with 0.007% BSA while exciting at λ_{ex} = 390 nm and following the emission at λ_{em} = 470 nm as NN was released following the enzymatic reduction of Q_3NN. A stock solution of 100 μM β-nicotinamide adenine dinucleotide, reduced disodium salt (β-

NADH, Sigma-Aldrich) was made using the PBS buffer and subsequently used to make all other solutions as to have a final concentration of 100 μM β-NADH in each assay. Solutions of Q_3NN were made from the NADH/0.1 M PBS solutions ranging from 2 to 60 μM. A 1.33 μg/mL stock solution of recombinant human NQO1 (Sigma-Aldrich) was prepared using the same buffer as above to give 20 μg hNQO1 per assay. Each assay was performed in a quartz fluorescence cuvette containing 1.5 mL Q_3NN solution and initialized by the addition of 1.5 mL hNQO1 solution. Measurements were collected every 30 seconds for five minutes. Fluorescence units were converted to concentration by creating stock solutions of Q_3NN containing the same concentration of NN and measuring the fluorescence with no hNQO1 present. Measurements were done in triplicate.

3.2.11 Flow Cytometry

Cells were suspended at a count of 1×10^6 in 1 mL of complete growth medium. To each suspension was added Q_3NN from a stock DMSO solution to give a final concentration of 20 μM of the sensor, while keeping the DMSO at approximately 1% or less after dilution. The suspension was incubated with the sensor for 10 or 60 minutes at 37 °C. After which 30 mL of 4% paraformaldehyde (maintained at 37.0 °C) in 0.1 M PBS was added to the mixture to fix the cells for 1 hour. After fixation, the cells were washed twice with 0.1 M PBS and resuspended in 1 mL PBS. Data acquisition was carried out on a iCyt Reflection flow cytometer (iCyt, Champaign, IL) configured for DAPI fluorescence measurements using the 405 nm excitation laser and a 457/60 nm bandpass filter for emission. Fluorescence measurements were made with logarithmic amplification. A total of 10,000 cells per sample were acquired using Winlist software (Verity Software House, Topshame, ME) and FlowJo software was used to plot the data.

3.2.12 Cell Viability

To determine cell viability, a suspension of HT-29, A549 and H596 cells were cultured in 5 mL of their respective complete growth medium in a sterile tube. To the medium was added Q_3NN (from a 1.8 mM stock solution) in DMSO, to give a 20 μM Q_3NN solution and the cells were incubated at 37 °C, 5% CO_2 for 60 minutes, after which 1 mL of the suspension was removed and 0.1 mL trypan blue was added. Cells were immediately counted using a hemocytometer with the aid of a microscope. The remainder of the 4 mL of suspended cells was left in the incubator for 24 hours. Cells were again removed and counted as above.

3.2.13 Optical Differentiation

HT-29, A549, and H596 cells were grown overnight on 22 x 22 mm glass cover slips in complete growth medium. Old growth medium was removed and replaced with a 20 μM Q_3NN solution in fresh growth medium. Cells were incubated at 37 °C with the sensor for 10 minutes and then rinsed with 0.1 M PBS. Cover slips of each cell line were immediately placed upside down on glass slides and visualized with a Mineralight Model UVGL-25 (365 nm, 0.16 amps, ~60 Hz). Image was taken using a Kodak digital camera.

3.2.14 Widefield Fluorescence Imaging of Fixed Cells

The images were acquired using a Leica DM RXA2 fluorescent microscope equipped with a 100x 1.4NA objective lens and a Cooke SensiCam QE. Slidebook software was used to control the camera and microscope as well as image renormalization, deconvolution and scale bar placement. The nucleus was stained with DRAQ5 and a Leica CY5 filter set (λ_{ex} 620/60, λ_{em} 700/75) was used when visualizing this dye. NN dye was visualized using a Leica A4 filter set (λ_{ex} 360/40 λ_{em} 470/40). HT-29, A549, and H596 cells were grown overnight on 22 x 22 mm glass cover slips in 6 well plates in their respective complete culture medium at 37 °C in 5%

CO_2. Prior to sensor addition the old growth medium was replaced with 2 mL of fresh medium maintained at 37 °C. A 1.87 mM solution of Q_3NN was made in DMSO and 21.4 μL was added to each well to give a 20 μM solution of the sensor. The cells were incubated with the Q_3NN in the 37 °C incubator for 10 minutes, after which the cover slips were removed and rinsed with pH 7.4, 0.1 M PBS. Cells were immediately fixed with 4% paraformaldehyde in pH 7.4, 0.1 M PBS for 30 minutes. After fixation, the cover slips were again rinsed with buffer and then submerged in a 3 μM DRAQ5 solution in 0.1 M PBS for 5 minutes. After staining, the cover slips were rinsed with buffer and mounted to glass slides using immu mount. Glass slides were left in the dark overnight to allow the immu mount to dry, after which the cells were imaged. Image analysis was performed in ImageJ.

3.2.15 Confocal Colocalization

Confocal fluorescence images were acquired with a Leica TCS SP5 tandem scanning multiphoton laser scanning microscope at the Cell Biology and Bioimaging Core within Pennington Biomedical Research Center at Louisiana State University, Baton Rouge. Experiments were performed using a 40x oil immersion objective lens (1.25 NA). Imaging of the lysotracker and Q_3NN loaded HT-29 cells was accomplished using a sequential scanning method with sensor excitation via a 405 nm laser at 10% output and collecting emitted light between 417-467 nm. Lysotracker Red was excited using a 561 nm laser at 10% output and emitted light collected between 574-621 nm. DIC images were collected using a PMT detector and 633 nm light at 3% output as an illumination source. All imaging was done at 37 °C using the Leica TCS SP5 in resonant scanning mode and collecting images bidirectionally (16 KHz) at a zoom setting of 3.6. Images were line averaged 64 times. HT-29 cells were incubated overnight in black 35 x 10 mm, 22 mm well glass bottom dishes (Chemglass Life Sciences) in its

complete growth medium at 37 °C with 5% CO_2. Prior to imaging, the medium was removed and replaced with F-12K medium (containing no phenol red) maintained 37 °C. From a concentrated solution of Q_3NN in DMSO, the sensor was added directly to the dish to give a concentration of 20 μM (while ensuring approximately 1% or less DMSO with respect to medium). Cells were incubated with Q_3NN for a total time of 20 minutes. Five minutes prior to imaging, Lysotracker Red-DND 99 was added from a stock solution in DMSO to give a concentration of 0.1 μM.

3.2.16 In vitro 2-Photon Imaging

2-photon confocal fluorescence images were acquired with a Leica TCS SP5 tandem scanning multiphoton laser scanning microscope at the Cell Biology and Bioimaging Core within Pennington Biomedical Research Center at Louisiana State University, Baton Rouge. Experiments were performed using a 40x oil immersion objective lens (1.25 NA). Imaging of live cells was accomplished using a MaiTai two-photon laser tuned to 750 nm (3% laser power, modelocked Ti:sapphire laser; Tsunami Spectra Physics) and emission was collected using a short-pass 680 nm filter. DIC images were collected using a PMT detector and 633 nm light at 3% output as an illumination source. All imaging was done at 37 °C using the Leica TCS SP5 in resonant scanning mode and collecting images bidirectionally (16 KHz) at a zoom setting of 3.6. Images were line averaged 64 times. HT-29, A549, H596, and H446 cells were incubated overnight in black 35 x 10 mm, 22 mm well glass bottom dishes (Chemglass Life Sciences) in their respective complete growth medium at 37 °C with 5% CO_2. Prior to imaging, the medium was removed and replaced with F-12K medium (containing no phenol red) maintained at 37 °C. From a concentrated solution of Q_3NN in DMSO, the sensor was added directly to the dish to give a concentration of 20 μM (while ensuring approximately 1% or less DMSO with respect to

medium). Cells were then imaged, with no washing or medium removal steps, after 10 minutes of incubation with Q_3NN. Image analysis was performed in ImageJ.

3.3 Results and Discussion

3.3.1 Thermodynamic Analysis for PeT Quenching

The sensor Q_3NN is of a *fluorophore-linker-trigger* format with a naphthalimide dye as the fluorophore, which has been shown to have its fluorescence modulated by PeT.[14] Scheme 3.1 shows the synthesis of Q_3NN and Q_1NN. The sensor utilizes a PeT quenching mechanism with a quinone as the trigger moiety that would not only act as an electron acceptor, but also as an electron donor when in the reduced hydroquinone state (Figure 3.2). When the naphthalimide is excited, the sensor undergoes oxidative electron transfer (OeT), with the excited electron in the fluorophore transferring to the electron poor quinone, thus quenching the fluorescence. After the quinone undergoes two-electron reduction to hydroquinone, the system is quenched via reductive electron transfer (ReT) by electron donation from the hydroquinone to the empty ground state in the dye. The fluorescence is finally revealed after cleavage of the hydroquinone unit (through lactonization).

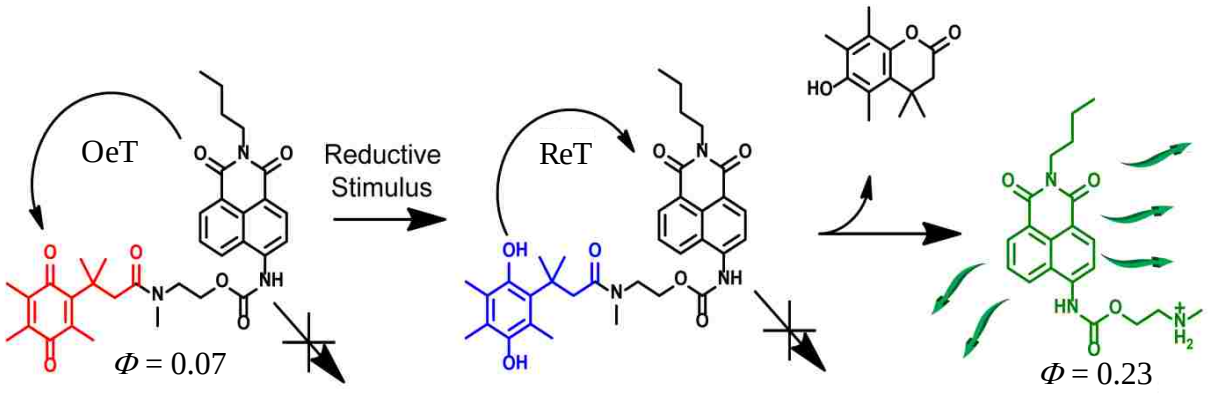

Figure 3.2. Schematic representation of the unique utilization of PeT in the hNQO1 sensor Q_3NN. Proposed quenching mechanisms for Q_3NN prior (OeT) and post (ReT) chemical/enzyme catalyzed reduction, and the subsequent release of the fluorescent NN dye.

This system would create a highly specific sensor towards the two electron reduction by hNQO1 and only reveal its fluorescence after the removal of the quinone subunit from the parent dye. This will not only produce a large fluorescence enhancement (FE), but also ensures minimal background signal from the quenched probe. The base dye chosen was a 1,8-naphthalimide-butyl fluorophore due to its versatility, biological inertness, and large fluorescence in aqueous media. [14, 24] Quinone propionic acid, which can be reduced via chemical or enzymatic catalyzed reactions, was chosen as the trigger group for its ability to react as an electron acceptor/donor (hydroquinone form) in the PeT quenching process, stability against biological reductants, and reactivity towards hNQO1.[22, 25-27] The quinone contains three methyls in the "trimethyl-lock" positions as to create a rapid and spontaneous release from the probe allowing for real-time detection of hNQO1.[28]

Given the nature of the fluorescence enhancement mechanism, *reductive-removal* of the trigger group, the Rehm-Weller equation was used to determine if quenching was thermodynamically possible prior to and post reduction by ensuring a sufficiently negative energy change for PeT (ΔG_{PeT}) until cleavage of the trigger group occurs, Equation 3.1.[29]

$$\Delta G_{PeT} = E_{ox} - E_{red} - \Delta G_{00} - \frac{e^2}{\varepsilon d} \qquad \textbf{Equation 3.1}$$

In this equation, E_{ox} is the oxidation potential of the donor, E_{red} is the reduction potential on the acceptor, ΔG_{00} is the energy of the first excited singlet state, and $\frac{e^2}{\varepsilon d}$ is the Coulombic interaction energy of the ion pair. To ensure complete quenching, the quinone was attached to the naphthalimide via a short *N*-methylethanolamine linker through a carbamate bond on the naphthalimide ring. This linker provides three crucial properties: it creates a tertiary amide at the

quinone end which prevents the formation of a non-activatable spirolactam, shifts the fluorescence of the dye in a hypsochromic shift increasing the energy of the first excited singlet state (decreasing ΔG_{PeT}), and is sufficiently short to allow for a high probability of electron transfer.[24, 30]

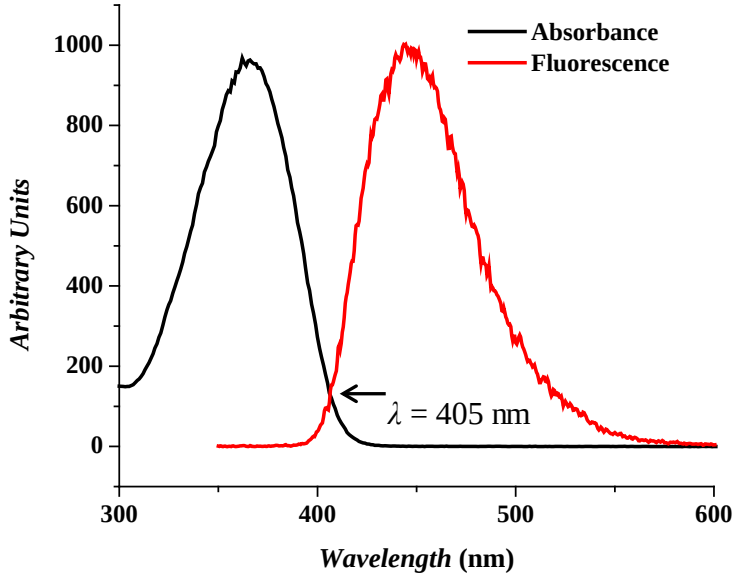

Figure 3.3. Intersection of the normalized absorbance spectrum of NN and its fluorescence spectrum; used to calculate the energy of the ground state to the fist excited state. Spectra were obtained in acetonitrile as the solvent.

The energy of the first excited singlet state of NN was measured to be 3.06 eV, by determining the interception of the normalized absorbance and fluorescence spectra (Figure 3.3), and the Coulombic interaction variable is known to be 0.06 eV.[29] In the first quenching step, prior to quinone reduction, oxidative electron transfer (OeT) takes place by the transfer of the excited electron to quinone. Using cyclic voltammetry (CV), the oxidation potential of NN (Figure 3.4) was measured as $E_{p,a}$ = 1.75 eV vs SHE and the reduction potential for the quinone was $E_{p,c}$ = -1.02 eV vs SHE (Figure 3.5). This generates -0.35 eV as ΔG_{PeT}, which leads to the thermodynamic possibility of electron transfer from the excited dye to the electron poor quinone. Post quinone reduction, the quenching system switches to a reductive electron transfer (ReT) mechanism. Again using CV, the reduction potential of NN (Figure 3.4) is $E_{p,c}$ = -1.33 eV vs

SHE and the oxidation potential for the 2-electron reduced quinone species (Figure 3.5) is $E_{p,c}$ = -0.9 eV vs SHE, also giving a sufficiently negative ΔG_{PeT} in -2.69 eV.

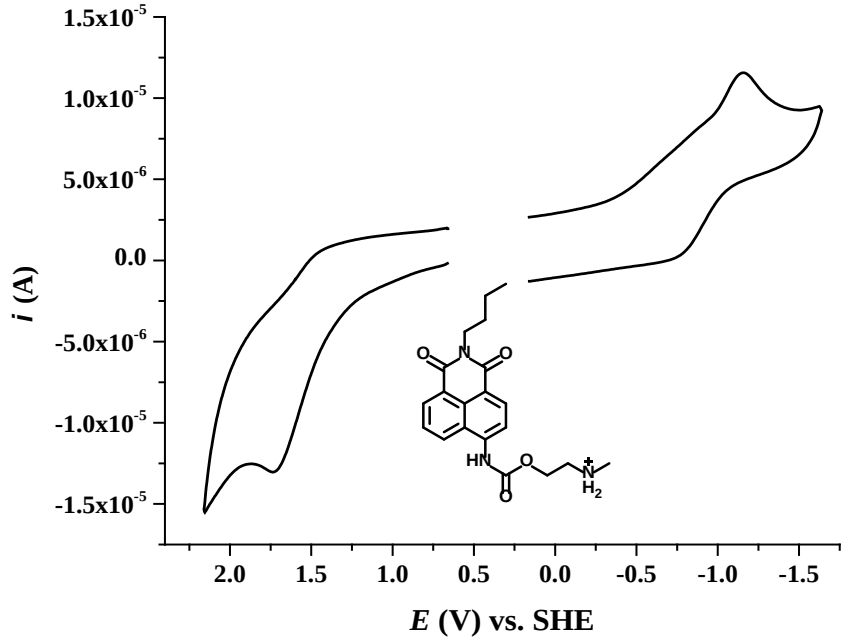

Figure 3.4. Cyclic voltammograms of NN showing the oxidation and reduction peaks used to calculate ΔG_{PeT}. Potential scans were conducted in a 0.1 M tetrabutylammonium perchlorate solution in acetonitrile.

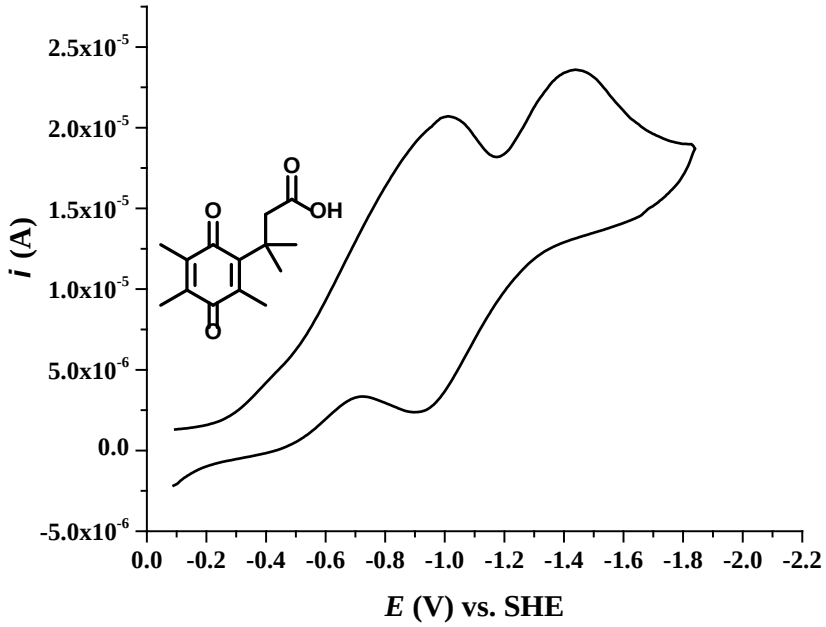

Figure 3.5. Cyclic voltammogram of Q_3PA showing the oxidation and reduction peaks used to calculate ΔG_{PeT}. Potential scans were conducted in a 0.1 M tetrabutylammonium perchlorate solution in acetonitrile.

3.3.2 Reduction Produces Dequenching of Q_3NN

The absorbance spectroscopy for Q_3NN and NN was found to be broad, ranging from 310 to 430 nm centered at 374 nm, Figure 3.6. As shown in Figure 3.7, fluorescence spectroscopy of 2 μM solutions of Q_3NN and NN displayed spectra ranging from 420 to 610 nm and containing a large Stokes shift of 116 nm, producing minimal overlap with its absorbance spectrum. Using quinine sulfate as a standard (Φ = 0.54),[31] quantum yields for Q_3NN and NN were obtained in aqueous media at physiological pH (0.1 M phosphate-buffered saline, PBS, pH = 7.4) and were calculated at 0.007 and 0.23 (33-fold FE), respectively.

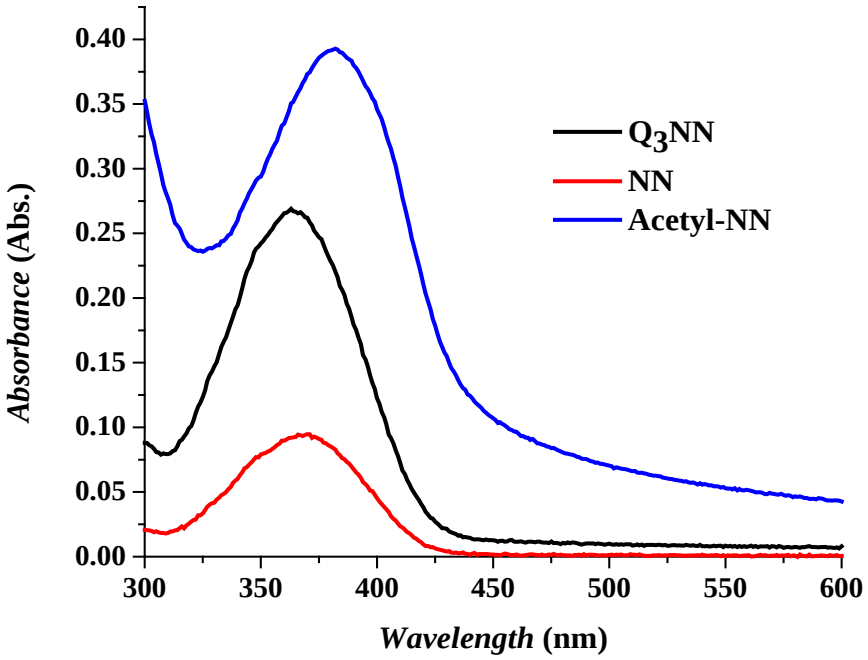

Figure 3.6. Absorbance spectra of 20 μM Q_3NN, NN, and Acetyl-NN in pH 7.4, 0.1 M PBS with 0.1 M KCl.

Quantum yield was determined using Equation 2.1. The quantum yield for NN is comparable to other sensors applied to cancer detection and localization that have yields ranging from 0.0028 for indocyanine green to 0.21 for Cy5.5 dyes.[6, 32] As proof positive that NN could indeed be released after quinone reduction, a strong reducing agent (sodium dithionite) was

added to a 10 μM solution of Q_3NN, Figure 3.8. While exciting the solution at 370 nm and following the emission intensity at 470 nm, it was found that NN was rapidly released post-reduction.

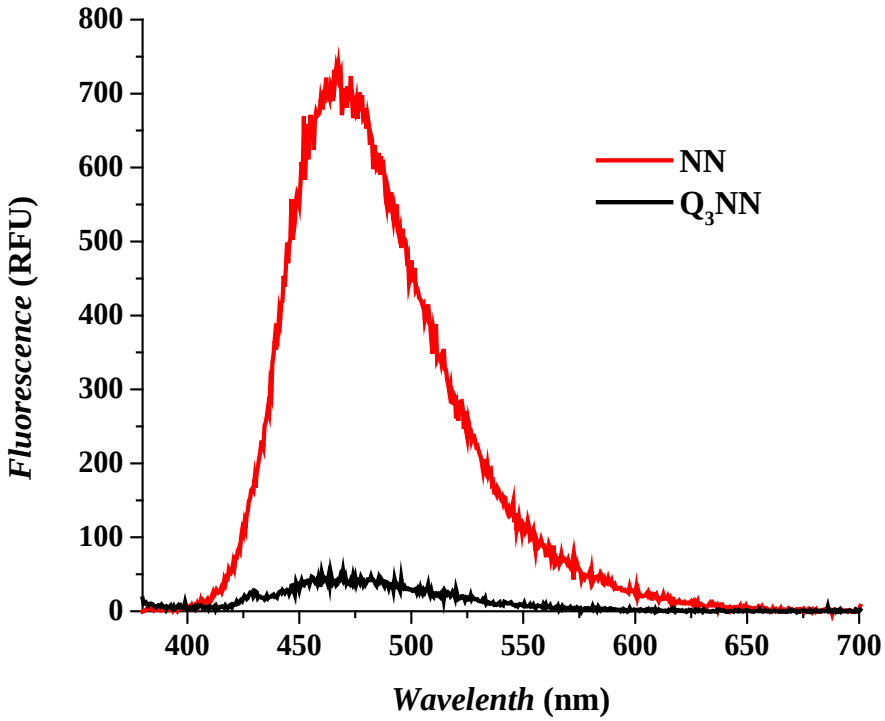

Figure 3.7. Fluorescence spectra of 2 μM solution of Q_3NN and NN in pH 7.4, 0.1 M PBS with 0.1 M KCl. λ_{ex} = 378 nm.

As method of checking the 2-step PeT mechanism, a second probe was synthesized (Q_1NN) where the quinone was lacking the two geminal methyls of the trimethyl-lock, thus significantly reducing cyclization and dye release.[22] As seen in Figure 3.8, Q_3NN undergoes a much more rapid dye release after the addition of sodium dithionite when compared to that of Q_1NN. Combining the very unique quenching mechanism, large Stokes shift, pronounced fluorescence signal enhancement, practicality of an off-on type sensor, and the biologically stable trigger-group, Q_3NN can then be utilized as an hNQO1 sensor in real-time applications such as flow cytometry and fluorescence imaging.

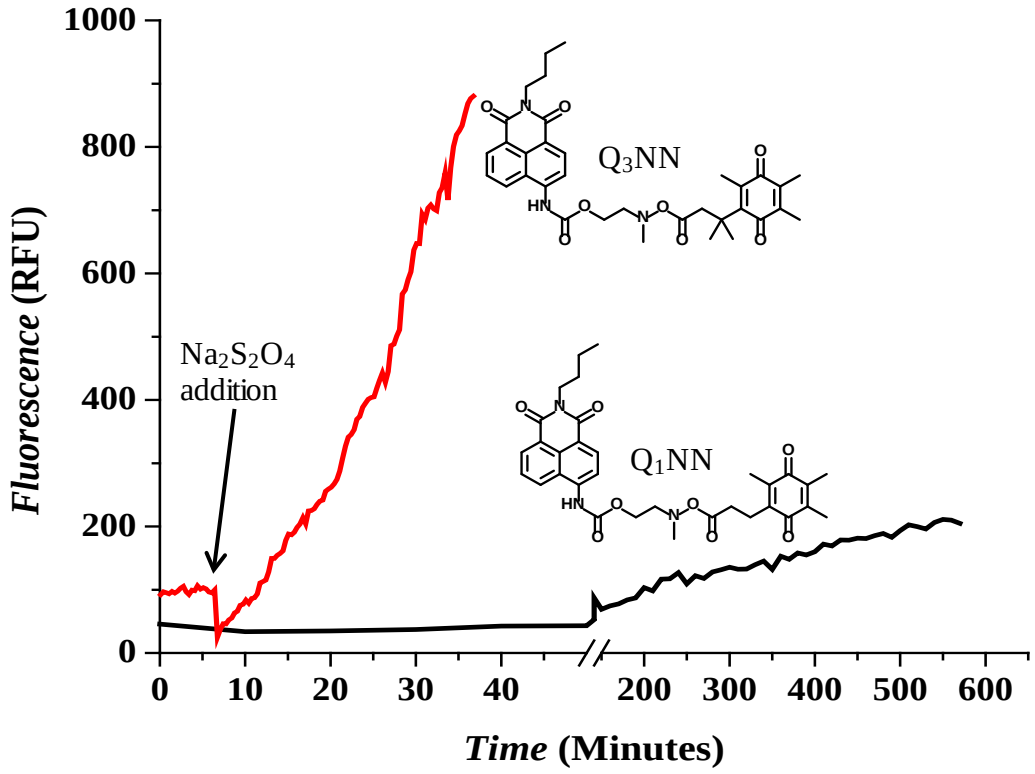

Figure 3.8. Comparing the release of NN in 10 μM solutions of Q_3NN and Q_1NN in pH 7.4, 0.1 M PBS following reduction via addition of 2.75 mg sodium dithionite into cuvettes. Solutions were excited at λ_{ex} = 370 nm and emission followed at λ_{em} = 470 nm.

3.3.3 Acetyl-NN and Other NN Properties

To ensure the amide bond connecting the linker and quinone did not significantly influence the optical properties of NN and Q_3NN, Acetyl-NN was synthesized (Scheme 3.2). Absorbance and fluorescence properties of Acetyl-NN were determined and then compared to NN and Q_3NN. The absorbance spectrum for 20 μM Acetyl-NN (Figure 3.6) had a similar maximum to that of NN, but appeared to have a higher extinction coefficient. Using Equation 2.1 and NN as the standard, the quantum yield for Acetyl-NN was calculated to be Φ = 0.35. Comparing the fluorescence spectra for NN, Q_3NN, and Acetyl-NN in pH 7.4, 0.1 M PBS demonstrates the increase in quantum yield for each compound while exciting at 365 nm, Figure 3.9.

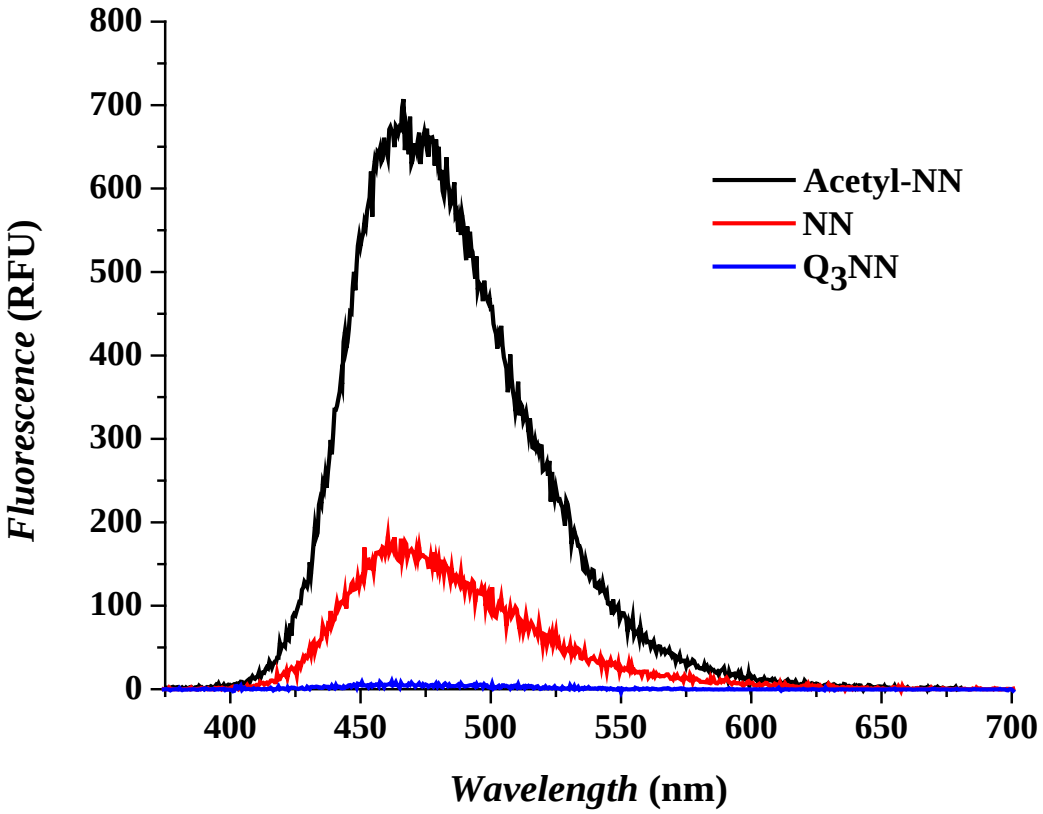

Figure 3.9. Fluorescence spectra of Q_3NN, NN, and Acetyl-NN in pH 7.4, 0.1 M PBS (each solution had an absorbance of 0.048 abs.). λ_{ex} = 365 nm.

As detailed in Chapter 2, one of the issues with the Q_3-Rho-Morph sensor was the quenching of the Rho-Morph product dye by NADH. This was an issue solved by using the naphthalimide dye scaffold. It was found that after one hour of mixing Rho-Morph into a 100 μM solution of NADH, the fluorescence of the dye was reduced by 26%. On the other hand, NN fluorescence was only reduced 4% while in the presence of NADH, Figure 3.10. Stability of Q_3NN at low pH was also tested to ensure no non-specific activation if the sensor accumulated in acidic compartments in cells. A 5.0 μM Q_3NN solution in 0.1 M PBS had its fluorescence spectrum observed every 10 minutes at a pH of 5.0 over a 50 minute period while exciting at λ = 380 nm, Figure 3.11. It was found that Q_3NN was relatively stable at a low pH and would be suitable for cellular imaging, even after longer incubation periods.

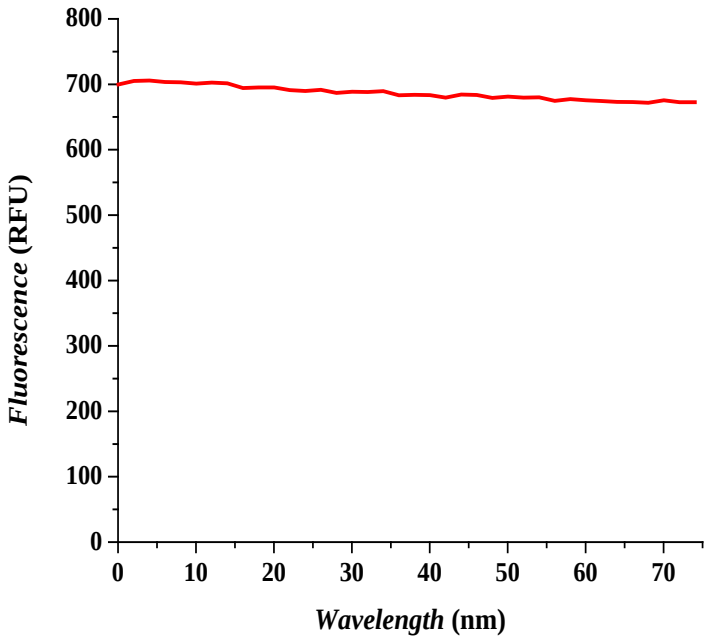

Figure 3.10. Observing the fluorescence of 2.0 μM NN in 0.1 M PBS pH 7.4 while in the presence of 100 µM NADH. λ_{ex} = 380 nm and λ_{em} = 470 nm.

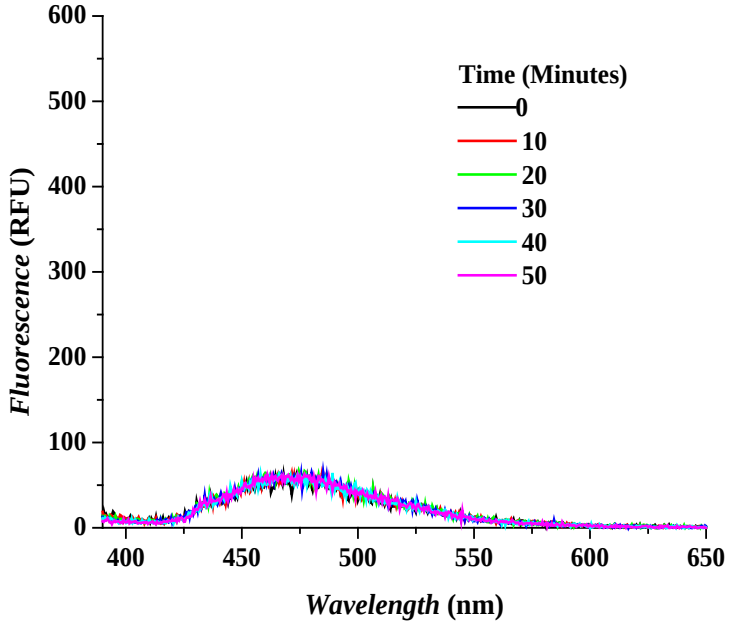

Figure 3.11. Fluorescence spectra of 5 μM Q_3NN in 0.1 M PBS at pH 5.0 over a 50 minute period. Scans were taken every 10 minutes while exciting at λ = 380 nm.

As seen with other amine-linker-naphthalimide dye systems, the fluorescence in NN is also PeT modulated by the p*K*a of the secondary amine at the end of the linker.[33-36] For this PeT

quenching system, the neutral secondary amine acts as an electron acceptor, quenching the naphthalimide dye. It was found that the p*K*a of NN was approximately 12.0, sufficiently high enough that physiological pH would have little effect on intensities for cellular imaging purposes, Figure 3.12.

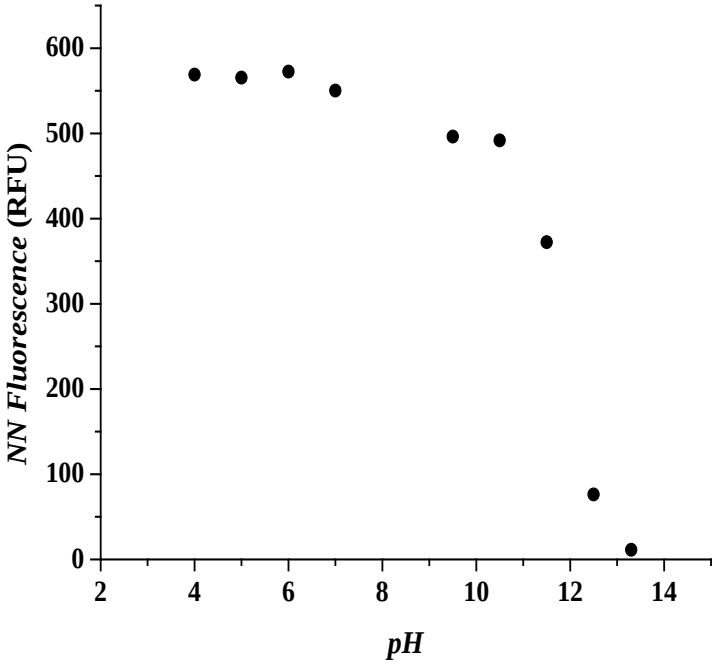

Figure 3.12. Fluorescence intensities of NN with respect to change in pH, λ_{ex} = 385 nm and λ_{em} = 480 nm.

3.3.4 Enzyme Kinetic Analysis With hNQO1

To confirm that Q_3NN was a suitable substrate for hNQO1 and to ensure the rate of release of the fluorophore in the presence of the enzyme, we measured the apparent kinetic activity of the enzyme relative to dye release. As shown in Figure 3.13, results displayed as Michaelis-Menten kinetics with K_m = 3.86 ± 0.79 μM, V_{max} = 0.037 ± 0.002 μmol min^{-1} mg·NQO1^{-1}, k_{cat} = 0.019 ± 0.001 sec^{-1}, and k_{cat}/K_m = 4.9 (± 1.0) × 10^3 M^{-1} sec^{-1}. Due to the single activation mechanism and the non-bulky linker, the kinetic constants are significantly higher than our reported hNQO1 activatable fluorophore (Q_3-Rho-Morph), Chapter 2.[25] This

higher enzymatic affinity and rapid dye release ensures sufficient signal enhancement for rapidly detecting hNQO1.

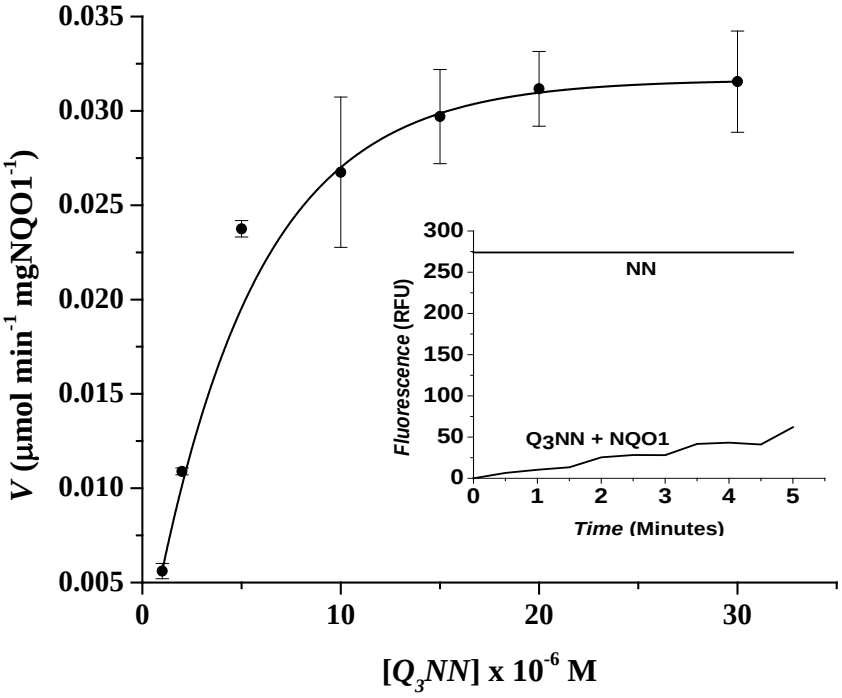

Figure 3.13. Michaelis-Menten kinetics plot of hNQO1 (20 μg) towards Q_3NN. Inset contains sample 1 μM Q_3NN assay observing NN release by fluorescence, relative to fluorescence signal of total release (1 μM NN).

3.3.5 Rapid Differentiation Between Target Cells

I next wanted to assess the ability to rapidly differentiate between cell lines known to contain hNQO1 and those devoid of the enzyme with and without the aid of instrumentation. The colorectal carcinoma cell line HT-29 and the non-small cell lung cancer (NSCLC) cell line A549 were both previously shown to contain hNQO1 activity and the NSCLC H596 is found to be devoid of hNQO1.[17, 37] Using cell lines originating from different organs demonstrates the breadth at which the probe can accurately detect hNQO1 in cells from varying locations. After a ten minute incubation period in a solution containing Q_3NN, it was possible to differentiate between the cells using only a fluorescent lamp emitting at 365 nm and the un-aided eye, Figure

3.14. Both HT-29 and A549 appeared fluorescent blue and the cell line H596 was found to emit no fluorescence. The ability to visually determine the presence of hNQO1 in cells is again due to the marked difference in fluorescence from the quenched Q_3NN and unquenched NN, the high quantum yield of NN, and the appearance of the fluorescence in the visual spectrum. This technique helps demonstrate the simplicity of the sensor as it comes to the rapid detection of tumor cells. Given the ability to visually detect tumor cells and determine accurate tumor/healthy tissue borders in real-time, without the aid of imaging equipment, would be highly beneficial for surgical resection of tumors with small foci.

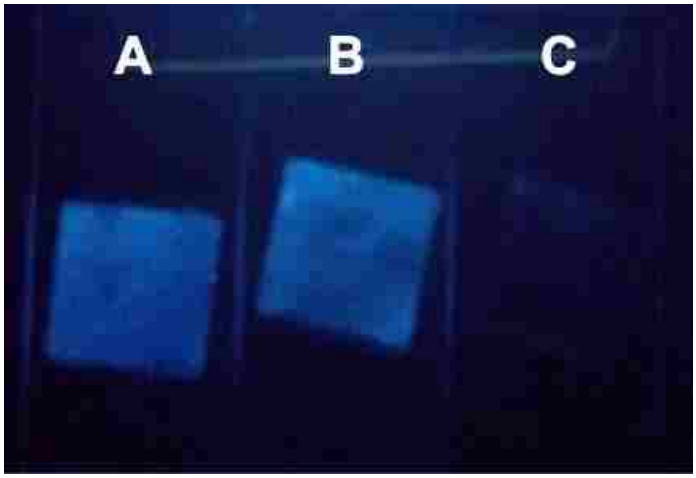

Figure 3.14. Optical differentiation between HT-29 (A), A549 (B), and H596 (C) cells after incubation with Q_3NN. Fluorophore is excited by a handheld lamp emitting 365-nm light.

Similarly, flow cytometry assays were used to assess the applicability of Q_3NN to rapidly detect hNQO1 in tumor cells. The probe was incubated in a suspension of HT-29, A549, and H596 cells for 10 or 60 minutes and a flow cytometer was used to detect the fluorescence in individual cells. In Figure 3.15 is depicted the fluorescence signal intensities per cells of each cell line in relation to the activation of Q_3NN. The results showed high intensity unimodal fluorescence signal from Q_3NN activation in HT-29/A549, while the negative cell line, H596, produced minimal fluorescence. It was also found that there was little to no increase in signal

when increasing the incubation time from ten to sixty minutes, demonstrating the rapid and substantial activation in A549/HT-29 and the stability Q_3NN in H596, Figure 3.15. With the low fluorescence in the H596 cells and no increase in signal over a longer incubation period, the results demonstrate lack of non-specific activation of Q_3NN. Given the stability and the very short incubation time to reveal sufficient fluorescence signal to differentiate between cells absent/containing hNQO1, it is indicated that Q_3NN is a highly sensitive and selective sensor and can be used as a rapid tumor cell detection sensor.

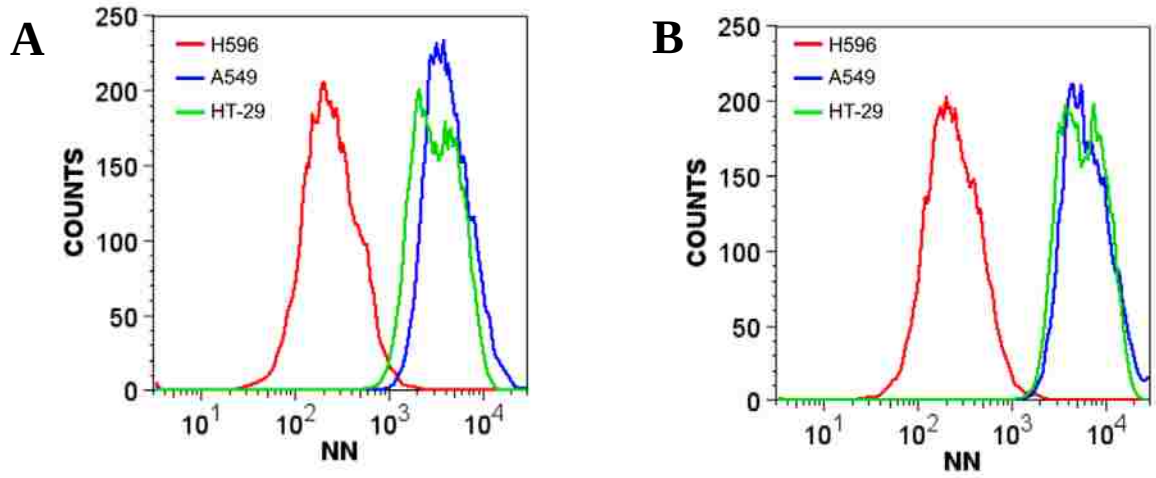

Figure 3.15. Flow cytometry assay of Q_3NN activation in 2 hNQO1-containing cell lines (A549 and HT-29) and a cell line with no hNQO1 activity (H596) after a 10 minute incubation period (A) or a 60 minute incubation period (B). Assay was performed by counting 10,000 cells and the concentration of Q_3NN was 20 μM.

3.3.6 Q_3NN for the Specific Detection of hNQO1 Overexpressing Cells

With the positive results from enzyme kinetics and flow cytometry, I sought to use a complimentary technique in fluorescence microscopy to further validate the effectiveness of Q_3NN to rapidly distinguish cells with hNQO1 activity and provide spatial resolution on the activation and compartmentalization of the NN dye released. In agreement with flow cytometry data, fluorescence microscopy on fixed cells and a ten minute incubation time also revealed significant sensor uptake and activation leading to intracellular fluorescence for the A549 and

HT-29 cell lines and minimal signal for H596, Figure 3.16. The average cytosolic signal was 9 times higher in A549 cells compared to H596, while the average intensities were 23 times higher in HT-29 compared to H596. Values of 9- to 23-fold increase from target cells to non-target cells is substantially higher than 2.5-fold increase, which previously was considered to be substantial accumulation.[38] Though the NN is excited near the ultraviolet region which can produce significant absorbance from hemoglobin and background fluorescence, the activation of Q_3NN to NN yields high signal-to-background relative to other exogenously introduced sensors ensuring sensitive tumor analysis.[15] From these results, it appears that paraformaldehyde fixation has little effect on dye quantum yield and also that there is no efflux of the dye from the fixed cells. Being able to retain its fluorescence after fixation gives it the potential to be invaluable for ex vivo quantitative analysis of excised tumors for a period of time after surgical removal.

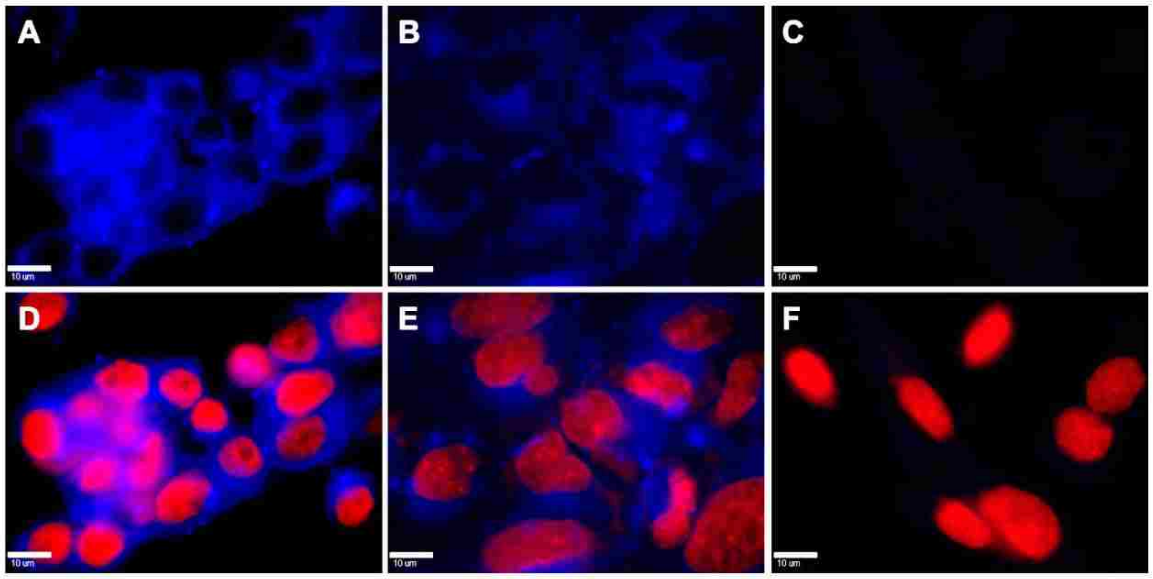

Figure 3.16. Widefield fluorescent imaging of fixed HT-29 (A,D), A549 (B,E), and H596 (C,F) cells after a 10 minute incubation with Q_3NN. Top row contains images of NN production (blue) and the bottom row is the overlays with the nuclei (red). Scale bars are 10 μm.

To determine the fate of the fluorophore NN after intracellular activation, confocal microscopy was used to localize NN in lysosomes using Lysotracker Red as an organelle-specific probe. For these experiments, live HT-29 cells were used after incubating for 20 minutes with Q_3NN, to which Lysotracker Red was added to the media in the imaging dish. It was found that a majority of the NN signal originated from the cytosol, while accumulation did occur in late endosomes/lysosomes, Figure 3.17. This was an expected fate for intracellular NN due to the ionizable amine at the end of the linker, because it is common for amine containing species to accumulate in acidic vesicles due to the pH difference with the cytosol. This accumulation of dye in late endosomes/lysosomes is beneficial in that it leads to slower efflux of NN and longer intracellular accumulation time, which can further lead to higher signal-to-background.

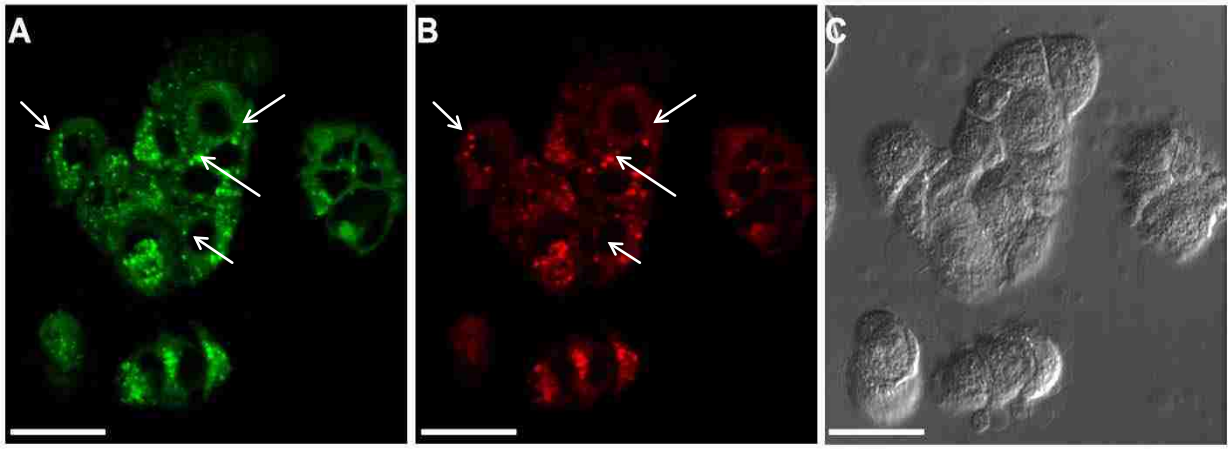

Figure 3.17. Confocal image of HT-29 cells depicting the accumulation of NN (A) in lysosomes (B) after intracellular production. DIC image is also provided for reference (C). Scale bars are 25 μm. Arrows points to localization of NN in lysosomes.

One of the more recent and powerful biologically relevant imaging techniques is multiphoton microscopy (MP) where fluorophores are excited by two, sometimes even three, photons at a much lower energy wavelength.[39] This system is more advantageous when

compared to traditional fluorescence microscopy in that longer wavelength photons have a lower probability of being scattered and can penetrate deeper into tissues, is less phototoxic to tissues, produces less background noise due to less out-of-focus excitation, and yields less photobleaching of the fluorophores allowing for longer imaging periods. MP imaging is ideal for ex vivo thick specimen sampling and in vivo experiments directly observing targets in their physiological environment where 2D and 3D maps can be generated.[6]

After incubating in complete growth medium containing Q_3NN, 2-photon microscopy revealed significant fluorescence signal enhancement in live HT-29 and A549 cells and minimal signal in two hNQO1-negative cell lines, H596 and H446 (a small cell lung carcinoma known to be devoid of hNQO1 activity), Figure 3.18.[37] It was calculated that the average cytosolic fluorescence signal was 13-fold higher in A549 compared to H596 and 3.66×10^4-fold higher in H446 cells. Similar results were obtained with the HT-29 cell line, with the cytosolic intensity being 15-fold higher compared to H596 and a 4.51×10^4 increase compared to H446. As before, the signal appears slightly heterogeneous throughout the cytosol with accumulation in small punctate organelles. To ensure prolonged exposure to Q_3NN and NN had little effect on cell health, cells were incubated in a 20 μM Q_3NN solution in complete growth medium for one hour and one day, after which a trypan blue assay was used to determine cell viability. After one hour, cell viability for HT-29, A549, and H596 was 97.7%, 98.8%, and 100%, respectively, and 97.7%, 98.7%, and 98.4%, respectively, after one day. Of note, due to the background-to-signal ratio, this assay requires no time consuming washing step as with "always-on" sensors. This is one of the more important aspects of the off-on nature of Q_3NN in that it significantly reduces the time between dye addition to detection producing a sensor ideal for a "real-time" detection technique.

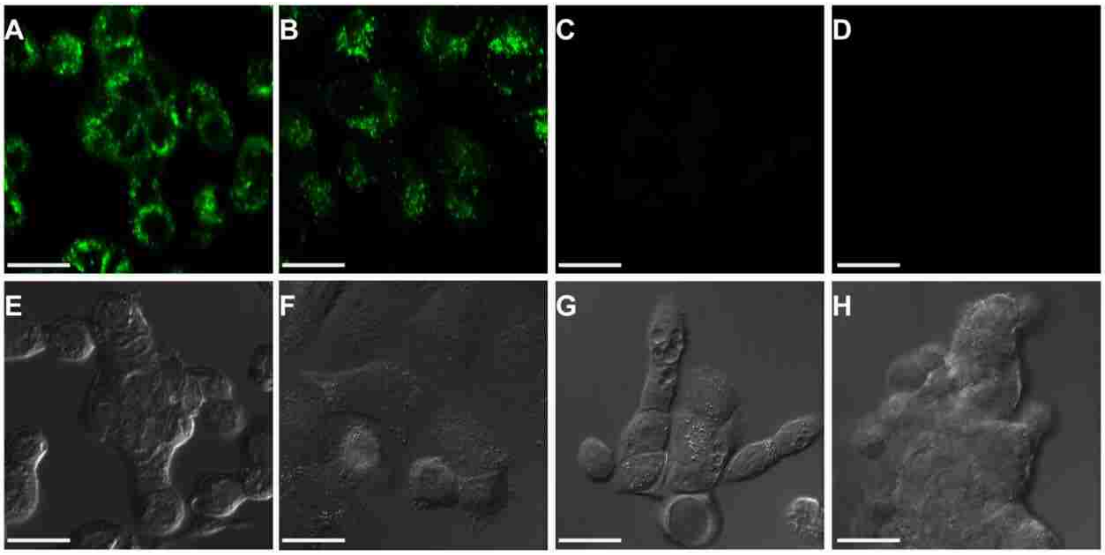

Figure 3.18. 2-Photon confocal microscopy imaging of live HT-29 (A,E), A549 (B,F), H596 (C,G), and H446 (D,H) cells following a 10 minute incubation time with Q_3NN. Fluorescence images of each cell line are on the top row with their respective differential interference contrast (DIC) image on the bottom row. Images were acquired while exciting at λ_{ex} = 750 nm (3% laser power) without any washing steps between sensor addition and imaging.

3.3.7 Quantitative Analysis of hNQO1 Probes

The rate of lactonization for Q_3-Rho-Morph and Q_3NN after reduction was determined to give a better understanding of the activation kinetics. This will provide valuable insight into future probe design to achieve the most effective probe possible. In the presence of excess sodium dithionite the quinone units in Q_3-Rho-Morph and Q_3NN should undergo near instantaneous reduction to the hydroquinone (less than 1 s for Q_3 propionic acid)[40], followed by the slow step of lactonization of the hydroquinone with concurrent release of the dye. Due the rapid reduction step, the dye release was considered to be a pseudo-first-order step. To determine the rate constant (k) for dye release, Equation 3.2 was used.

$$\ln\left[\frac{[\mathrm{A}]_t}{[\mathrm{A}]_0}\right] = -kt \qquad \textbf{Equation 3.2}$$

In this equation, $[\mathrm{A}]_t$ and $[\mathrm{A}]_0$ are the concentrations of the reduced probe at time t and time 0, respectively. An approximate rate constant for each probe was determine by adding

excess sodium dithionite to a dilute solution (5 μM) of probe in pH 7.4 0.1 M PBS with 0.1M KCl and following the fluorescence increase over a long period of time. The rate constant was calculated by taking the time at which half the maximum signal was achieved and recognizing that at this point $[A]_t/[A]_0 = 0.5$. For Q_3NN, the time was 54 minutes for 50% consumption of Q3NN, yielding a rate constant of $k = 2.1 \times 10^{-4}$ sec^{-1}. For Q_3-Rho-Morph, the time was 2.5 minutes resulting in a rate constant of $k = 4.62 \times 10^{-3}$ sec^{-1}. This shows that Q_3-Rho-Morph undergoes dye significantly faster than Q_3NN, with the rate constant is only 20-fold higher. This increase in lactonization for Q_3-Rho-Mrph could be due to the electronic effect of the attached dye on the amide and the lack of the methyl on the nitrogen in the amide versus Q_3NN. The latter is supported in studies by Iresha Perera in the McCarley Group, as it was found that the Q_3PA derivative of N-methyl-ethanolamine cyclized at least two times slower than the ethanolamine derivative in D_2O) medium.[41]

A second experiment was also used to highlight the effect the lactonization rate has on dye release, in which enzyme kinetics were again performed on Q_3-Rho-Morph where the oxidation of NADH to NAD^+ was followed over time instead of following the formation of Rho-Morph. Due to absorbance overlap at 340 nm this experiment was not possible for Q_3NN. Kinetics was performed exactly as written in Chapter 2, except the fluorescence change observed was from the fluorescent NADH to the nonfluorescent NAD^+. Here, NADH was excited at 340 nm and the emission was observed at 460 nm. The results are displayed in Figure 3.19.

From this, it was found that $K_m = 5.37 \pm 0.67$ μM, $V_{max} = 0.019 \pm 0.001$ μmol min^{-1} mg·NQO1^{-1}, $k_{cat} = 0.01 \pm 0.001$ sec^{-1}, and $k_{cat}/K_m = 1.8 (\pm 0.4) \times 10^3$ M^{-1} sec^{-1}. When compared to the assay in Chapter 2 where the formation of Rho-Morph was followed, the V_{max} for this NADH fluorescence assay was 9-fold higher. This outcome is as expected due to the two-step

process of NQO1 reduction then hydroquinone lactonization to yield the free Rho-Morph. At this stage, I do not have any direct evidence that would indicate more/less rapid reduction of Q_3NN by NQO1 (due to the spectral overlap of the NADH and NN species). However, it is clear from the dithionite reduction results discussed above that the cyclization process is slower for Q_3NN vesus Q_3-Rho-Morph, and this is probably the major contributor to the somewhat expected slow V_{max} value for its NQO1 activation (reduction and cyclization). Future studies should target enzyme parameters for the NQO1 activation of Q_3PA linked directly to the aromatic amine of the naphthalimide or a Q_3NN-like derivative having a naphthalimide absorption/emission that is significantly shifted from that of NADH so that the reduction cyclization steps can be separated, as was possible with the Q_3-Rho-Morph.

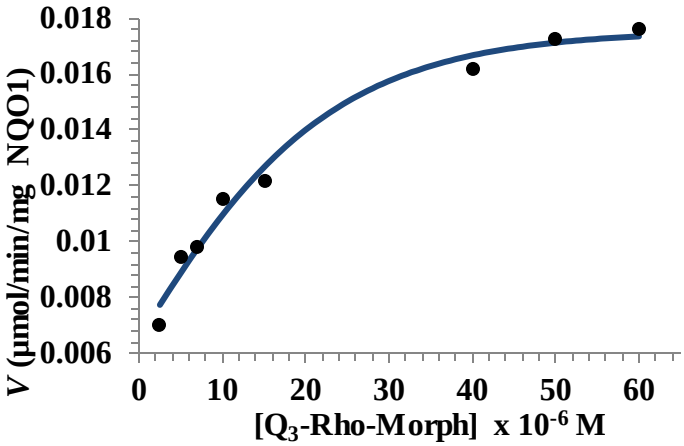

Figure 3.19. Kinetic plot for recombinant human NQO1 (1×10^{-5} g) towards Q_3-Rho-Morph in pH 7.4, 0.1 M PBS, and 0.007% bovine serum albumin while observing the oxidation of NADH. Solid blue line indicates best fit to Michaelis–Menten equation.

3.4 Conclusions

I have developed a first-generation sensor utilizing a unique use of PeT quenching for use as an off-on sensor for the rapid, sensitive, and specific detection of hNQO1-containing tumor cells. Following activation of the non-fluorescent capped Q_3NN, the highly fluorescent NN dye is released leading to high signal-to-background ratios with respect to non-targeted cells. Given

the enzymatic efficiency of Q_3NN and the rapid single step activation mechanism post-reduction, Q_3NN was found to be a better substrate for hNQO1 when compared to other rhodamine-containing sensors and also sensors that require a slow linker cyclization step to dequench the fluorophore.[25, 42-43] Flow cytometry analysis revealed Q_3NN to be highly specific and sensitive for tumor cells containing hNQO1 after a short incubation period with the sensor, allowing for easy differentiation between targeted and non-targeted cells. Q_3NN and NN were found to be biologically compatible to where they were not detrimental to cell health. Confocal microscopy revealed NN to be found mostly in the cytosol with partial accumulation in acidic vesicles. The fluorophore NN was found to be easily excited via a multiphoton laser which is becoming an increasingly useful medical diagnostic tool given the lower background signal multiphoton microcopy generates along with the deeper sample penetration, lower phototoxicity, and less photobleaching. Given the need for real-time analysis of tumor/healthy tissue, Q_3NN has the potential to aid in ex vivo analysis and in vivo detection and resection of tumors of varying origin. This is thanks in part to the accumulation in acidic cellular organelles, high background-to-signal ratio, specificity to hNQO1 leading to high sensitivity to tumor cells, and stability.

3.5 References

(1) Siegel, R.; Naishadham, D.; Jemal, A., Cancer Statistics, 2012. *CA Cancer J Clin* 2012, *62* (1), 10-29.

(2) Nguyen, Q. T.; Olson, E. S.; Aguilera, T. A.; Jiang, T.; Scadeng, M.; Ellies, L. G.; Tsien, R. Y., Surgery with Molecular Fluorescence Imaging Using Activatable Cell-Penetrating Peptides Decreases Residual Cancer and Improves Survival. *Proc Natl Acad Sci U S A* 2010, *107* (9), 4317-4322.

(3) Elfriede, S., Biological and Chemical Sensors for Cancer Diagnosis. *Meas Sci Technol* 2010, *21* (11), 112002-112026.

(4) Mieog, J.; Hutteman, M.; van der Vorst, J.; Kuppen, P.; Que, I.; Dijkstra, J.; Kaijzel, E.; Prins, F.; Löwik, C.; Smit, V.; van de Velde, C.; Vahrmeijer, A., Image-guided Tumor Resection Using Real-time Near-infrared Fluorescence in a Syngeneic Rat Model of Primary Breast Cancer. *Breast Cancer Res Treat* 2011, *128* (3), 679-689.

(5) Liu, Y.; Bauer, A. Q.; Akers, W. J.; Sudlow, G.; Liang, K.; Shen, D.; Berezin, M. Y.; Culver, J. P.; Achilefu, S., Hands-free, Wireless Goggles for Near-infrared Fluorescence and Real-time Image-guided Surgery. *Surgery* 2011, *149* (5), 689-698.

(6) van den Berg, N. S.; van Leeuwen, F. W.; van der Poel, H. G., Fluorescence Guidance in Urologic Surgery. *Curr Opin Urol* 2012, *22* (2), 109-120.

(7) Blum, G.; von Degenfeld, G.; Merchant, M. J.; Blau, H. M.; Bogyo, M., Noninvasive Optical Imaging of Cysteine Protease Activity Using Fluorescently Quenched Activity-based Probes. *Nat Chem Biol* 2007, *3* (10), 668-677.

(8) Urano, Y.; Sakabe, M.; Kosaka, N.; Ogawa, M.; Mitsunaga, M.; Asanuma, D.; Kamiya, M.; Young, M. R.; Nagano, T.; Choyke, P. L.; Kobayashi, H., Rapid Cancer Detection by Topically Spraying a Gamma-Glutamyltranspeptidase-Activated Fluorescent Probe. *Sci Transl Med* 2011, *3* (110), 110-119.

(9) Shi, H.; He, X.; Wang, K.; Wu, X.; Ye, X.; Guo, Q.; Tan, W.; Qing, Z.; Yang, X.; Zhou, B., Activatable Aptamer Probe for Contrast-Enhanced in vivo Cancer Imaging Based on Cell Membrane Protein-Triggered Conformation Alteration. *Proc Natl Acad Sci U S A* 2011, *108* (10), 3900-3905.

(10) Tung, C.-H., Fluorescent Peptide Probes for in vivo Diagnostic Imaging. *Peptide Science* 2004, *76* (5), 391-403.

(11) Bremer, C.; Tung, C.-H.; Weissleder, R., In Vivo Molecular Target Assessment of Matrix Metalloproteinase Inhibition. *Nat Med* 2001, *7* (6), 743-748.

(12) Jaffer, F. A.; Kim, D. E.; Quinti, L.; Tung, C. H.; Aikawa, E.; Pande, A. N.; Kohler, R. H.; Shi, G. P.; Libby, P.; Weissleder, R., Optical Visualization of Cathepsin K Activity in Atherosclerosis with a Novel, Protease-activatable Fluorescence Sensor. *Circulation* 2007, *115* (17), 2292-2298.

(13) Luo, S.; Zhang, E.; Su, Y.; Cheng, T.; Shi, C., A Review of NIR Dyes in Cancer Targeting and Imaging. *Biomaterials* 2011, *32* (29), 7127-7138.

(14) Duke, R. M.; Veale, E. B.; Pfeffer, F. M.; Kruger, P. E.; Gunnlaugsson, T., Colorimetric and Fluorescent Anion Sensors: An Overview of Recent Developments in the Use of 1,8-naphthalimide-Based Chemosensors. *Chem Soc Rev* 2010, *39* (10), 3936-3953.

(15) Razgulin, A.; Ma, N.; Rao, J., Strategies for in vivo Imaging of Enzyme Activity: An Overview and Recent Advances. *Chem Soc Rev* 2011, *40* (7), 4186-4216.

(16) Danson, S.; Ward, T. H.; Butler, J.; Ranson, M., DT-Diaphorase: A Target for New Anticancer Drugs. *Cancer Treat Rev* 2004, *30* (5), 437-449.

(17) Smitskamp-Wilms, E.; Hendriks, H. R.; Peters, G. J., Development, Pharmacology, Role of DT-Diaphorase and Prospects of the Indoloquinone EO9. *Gen Pharmacol* 1996, *27* (3), 421-429.

(18) Bongard, R. D.; Lindemer, B. J.; Krenz, G. S.; Merker, M. P., Preferential Utilization of NADPH as the Endogenous Electron Donor for NAD(P)H:quinone Oxidoreductase 1 (NQO1) in Intact Pulmonary Arterial Endothelial Cells. *Free Radic Biol Med* 2009, *46* (1), 25-32.

(19) Hernick, M.; Flader, C.; Borch, R. F., Design, Synthesis, and Biological Evaluation of Indolequinone Phosphoramidate Prodrugs Targeted to DT-Diaphorase. *J Med Chem* 2002, *45* (16), 3540-3548.

(20) Dinkova-Kostova, A. T.; Talalay, P., NAD(P)H:quinone Acceptor Oxidoreductase 1 (NQO1), a Multifunctional Antioxidant Enzyme and Exceptionally Versatile Cytoprotector. *Arch Biochem Biophys* 2010, *501* (1), 116-123.

(21) Goloudina, A. R.; Tanoue, K.; Hammann, A.; Fourmaux, E.; Le Guezennec, X.; Bulavin, D. V.; Mazur, S. J.; Appella, E.; Garrido, C.; Demidov, O. N., Wip1 Promotes RUNX2-dependent Apoptosis in p53-negative Tumors and Protects Normal Tissues During Treatment with Anticancer Agents. *Proc Natl Acad Sci U S A* 2012, *109* (2), 68-75.

(22) Ong, W.; Yang, Y.; Cruciano, A. C.; McCarley, R. L., Redox-Triggered Contents Release from Liposomes. *J Am Chem Soc* 2008, *130* (44), 14739-14744.

(23) Friis, E. P.; Andersen, J. E. T.; Madsen, L. L.; Bonander, N.; Møller, P.; Ulstrup, J., Dynamics of Pseudomonas aeruginosa azurin and its Cys3Ser Mutant at Single-crystal Gold Surfaces Investigated by Cyclic Voltammetry and Atomic Force Microscopy. *Electrochim Acta* 1997, *42* (19), 2889-2897.

(24) Qian, X.; Xiao, Y.; Xu, Y.; Guo, X.; Qian, J.; Zhu, W., "Alive" Dyes as Fluorescent Sensors: Fluorophore, Mechanism, Receptor and Images in Living Cells. *Chem Commun* 2010, *46* (35), 6418-6436.

(25) Silvers, W. C.; Payne, A. S.; McCarley, R. L., Shedding Light by Cancer Redox-human NAD(P)H:quinone Oxidoreductase 1 Activation of a Cloaked Fluorescent Dye. *Chem Commun* 2011, *47* (40), 11264-11266.

(26) Carpino, L. A.; Triolo, S. A.; Berglund, R. A., Reductive Lactonization of Strategically Methylated Quinone Propionic Acid Esters and Amides. *J Org Chem* 1989, *54* (14), 3303-3310.

(27) Ward, M. D., Photo-induced Electron and Energy Transfer in Non-covalently Bonded Supramolecular Assemblies. *Chem Soc Rev* 1997, *26* (5), 365-375.

(28) Ong, W.; McCarley, R. L., Chemically and Electrochemically Mediated Release of Dendrimer End Groups. *Macromolecules* 2006, *39* (21), 7295-7301.

(29) Lakowicz, J. R., Mechanisms and Dynamics of Fluorescence Quenching. In *Principles of Fluorescence Spectroscopy*, Third ed.; Springer: 2006; pp 331-351.

(30) Nicolaou, M. G.; Wolfe, J. L.; Schowen, R. L.; Borchardt, R. T., Facilitated Intramolecular Conjugate Addition of Amides of 3-(3',6'-Dioxo-2',4'-dimethyl-1',4'-cyclohexadienyl)-3,3-dimethylpropionic Acid 2. Kinetics of Degradation. *J Org Chem* 1996, *61* (19), 6633-6638.

(31) Melhuish, W. H., Quantum Efficiencies of Fluorescence of Organic Substances: Effect of Solvent and Concentration of the Fluorescent Solute. *J Phys Chem* 1961, *65* (2), 229-235.

(32) Gioux, S.; Choi, H. S.; Frangioni, J. V., Image-guided Surgery Using Invisible Near-infrared Light: Fundamentals of Clinical Translation. *Mol Imaging* 2010, *9* (5), 237-255.

(33) de Silva, A. P.; Gunaratne, H. Q. N.; Habib-Jiwan, J.-L.; McCoy, C. P.; Rice, T. E.; Soumillion, J.-P., New Fluorescent Model Compounds for the Study of Photoinduced Electron Transfer: The Influence of a Molecular Electric Field in the Excited State. *Angew Chem, Int Ed* 1995, *34* (16), 1728-1731.

(34) Bissell, R. A.; de Silva, A. P.; Gunaratne, H. Q. N.; Lynch, P. L. M.; Maguire, G. E. M.; Sandanayake, K. R. A. S., Molecular Fluorescent Signalling with 'Fluor-Spacer-Receptor'

Systems: Approaches to Sensing and Switching Devices via Supramolecular Photophysics. *Chem Soc Rev* 1992, *21* (3), 187-195.

(35) Staneva, D.; McKena, M.; Bosch, P.; Grabchev, I., Synthesis and Spectroscopic Studies of a New 1,8-naphthalimide Dyad as Detector for Metal Cations and Protons. *Spectrochim Acta A* 2010, *76* (2), 150-154.

(36) Georgiev, N. I.; Bojinov, V. B.; Nikolov, P. S., The Design, Synthesis and Photophysical Properties of Two Novel 1,8-naphthalimide Fluorescent pH Sensors Based on PET and ICT. *Dyes Pigments* 2011, *88* (3), 350-357.

(37) Beall, H. D.; Murphy, A. M.; Siegel, D.; Hargreaves, R. H.; Butler, J.; Ross, D., Nicotinamide Adenine Dinucleotide (Phosphate): Quinone Oxidoreductase (DT-diaphorase) as a Target for Bioreductive Antitumor Quinones: Quinone Cytotoxicity and Selectivity in Human Lung and Breast Cancer Cell Lines. *Mol Pharmacol* 1995, *48* (3), 499-504.

(38) Shi, C., Comment on "Rapid Cancer Detection by Topically Spraying a γ-Glutamyltranspeptidase–Activated Fluorescent Probe". *Sci Transl Med* 2012, *4* (121), 121le1.

(39) Peti-Peterdi, J.; Burford, J. L.; Hackl, M. J., The First Decade of Using Microscopy for High-power Kidney Imaging. *Am J Physiol - Renal* 2012, *302* (2), F227-F233.

(40) Balamurugan, S., Unpublished Results.

(41) Perera, K. L. I. Kinetic Studies on Lactonization of Quinone Propionic Acid Derivatives for the Development of Redox-responsive Liposomes. Louisiana State University, 2012.

(42) Huang, S. T.; Peng, Y. X.; Wang, K. L., Synthesis of a new long-wavelength latent fluorimetric indicator for analytes determination in the DT-Diaphorase coupling dehydrogenase assay system. *Biosens Bioelectron* 2008, *23* (12), 1793-8.

(43) Huang, S. T.; Lin, Y. L., New Latent Fluorophore for DT Diaphorase. *Org Lett* 2006, *8* (2), 265-268.

CHAPTER 4

SOLVENT DEPENDENCE EFFECTS ON HUMAN NAD(P)H:QUINONE OXIDOREDUCTASE-1 ACTIVITY

4.1 Introduction

With the growing number of NQO1 substrates and inhibitors for cancer treatment,[1-7] there is a pressing need for consistency when determining substrate specificity allowing for more accurate comparison between substrates. The most common way to compare substrate specificity for enzymes is to determine and compare kinetic parameters such as: the theoretical maximum velocity (V_{max}), Michaelis constant (K_m), catalytic turnover (k_{cat}), and catalytic efficiency (k_{cat}/K_m).[8] This is accomplished by performing enzyme assays in very similar environments, such as in specific buffers, buffer and salt concentrations, pH, same enzyme activators (such as fetal bovine serum), etc. One of the issues in the execution of enzyme assays is that a majority of substrates are not highly water soluble, while the native environment of enzymes is aqueous media.[8] To circumvent this problem, solutes are generally dissolved in organic solvents that are miscible with water. This inherently imparts a new variable in determining the ability of an enzyme to catalyze a specific reaction. As enzymes are intricate machinery whose nature is to catalyze reactions in specific environments, any perturbation to that environment can cause drastic changes in enzyme structure and catalytic activity. One of the largest effects organic solvents have on enzymes is the removal of water from the hydration shell or the active site in the enzyme causing drastic changes in the solvation of the enzyme. [9-13] This removal of water leads to denaturation of the 3D structure of the enzyme. These forces include: hydrogen bonding, van der Waals, and hydrophobic interactions.[9] By altering this balance of forces, a change is created in the enzyme rigidity and the ability to catalyze its specific reaction. From previous work, it has been found that polar solvents have the ability to penetrate deeper

into an enzyme, whereas nonpolar solvents have a more limited penetration.[9] Along with polarity, solvents with lower dielectric constants impart stronger electrostatic interactions leading to more rigid enzymes.[11, 14] NQO1 utilizes a flavin adenine dinucleotide (FAD) cofactor in the active site to catalyze its 2-electron reduction reactions. Faig et al. elucidated the structure of the FAD unit in the active site of human-NQO1 (hNQO1) and were able to reveal the hydrogen bonding, van der Waals interactions, and the water molecules between FAD and the hNQO1 protein, Figure 4.1.[15]

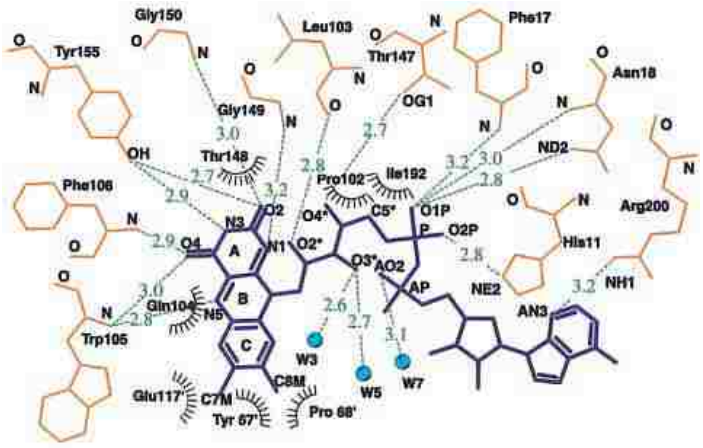

Figure 4.1. Hydrogen bonding and van der Waals interaction observed between FAD and protein in hNQO1. Open radiated circles indicate hydrophobic interactions. Hydrogen bonds are represented by dashed green lines; water molecules are shown as blue filled circles.[15]

As seen in Figure 4.1, there are multiple interactions which are a part of the FAD and NQO1 protein where the catalysis occurs. Perturbation of this substructure, and also the solvation of the enzyme, has the potential to cause drastic fluctuations in enzymes ability to catalyze the reduction of quinones. As mentioned above, many enzyme substrates are only soluble in organic solvents. This introduction of non-native species to the NQO1 assay environment can produce inconsistent results in substrate analysis. Previous work on producing NQO1 substrates and determining the ability of NQO1 to reduce these compounds has produced a variety of assay conditions in which different organic solvents are used at low concentrations

ranging from 0.5% to 2%, or even unspecified amounts.[2, 4-5, 16-19] Here, the ability of hNQO1 to catalyze the reduction of 3-(3',6'-dioxo-2',4',5'-trimethylcyclohexa-1',4'-diene)-3,3-dimethylpropionic acid (Q_3PA) to its hydroquinone under various solvent-buffer systems is analyzed, Scheme 4.1. To test hNQO1 activity, multiple assays were performed with only one variable, the solvent. The solvents tested are the most commonly used water miscible organic solvents used in hNQO1 assays: acetonitrile (ACN), ethanol (EtOH), and dimethyl sulfoxide (DMSO). By changing only the solvent type and the overall solvent percentage, it will be possible to elucidate the effect of different organic solvents on the ability of hNQO1 to catalyze the reduction of quinones.

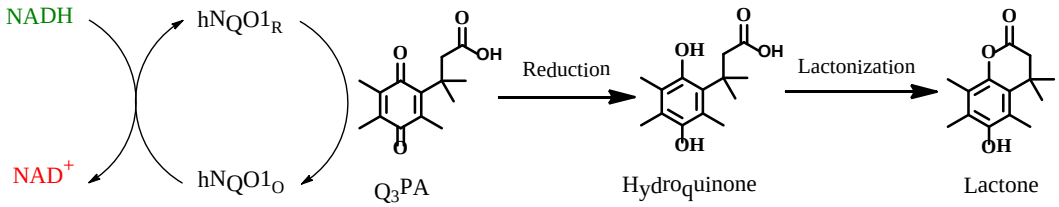

Scheme 4.1. Reduction and lactonization of Q_3PA by NQO1.

4.2 Experimental Section

4.2.1 Materials and Methods

All chemicals were purchased from Sigma-Aldrich or Fisher Scientific and used as received. 3-(3',6'-dioxo-2',4',5'-trimethylcyclohexa-1',4'-diene)-3,3-dimethylpropionic acid (Q_3PA) was prepared according to literature procedures.[20] Enzyme assays were performed using a quartz 96-well plate (Hellma) on a FLUOstar OPTIMA plate reader from BMG LABTECH.

4.2.2 NADH Calibration Curve Preparation

Phosphate-buffered saline (PBS) solutions were prepared by dissolving potassium phosphate monobasic (4.54 g, 0.033 mol), potassium phosphate dibasic (11.6 g, 0.067 mol), and potassium chloride (7.45 g, 0.1 M) in one liter of nanopure water/organic solvent. The pH was

adjusted by adding a concentrated solution of potassium hydroxide dropwise. Fetal bovine serum (FBS) was added to give a final concentration of 0.007% w/v. Standard solutions of β-nicotinamide adenine dinucleotide reduced disodium salt (NADH) were prepared by diluting stock NADH solutions in solvent-PBS into the same solvent system. A calibration curve for each solvent-PBS system was obtained by placing 200 μL of the NADH standard solutions into the quartz 96-well plate. Absorbance measurements were obtained using the λ = 340 nm filter with each scan containing 40 flashes. Each experiment was done in triplicate.

4.2.3 Enzyme Assay Conditions

NQO1 assays for the reduction of Q_3PA were performed by following reduction in absorbance at 340 nm for the conversion of reduced NADH to the oxidized form NAD^+. Scans were taken every 4 seconds for 44 seconds at room temperature (22 to 24 °C) using a FLUOstar OPTIMA plate reader, and the assays were performed in a quartz 96-well plate (Hellma). Recombinant human NQO1 (Sigma-Aldrich) in pH 7.4, 0.1 M solvent-PBS and supplemented with 0.007% bovine serum albumin (BSA) was used. Stock solutions of Q_3PA were prepared in the 0.1 M solvent-PBS and diluted in buffer to a final concentration between 25×10^{-6} and 350×10^{-6} M. Total volume per well was 200×10^{-6} L with a final NQO1 content of 5×10^{-7} g. Assays were initiated by the instrument-injection of NADH so as to yield a final NADH concentration of 100×10^{-6} M. All assays were performed in triplicate. Rate versus [Q_3PA] curves were fitted with a non-linear least-squares algorithm so as to obtain apparent K_m and V_{max} values.

4.3 Results and Discussion

4.3.1 NADH Calibration Curves

To determine the kinetic parameters for hNQO1 in each solvent system, the oxidation of NADH to NAD^+ was followed over 44 seconds. This is possible because NADH strongly

absorbs at 340 nm and NAD^+ does not. To ensure proper conversion from absorbance units to concentration units for each assay, a calibration curve for NADH was produced for all solvent-PBS systems, Figure 4.2.

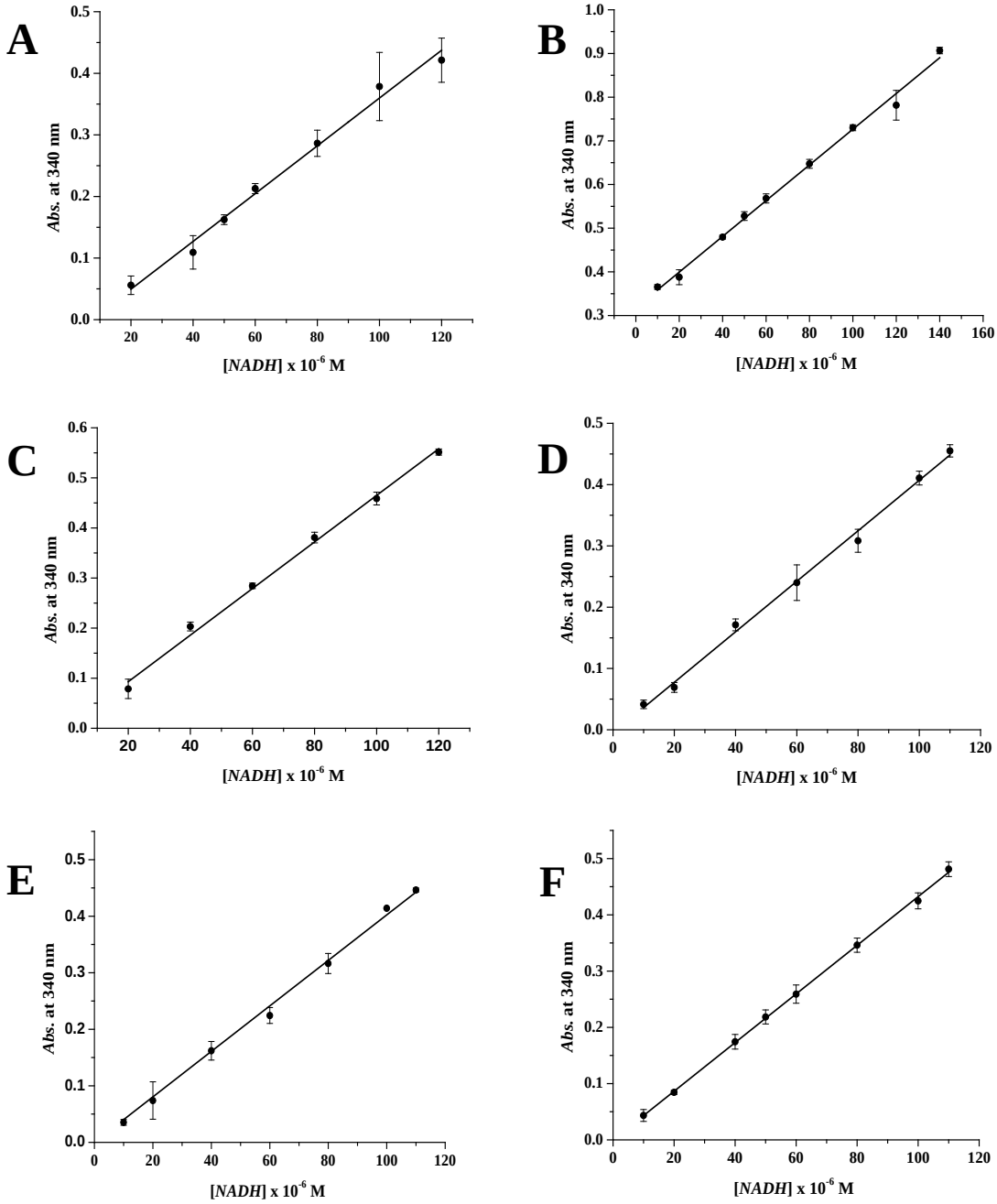

Figure 4.2. Calibration curves for NADH in 5% DMSO-PBS (A), 10% DMSO-PBS (B), 5% Ethanol-PBS (C), 10% Ethanol-PBS (D), 5% ACN-PBS (E), and 10% ACN-PBS (F) a quartz 96-well plate. Each solution contained 0.1M PBS supplemented with 0.007% FBS and had a pH of 7.4. λ = 340 nm.

While each extinction coefficient was relatively close to that of NADH in pH 7.4, 0.1 M PBS with 0.007% FBS (4390 $M^{-1}cm^{-1}$)[16], they did vary slightly. Extinction coefficients (ε) for 5% and 10% DMSO-PBS were measured to be 3879 ± 170 $M^{-1}cm^{-1}$ and 4090 ± 106 $M^{-1}cm^{-1}$, respectively. While ε in 5% and 10% ethanol-PBS systems was 4610 ± 62 $M^{-1}cm^{-1}$ and 4120 ± 111 $M^{-1}cm^{-1}$, respectively; in 5% and 10% ACN-PBS, ε was found to be 4020 ± 51 $M^{-1}cm^{-1}$ and 4323 ± 20 $M^{-1}cm^{-1}$, respectively. Because all calibration curves were run in triplicate and produced expected results, the values were considered acceptable and used for each assay.

4.3.2 Solvent Effect on NQO1 Kinetics

To determine what effect, if any, organic solvents would impact the ability of hNQO1 to catalyze the reduction of quinones, multiple enzyme assays were performed in a wide variety of solvent-containing systems with differing percentages of solvent in each system. To ensure it was a solvent-dependent experiment, all other parameters except solvent type and percentage were kept constant. For all systems, the pH was adjusted to 7.4, the substrate used was always Q_3PA each system contained 0.007% FBS, every assay contained 0.5 μg enzyme from the same batch, assays were run in triplicate, NADH concentration was 100 μM, and all systems contained 0.1 M PBS and 0.1 M KCl. The solvents tested were ACN, EtOH, and DMSO at 5% and 10% in each solvent-PBS system, Figure 4.3.

After each assay was completed, apparent Michaelis-Menten kinetic parameters were obtained using the computer program from Cleland, Table 4.1.[21] This program determines values and their error from least squares fitting to the equation:

$$V = \frac{V_{\max} \times [S]}{K_m + [S]} \qquad \text{Equation 4.1}$$

where V is the initial velocity of catalysis at a given concentration, [S] is substrate concentration, V_{max} is theoretical maximum velocity, and K_m is the substrate concentration of an estimate for the equilibrium constant for S binding to an enzyme. Though there was error between the individual replicates, the averages for each assay produced quality data for fitting to Equation 4.1. Comparison of all V_{max} values showed low calculated error from the least squares fit equation, with 12% error or less.

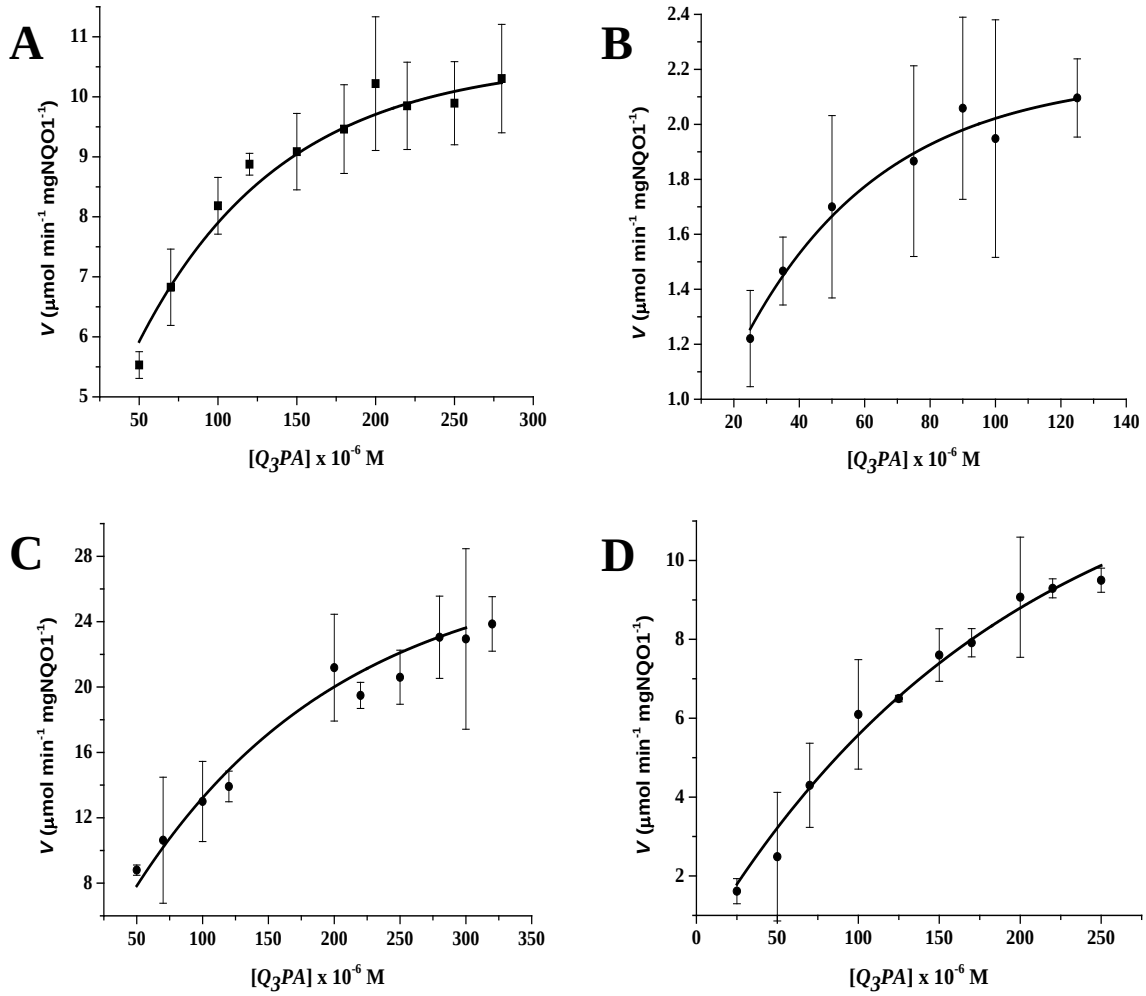

Figure 4.3. Michaelis-Menten kinetics plot of hNQO1 (0.5 μg) towards Q_3PA in different solvent systems. Solvent systems in PBS are: 5% DMSO (A), 10% DMSO (B), 5% EtOH (C), 10% EtOH (D), 5% ACN (E), 10% ACN (F).

Figure 4.3 Continued

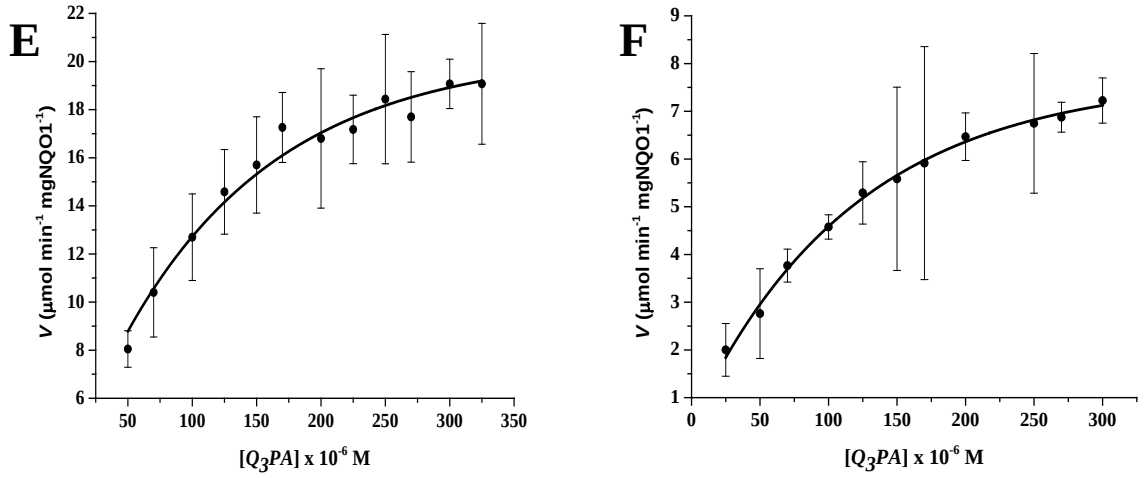

Table 4.1. Kinetic parameters for the reduction of Q_3PA by hNQO1 in different solvent-PBS systems.

	% Solvent	K_m (μM)	V_{max} (μmol·min^{-1}·mg^{-1} hNQO1	k_{cat} (sec^{-1})	k_{cat}/K_m (M^{-1}·sec^{-1})
	0	158 ± 41	38 ± 5	19.6 ± 2.6	(1.2 ± 0.4) × 10^5
DMSO	**5**	55 ± 5	12.3 ± 0.3	6.33 ± 0.15	(1.1 ± 0.1) × 10^5
	10	26 ± 3	2.54 ± 0.08	1.31 ± 0.00	(5.8 ± 0.6) × 10^4
EtOH	**5**	180 ± 20	37 ± 2	19.1 ± 1.0	(1.1 ± 0.1) × 10^5
	10	264 ± 54	20.4 ± 2.5	10.5 ± 1.3	(4.0 ± 0.2) × 10^4
ACN	**5**	94 ± 9	25 ± 1	5.4 ± 0.5	(5.7 ± 0.6) × 10^4
	10	115 ± 8	9.9 ± 0.3	5.1 ± 0.2	(4.4 ± 0.4) × 10^4

When compared to the V_{max} obtained for hNQO1 towards Q_3PA in buffer only (38 μmol·min^{-1}·mg^{-1}), measurement of the solvent in all cases appears to cause an inhibition of the enzyme. It is also seen that increasing the amount of solvent in the assay environment substantially decreases the V_{max} for hNQO1, Figure 4.5. For all three solvents at 10%, hNQO1 is

inhibited by 93% in DMSO, 46% in EtOH, and 74% in ACN. As for the 5% systems, hNQO1 has 68%, 3%, and 34% lower V_{max} in DMSO, EtOH, and ACN, respectively. It is clear that DMSO has the most detrimental effect on hNQO1 catalysis when compared to ACN and EtOH, and ACN has more of an effect than EtOH. As stated above, more polar solvents can penetrate into enzymes further creating a more perturbed state. The order of polarity for the three solvents is: DMSO > ACN > EtOH.[22] Also stated above is the fact that solvents with higher dielectric constants produce more electrostatic interactions causing the enzyme to be more rigid. The order of increasing dielectric constants is: DMSO (46.7) > ACN (37.5) > EtOH (24.3).[14] This order of polarity and dielectric constants correlates well with the V_{max} values decreasing from EtOH, to ACN, and then to DMSO. From this analysis, it is clear that ethanol provides the best organic solvent when a substrate needs to be dissolved before introduction into an assay. Even at just a 5% solvent amount, DMSO and ACN considerably reduced the ability of hNQO1 to catalyze the reaction, while hNQO1 remains essentially completely active in ethanol. The same cannot be said for assays containing 10% organic solvent, where hNQO1 retains only 54% of its activity or less.

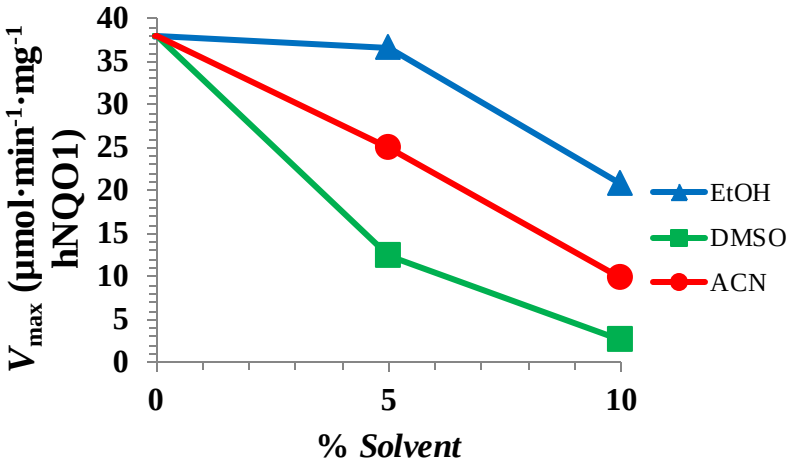

Figure 4.4. Comparison of the V_{max} values calculated for hNQO1 towards Q_3PA in different solvent-PBS systems.

Using the molecular weight of 31,000 g/mol for the hNQO1 monomer, catalytic activity (k_{cat}) was calculated from the V_{max} values.[23] From this, catalytic efficiencies (k_{cat}/K_m) were calculated for hNQO1 in each solvent-PBS system, Table 4.1. When comparing these values, it was noticed that hNQO1 was actually least efficient in ACN and was similarly efficient in DMSO and EtOH. For the 5% solvent systems, ACN was only 46% as efficient as hNQO1 in only buffer; while EtOH and DMSO were 85% and 93% as efficient, respectively. But, the ability of hNQO1 to work properly was significantly reduced to 36%, 32%, and 47% for ACN, EtOH, and DMSO, respectively, when the assay was performed in 10% solvent-PBS. This comparison demonstrates that even though the enzyme loses a majority of its activity in DMSO at 5%, its efficiency is relatively close to that of an assay with no organic solvent. This is possible even though V_{max} is substantially reduced, K_m is also reduced by a large amount indicating a tighter substrate binding to the enzyme. An increase in organic solvent from 5% to 10% produces an enzyme that maintains less than half of its catalytic efficiency.

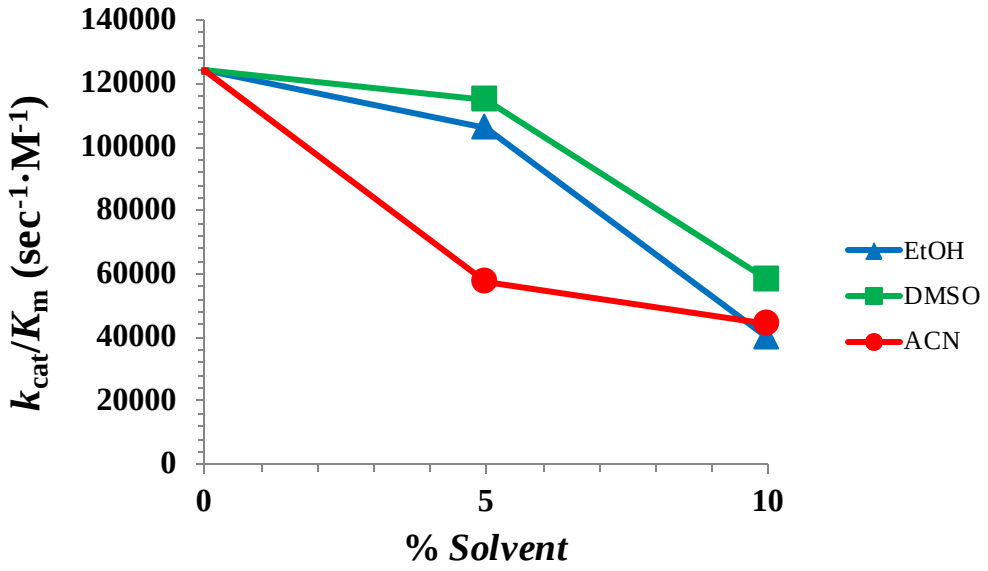

Figure 4.5. Comparison of the k_{cat}/K_m values calculated for hNQO1 towards Q_3PA in different solvent-PBS systems.

4.4 Conclusions

Here, it was demonstrated the effect of three different organic solvents (ACN, EtOH, and DMSO) had on the ability of hNQO1 to catalyze the reduction of Q_3PA to a hydroquinone. These three solvents produced results using Michaelis-Menten kinetics that followed previous trends of more polar solvents penetrating deeper into enzymes causing a more drastic change in the 3D shape of the enzyme and solvents with higher dielectric constants producing more rigid enzymes.[9] DMSO has been previously used to study the overall and secondary structures of proteins because it strongly perturbs proteins.[24-25] While the two methyls in DMSO are thought to interact with the hydrophobic residues in proteins, the strong proton-accepting nature of the sulfoxide is thought to be the driving force behind the ability of DMSO to strongly denature proteins.[25] This strong affinity for protons leads to the disruption of hydrogen-bonding and weakening the hydrophobic interactions throughout the protein and its secondary structures, leading to a more unfolded state as the concentration of DMSO is increased.[24, 26] Alcohols have also been used to study the structures of proteins because they have not only been found to denature proteins in some cases, but also stabilized helixes, β-sheet hairpins, and other secondary structures.[27-29] This stabilization effect can be partially explained by the decrease in polarity in the ethanol-water solvent system where ethanol preferentially associates with protein surface hydrophobic sites, which weakens the hydrophobic interactions and strengthens the hydrogen-bonds in helixes and other secondary structures.[27-28] Though ethanol is a proton donor, it has been shown to bind to hydrogen donors (amides) and hydrogen acceptors (carbonyls) equally.[27] Though enzyme properties in the presence of DMSO vary from enzyme-to-enzyme, with some being activated and other having negligible catalytic differences[30], NQO1 is greatly inhibited when in the presence of DMSO. From the results above, it was found that DMSO and ACN

drastically reduced the enzymes V_{max} by 68% and 34%, respectively, at only a 5% solvent level. On the other hand, hNQO1 retained all of its activity in 5% EtOH. But, the shift from 5% solvent to 10% solvent created a poorly catalyzing hNQO1 which had 54% of its activity in EtOH, 7% in DMSO, and 26% in ACN. With the sharp reduction of V_{max} in DMSO, hNQO1 retains a majority of its efficiency at 5% DMSO. This was due to the concurrent reduction in K_m, which demonstrates tighter binding substrates along with slower turnover. From the three solvents tested, EtOH is superior to ACN and DMSO at 5% levels, allowing the enzyme to retain 97% of its V_{max} and remain 87% efficient. Though DMSO is most commonly used to dissolve substrates for assays, ethanol is now shown to be the better option to obtain kinetic values which should more closely resemble those obtained in 100% buffer.

4.5 References

(1) Beall, H. D.; Winski, S.; Swann, E.; Hudnott, A. R.; Cotterill, A. S.; O'Sullivan, N.; Green, S. J.; Bien, R.; Siegel, D.; Ross, D.; Moody, C. J., Indolequinone Antitumor Agents: Correlation Between Quinone Structure, Rate of Metabolism by Recombinant Human NAD(P)H:Quinone Oxidoreductase, and in Vitro Cytotoxicity. *J Med Chem* 1998, *41* (24), 4755-4766.

(2) Hernick, M.; Flader, C.; Borch, R. F., Design, Synthesis, and Biological Evaluation of Indolequinone Phosphoramidate Prodrugs Targeted to DT-Diaphorase. *J Med Chem* 2002, *45* (16), 3540-3548.

(3) Volpato, M.; Abou-Zeid, N.; Tanner, R. W.; Glassbrook, L. T.; Taylor, J.; Stratford, I.; Loadman, P. M.; Jaffar, M.; Phillips, R. M., Chemical Synthesis and Biological Evaluation of a NAD(P)H:quinone Oxidoreductase-1 Targeted Tripartite Quinone Drug Delivery System. *Molecular cancer therapeutics* 2007, *6* (12 Pt 1), 3122-3130.

(4) Winski, S. L.; Faig, M.; Bianchet, M. A.; Siegel, D.; Swann, E.; Fung, K.; Duncan, M. W.; Moody, C. J.; Amzel, L. M.; Ross, D., Characterization of a Mechanism-Based Inhibitor of NAD(P)H:Quinone Oxidoreductase 1 by Biochemical, X-ray Crystallographic, and Mass Spectrometric Approaches. *Biochem* 2001, *40* (50), 15135-15142.

(5) Lee, Y. Y.; Westphal, A. H.; de Haan, L. H. J.; Aarts, J. M. M. J. G.; Rietjens, I. M. C. M.; van Berkel, W. J. H., Human NAD(P)H:Quinone Oxidoreductase Inhibition by Flavonoids in Living Cells. *Free Radic Biol Med* 2005, *39* (2), 257-265.

(6) Gibson, N. W.; Hartley, J. A.; Butler, J.; Siegel, D.; Ross, D., Relationship Between DT-Diaphorase-Mediated Metabolism of a Series of Aziridinylbenzoquinones and DNA Damage and Cytotoxicity. *Mol Pharm* 1992, *42* (3), 531-536.

(7) Reigan, P.; Colucci, M. A.; Siegel, D.; Chilloux, A.; Moody, C. J.; Ross, D., Development of Indolequinone Mechanism-Based Inhibitors of NAD(P)H:Quinone Oxidoreductase 1 (NQO1): NQO1 Inhibition and Growth Inhibitory Activity in Human Pancreatic MIA PaCa-2 Cancer Cells. *Biochem* 2007, *46* (20), 5941-5950.

(8) *Enzyme Assays: A Practical Approach*. Second ed.; Oxford University Press: USA, 2002.

(9) Serdakowski, A. L.; Dordick, J. S., Enzyme Activation for Organic Solvents Made Easy. *Trends Biotechnol* 2008, *26* (1), 48-54.

(10) Zaks, A.; Klibanov, A. M., Enzyme-catalyzed Processes in Organic Solvents. *Proc Natl Acad Sci U S A* 1985, *82* (10), 3192-3196.

(11) Klibanov, A. M., Why are Enzymes Less Active in Organic Solvents than in Water? *Trends Biotechnol* 1997, *15* (3), 97-101.

(12) van Erp, S. H. M.; Kamenskaya, E. O.; Khmelnitsky, Y. L., The Effect of Water Content and Nature of Organic Solvent on Enzyme Activity in Low-water Media. *Eur J Biochem* 1991, *202* (2), 379-384.

(13) Gorman, L. A. S.; Dordick, J. S., Organic Solvents Strip Water Off Enzymes. *Biotechnol Bioeng* 1992, *39* (4), 392-397.

(14) Affleck, R.; Haynes, C. A.; Clark, D. S., Solvent Dielectric Effects on Protein Dynamics. *Proc Natl Acad Sci U S A* 1992, *89* (11), 5167-5170.

(15) Faig, M.; Bianchet, M. A.; Talalay, P.; Chen, S.; Winski, S.; Ross, D.; Amzel, L. M., Structures of Recombinant Human and Mouse NAD(P)H:Quinone Oxidoreductases: Species Comparison and Structural Changes with Substrate Binding and Release. *Proc Natl Acad Sci U S A* 2000, *97* (7), 3177-3182.

(16) Mendoza, M. Characterization of Triggerable Quinones for the Development of Enzyme-Responsive Liposomes. Research, Louisiana State University, 2012.

(17) Buffinton, G. D.; Ollinger, K.; Brunmark, A.; Cadenas, E., DT-Diaphorase-Catalysed Reduction of 1,4-naphthoquinone Derivatives and Glutathionyl-Quinone Conjugates. Effect of Substituents on Autoxidation Rates. *Biochem J* 1989, *257* (2), 561-571.

(18) Phillips, R. M., Bioreductive Activation of a Series of Analogues of 5-aziridinyl-3-hydroxymethyl-1-methyl-2-[1H-indole-4, 7-dione] prop-β-en-α-ol (EO9) by Human DT-Diaphorase. *Biochem Pharmacol* 1996, *52* (11), 1711-1718.

(19) Osman, A. M.; Boeren, S., Studies on the DT-diaphorase-catalysed Reaction Employing Quinones as Substrates: Evidence for a Covalent Modification of DT-diaphorase by Tetrachloro-p-benzoquinone. *Chem Biol Interact* 2004, *147* (1), 99-108.

(20) Carpino, L. A.; Triolo, S. A.; Berglund, R. A., Reductive Lactonization of Strategically Methylated Quinone Propionic Acid Esters and Amides. *J Org Chem* 1989, *54* (14), 3303-3310.

(21) Cleland, W. W., Computer Programmes for Processing Enzyme Kinetic Data. *Nature* 1963, *198* (487), 463-465.

(22) Sadek, P. C., *The HPLC Solvent Guide*. Second ed.; Wiley: 2002.

(23) Huang, S. T.; Lin, Y. L., New Latent Fluorophore for DT Diaphorase. *Org Lett* 2006, *8* (2), 265-268.

(24) Jackson, M.; Mantsch, H. H., Beware of Proteins in DMSO. *Biochim Biophys Acta* 1991, *1078* (2), 231-235.

(25) Bhattacharjya, S.; Balaram, P., Effects of Organic Solvents on Protein Structures: Observation of a Structured Helical Core in Hen Egg-White Lysozyme in Aqueous Dimethylsulfoxide. *Proteins: Struct, Func, and Bioinf* 1997, *29* (4), 492-507.

(26) Huang, P.; Dong, A.; Caughey, W. S., Effects of dimethyl sulfoxide, glycerol, and ethylene glycol on secondary structures of cytochrome c and lysozyme as observed by infrared spectroscopy. *Journal of Pharmaceutical Sciences* 1995, *84* (4), 387-392.

(27) Buck, M., Trifluoroethanol and Colleagues: Cosolvents Come of Age. Recent Studies with Peptides and Proteins. *Q Rev Biophys* 1998, *31* (03), 297-355.

(28) Hirota, N.; Mizuno, K.; Goto, Y., Group Additive Contributions to the Alcohol-Induced α-Helix Formation of Melittin: Implication for the Mechanism of the Alcohol Effects on Proteins. *J Mol Bio* 1998, *275* (2), 365-378.

(29) Hwang, S.; Shao, Q.; Williams, H.; Hilty, C.; Gao, Y. Q., Methanol Strengthens Hydrogen Bonds and Weakens Hydrophobic Interactions in Proteins – A Combined Molecular Dynamics and NMR study. *J Phys Chem B* 2011, *115* (20), 6653-6660.

(30) Somasundaran, P., *Encyclopedia of Surface and Colloid Science*. 2nd ed.; CRC: 2006; Vol. 7.

CHAPTER 5

CONCLUSIONS AND OUTLOOK

5.1 Summary

The overall goal of this research was the development and implementation of an activatable latent fluorophore for intracellular NQO1 detection. The fluorescent probe was designed to be sensitive by having a nearly non-fluorescent quenched state and a highly fluorescent free dye. The probe's receptor unit needed to be highly selective for NQO1 2-electron reduction catalysis and undergo rapid lactonization from the probe to reveal the dye's fluorescent signal. The probe was analyzed by determining the quantum yield of each free dye and capped dye, determining enzyme kinetic parameters, imaging the probe in different cell lines using fluorescence microscopy, and determining the ability to differentiate between hNQO1-positive and hNQO1-negative cell lines using flow cytometry.

Quantum yield values for rhodamine110-based latent fluorophores in pH 7.4, 0.1 M PBS yielded 0.005 for Q_3-Rho-Morph and 0.48 for Rho-Morph, which leads to a 96-fold increase in fluorescence. Rho-Morph excitation and emission maxima were measured to be λ_{ex} = 490 nm and λ_{em} = 520 nm. Q_3-Rho-Morph was found to be rapidly activated with the release of Rho-Morph by sodium dithionite and was highly stable in the presence of high concentrations of glutathione, ascorbic acid, and dithiothreitol. Along with sodium dithionite, it was observed that Q_3-Rho-Morph was activated by NQO1 in the presence of NADH and was very stable while in a solution of NADH only. The kinetic parameters were measured to be 0.00214 ± 0.00013 μmol min^{-1} mg·$NQO1^{-1}$ for V_{max} and 46.4 ± 7.4 M^{-1} sec^{-1} for k_{cat}/K_m. The low catalytic efficiency for NQO1 towards Q_3-Rho-Morph is most likely due to the steric hindrance of the rhodamine species in close proximity to the quinone substrate, thus preventing the probe from effectively

entering the active site. Using fluorescence and absorbance spectroscopy, it was found that the Rho-Morph species was readily reduced by a low concentration in NADH in a pH 7.4, 0.1 M PBS solution. The reduction led to a rapid loss of absorbance at λ = 485 nm and, coincidentally, a loss of fluorescence. This catalytic inefficiency and reduction by NADH led to the inability to image the probe intracellularly in two NQO1-positive cell lines (HT-29 and A549). Images obtained for the positive cell lines looked very similar to the negative cell line (H596), where all three contained a faint fluorescent intracellular signal. This signal most likely derived from the background of the capped probe. It has also been reported that a Rho-Morph analogue switches to a cell permeant lactone form in polar media, which can also lead to a loss of intracellular signal.[1] This inability to image the probe was found to occur even after adjusting the probe concentration and a wide range of incubation times.

Q_3NN was designed to attach the quinone to the fluorophore via a short ethylene spacer as to minimize the steric hindrance and allow the probe to freely enter the enzyme active site, which in turn should increase the V_{max} and catalytic efficiency. The fluorophore used was a naphthalimide-butyl species that has a large Stokes shift of 116 nm and was measured to excite at 374 nm and emit at 490 nm. Quantum yields for Q_3NN and NN were calculated at 0.23 and 0.007, with a 33-fold fluorescence enhancement. Where Q_3-Rho-Morph was quenched by a structural change of the Rho-Morph species, Q_3NN possessed a much different quenching mechanism. It used a photoinduced electron transfer (PeT) process, prior to and post-reduction of the quinone, to prevent the excited electron in the fluorophore from relaxing and emitting a photon. To determine if this PeT process between the naphthalimide dye and the quinone was possible, the PeT free energy change was calculated using the Rehm-Weller equation. To accomplish this, the oxidation and reduction potentials were measured for NN and the trimethyl-

quinone acid. ΔG_{PeT} for the oxidative electron transfer prior to quinone reduction was calculated to be -0.35. Post-reduction was calculated at -2.69 for the reductive electron transfer. Both are sufficiently negative to give nearly complete quenching of the fluorophore. Only after the quinone is removed by lactonization is the fluorophore's signal revealed. Similar to Q_3-Rho-Morph, Q_3NN was rapidly activated in the presence of sodium dithionite. As a control to ensure PeT is the quenching mechanism after hydroquinone formation, a second probe (Q_1NN) was synthesized that contained a similar quinone without the trimethyl-lock. This probe was also mixed with sodium dithionite, of which the fluorescence signal was revealed at a much slower rate. By conjugating the quinone to a short linker, the enzymatic efficiency was raised when compared to Q_3-Rho-Morph, where V_{max} = 0.037 ± 0.002 μmol min^{-1} mg·NQO1^{-1} and k_{cat}/K_m = 4.9 (± 1.0) x 10^3 M^{-1} sec^{-1}. And of high importance, NADH caused a minimal decrease in the fluorescence signal of NN in pH 7.4, 0.1 M PBS. To determine if it was possible to visually observe the difference between cell lines with and without NQO1, HT-29, A549, and H596 cells were incubated with 20 μM Q_3NN for 10 minutes. These cells were then observed under a 365 nm lamp, where HT-29 and A549 were easily distinguishable from H596. The NQO1-positive cells emitted a blue light and H596 cells were colorless. The same cell lines were also analyzed using flow cytometry and widefield imaging. In both cases, the two NQO1-positive cell lines were easily differentiated from H596 with a very short incubation period of 10 minutes. Fluorescence imaging was also performed using two-photon confocal microscopy. The three cell lines used previously were used again, along with a second negative cell line (H446). As before, the negative and positive cell lines were differentiated with only a 10 minute incubation period. It was calculated that the average cytosolic fluorescence signal was 13-fold higher in A549 compared to H596 and 3.66 x 10^4-fold higher than H446 cells. Similar results were

obtained with the HT-29 cell line, with the cytosolic intensity being 15-fold higher compared to H596 and a 4.51 x 10^4 increase compared to H446. The released dye, NN, was colocalized with a lysotracker dye in the HT-29 cells and it was determined that the free dye preferentially accumulated in acidic compartments. Important to future applications of the probe for in vivo analysis is the effect it has on cell health. After one hour, cell viability for HT-29, A549, and H596 was 97.7%, 98.8%, and 100%, respectively, and 97.7%, 98.7%, and 98.4%, respectively, after one day.

To develop better enzyme assay conditions that should be more reliable and consistent between compound testing, solvent effects were determined on the ability of NQO1 to catalyze the reduction of a simple quinone trimethyl-lock system. One effect that is rarely taken into account is the solvent in which the substrate is dissolved. These solvents can perturb the enzyme's 3D structure by altering the hydrogen bonding of water to the protein or by changing the polarity of the medium. To determine how different solvents can affect the ability of NQO1 to catalyze a reaction, acetonitrile (ACN), ethanol (EtOH), and dimethyl sulfoxide (DMSO) were used in assays at 5% or 10%. While each solvent percentage was changing, the buffer (0.1 M PBS), salt (0.1 M potassium chloride), and pH 7.4 stayed constant. The results revealed that the high polar solvents (DMSO) negatively affected NQO1 more than the less polar solvents (ACN and EtOH). This trend was reasonable because higher polar solvents have the ability to penetrate deeper into the enzyme structure. This further penetration would create a larger shift in the 3D structure of the enzyme, specifically the active site. It was found that DMSO and ACN drastically reduced the enzyme's V_{max} by 68% and 34% when compared to an assay with no solvent, respectively, and NQO1 retained all of its activity in 5% EtOH. However, the shift from 5% solvent to 10% solvent was more detrimental to hNQO1 and had 54% of its activity in

ethanol, 7% in DMSO, and 26% in ACN. Catalytic efficiencies (k_{cat}/K_m) were calculated for each solvent-PBS system and compared to each other. For the 5% solvent systems, NQO1 in ACN was only 46% as efficient as compared to 100% buffer, while EtOH and DMSO were 85% and 93% as efficient, respectively. The k_{cat}/K_m was significantly reduced to 36%, 32%, and 47% for ACN, EtOH, and DMSO, respectively, when the assay was performed in 10% solvent-PBS. From the solvents tested, it was apparent that NQO1 assays containing 5% EtOH would be preferable for future assays since NQO1 retained all of its activity. Though DMSO is more commonly used in vitro, due to its minimal effect on cells, it is not as suitable for enzymatic assays involving NQO1.

5.2 Conclusions

The results demonstrated in this research outline the development and use of off-on latent fluorophores for the detection of hNQO1. Though the rhodadamine110-based probe was unsuccessfully used in vitro, it was found to be activated by hNQO1 in a timely manner and was stable towards biological reductants such as glutathione, ascorbic acid, and even dithiothreitol. The probe's main failures for in vitro imaging were associated with the fluorescent dye itself. Though the rhodamine-morpholino urea species was highly fluorescent, it was also susceptible to reduction by low concentrations of NADH. Along with the loss of fluorescence from reduction, it has been previously reported by a different research group that it forms a membrane permeant lactone form.[1] These two factors appeared to be detrimental in the ability of the probe to be fluorescently imaged in cell lines with hNQO1 activity.

A second probe was synthesized in which the quinone receptor group was attached to a short ethylene linker and attached to a naphthalimide dye. This probe exhibited a unique off-on type activation in that the quinone acted as an electron acceptor in a photoinduced electron

transfer quenching mechanism. By studying a negative control type dye that did not contain the trimethyl-lock and by using cyclic voltammetry to determine oxidation/reduction potentials in order to calculate the free energy change uing the Rehm-Weller equation, it was determined that the naphthalimide-based probe actually underwent a two-stage quenching mechanism. The first stage was prior to reduction, in which the quinone acts as the electron acceptor for the excited dye and caused a quenching effect. The second state was post-reduction, where the hydroquinone acted as an electron donor to the excited fluorophore, also causing quenching until cyclization and lactone release. This probe was found be a better NQO1 substrate substantially better than the rhodamine110-based probed. This would be most likely due to the bulky rhodamine-110 group attached directly to the quinone, rather than a much smaller ethylene linker. The naphthalimide probe was also found to be effective in tumor cell differentiation between cells known to contain NQO1 activity and cells with no enzyme activity. This was proved by performing widefield fluorescence imaging, confocal and multiphoton microscopy, and flow cytometry. Most importantly, the probe was rapidly activated in the NQO1-positive cells (<10 minutes) and did not show to be cytotoxic to any of the cell lines studied. It was also demonstrated that the type and percentage of solvent used in the NQO1 enzyme assay can be detrimental to the enzyme activity. Here, it was found that DMSO at only 5% reduced the enzyme activity by 68%, while EtOH and ACN only reduced the activity by 3% and 34%, respectively.

5.3 Outlook

With fluorescence-based optical imaging for the diagnosis and treatment of diseases still in its infancy, there is much work left to be accomplished to have a greater impact in the clinic. This development of fluorescent probes has the potential to aid in the design of drugs by

obtaining pharmacokinetic and biodistribution information, along with aiding in fields such as diagnosis and real-time surgical guidance. The goal of all fluorogenic probes for disease detection and analysis is to have high selectivity and sensitivity. This is attainable by obtaining a better understanding of the macro- and microenvironments of the tissue being studied, and utilizing the unique features that differentiates them from healthy tissues.

With the amount of previously reported information on the design and implementation of drug molecules that are selectively activated by NQO1, it is rather surprising NQO1 has not been used in the detection and treatment of cancer using biomedical imaging. Information in this dissertation provides an excellent starting point towards the design of next generation NQO1-activatable fluorophores. The probe structure contains two moieties, quinone and fluorophore, that can readily be changed to increase the substrate efficiency and allow adjustment of the optical properties to obtain a more biologically useable fluorophore. These properties can be adjusted while maintaining the selectivity for activation and still maintain a high signal-to-background ratio. The naphthalimide probe possesses the capability to conjugate the probe to different entities, such as other fluorophores and nanomaterials. By attaching fluorophores which emit in the red, there is the ability to create a pseudo-dual color probe using Förster resonance energy transfer (FRET) and giving the user more quantitative information. This could be accomplished by observing the red-emitting fluorescence and the change in fluorescence through FRET by exciting the naphthalimide probe as it is activated. These probes can also be attached to biomaterials, such as dextrans, to determine if there is any NQO1 activity in endosomes or lysosomes. One could easily attach lipids to the naphthalimide probe to create a probe-capped liposome system to observe the kinetics of activation and release of the vesicle's contents. More recently, reports have been published about the development of multimodal

probes that contain an optical imaging motif and a nuclear or magnetic resonance imaging motif.[2,3] This combination of incorporating a biomedical imaging technique commonly used clinically with an optical imaging agent allows for the development of a two function probe. One can be used to locate disease sites prior to surgery and a second can give real-time information during intraoperative procedures. Whether it's creating a second generation probe system or utilizing the probes presented here for in vivo analysis, there is still a large amount of research left to be performed to develop an NQO1-selective fluorophore which is capable for clinical applications.

5.4 References

(1) Watkins, R. W.; Lavis, L. D.; Kung, V. M.; Los, G. V.; Raines, R. T., Fluorogenic Affinity Label for the Facile, Rapid Imaging of Proteins in Live Cells. *Org. Biomol. Chem*. 2009, *7*, 3969-3975.

(2) Liu, Y.; Yu, G.; Tian, M.; Zhang, H., Optical probes and the applications in multimodality imaging. *Contrast Media Mol Imaging* 2011, *6*, 169-177.

(3) Azhdarinia, A.; Ghosh, P.; Ghosh, S.; Wilganowski, N.; Sevick-Muraca, E. M., Dual-labeling strategies for nuclear and fluorescence molecular imaging: a review and analysis. *Mol Imaging Biol* 2012, *14*, 261-276.

VITA

William Silvers was born in Bryan, Texas, and two years later, he moved to Kerrville, Texas where he lived through completion of high school. He obtained his Bachelor of Science degree in chemistry from Texas State University in the spring of 2007. He enrolled in the doctoral program in the Department of Chemistry at Louisiana State University in the fall of 2007, where he later joined the research lab of Dr. Robin L. McCarley. The degree of Doctor of Philosophy will be conferred at the Fall 2012 Commencement.